MIAMI UNIVERSITY
The Graduate School

Certificate for Approving the Dissertation

We hereby approve the Dissertation

of

Rebecca Stowe

Candidate for the Degree

DOCTOR OF PHILOSOPHY

_____
Dr. Gary A. Lorigan, Director

_____
Dr. Carole Dabney-Smith, Reader

_____
Dr. Andrea Kravats, Reader

_____
Dr. Kevin Yehl, Reader

_____
Dr. Tracy Haynes, Graduate School Representative

ABSTRACT

A SPECTROSCOPIC AND BIOCHEMICAL STUDY OF PROTEIN INTERACTIONS AND MEMBRANE MIMETIC SYSTEMS

by

Rebecca B. Stowe

The local environment of a protein determines whether it can perform its functions properly. Studying proteins in their native environment provides the most accurate information on their structure, function, dynamics, and interactions with other proteins. Membrane proteins are especially sensitive to their environment. In vitro studies require solubilization in a compatible membrane mimetic to allow membrane proteins to adopt native conformations and interact with binding partners. In this work, protein-protein interactions, aggregation and novel membrane mimetics are studied with EPR spectroscopy complemented by biochemical techniques. KCNQ1 is a six pass transmembrane protein that forms a potassium channel responsible for the regulation of many physiological processes including heartbeat by interacting with an accessory protein, KCNE1. In this dissertation the interactions between KCNQ1 monomers are further clarified by demonstrating the role of the transmembrane region in tetramer formation, and the interactions of KCNQ1 and KCNE1 are observed from the perspective of KCNE1 side chain dynamics with CW EPR spectroscopy. The novel membrane mimetic SMALPs were used to purify KCNE1 directly from inclusion bodies, expanding the potential applications for SMALPs to be used with proteins that denature upon removal from the native membrane. EPR spectroscopy can also be used to track protein-protein interactions that are detrimental to an organism, such as tau aggregation. Tau is an intrinsically disordered protein that is prone to degradation and has proven to be difficult to study in its full-length form. In this work, a method for spin labeling full-length Tau was developed as a screening tool to quickly and cost effectively estimate the location of aggregate cores. Lastly, the spectroscopic methods used in this work were used to spin label and observe the dynamics and interhelical distances of the human TRPV1 channel for the first time. This method can be used to observe dynamic and conformational changes that occur within the protein as a result of interactions with different agonists and environmental changes. The work presented in this dissertation uses EPR spectroscopy and various biochemical methods to solve problems related to protein interactions and membrane mimetics that have not been adequately addressed with other techniques.

A SPECTROSCOPIC AND BIOCHEMICAL STUDY OF PROTEIN INTERACTIONS AND MEMBRANE MIMETIC SYSTEMS

A DISSERTATION

Presented to the Faculty of

Miami University in partial

fulfillment of the requirements

for the degree of

Doctor of Philosophy

Department of Chemistry and Biochemistry

by

Rebecca B. Stowe

The Graduate School
Miami University
Oxford, Ohio

2023

Dissertation Director: Gary A. Lorigan

TABLE OF CONTENTS

LIST OF FIGURES

DEDICATION

The work discussed in this dissertation is dedicated to my parents, who have always encouraged me to pursue my dreams to the very end. To my dad for instilling a love of science and discovery in me from a young age with all the museums visited and documentaries watched. To my mom for always encouraging me to achieve my dreams even when they changed every other day.

ACKNOWLEDGEMENTS

First, I would like to thank my advisor Gary A. Lorigan for the opportunity to work in his group and for all the support he's offered throughout my time at Miami.

I would also like to thank all the members of my committee for their advice throughout the years: Dr. Carole Dabney-Smith, Dr. Andrea Kravats, Dr. Kevin Yehl, and Dr. Tracy Haynes.

I would like to thank Dr. Rob McCarrick for all the time spent training and helping me with EPR instrumentation.

I would also like to thank Dr. Carole Dabney-Smith for all her guidance when it felt like I'd never get the perfect gel.

I am grateful to have worked with members of the Lorigan group. Dr. Indra Sahu for all the help when things go wrong, especially during my first year. Alison Bates for being a great labmate and friend, and always coming through when life gets crazy. Thank you to Dr. Gunjan Dixit, Rasal Khan, Nancy Rotich, Lauryn Cook, Dr. Andrew Morris, and many more.

Thank you to all the friends I've made throughout my time at Miami, but especially Courtney Chatha and Emma Gordon. You guys have kept me sane with all the margaritas, movie nights, and adventures. Let's see each other again soon.

I am forever grateful for all my friends who have stuck with me for years and have supported this journey through the highs and the lows. Thank you, Haleigh Marlowe, for still being my best friend even though you knew me when I was 12, and thank you to all my friends from UNCA, Jacob Chappell, Dani Davis, Alex Hanamean, Abbie Sigmon, Giacomo Riva, Mikayla Bennet, and Rachel Maynard for getting me through the first degree, so that I could get this one.

Thank you to my parents for their endless love and support; and Doug for always being a comforting presence when I get home, no matter how the day went.

"When my little steps pile up, they will form a firm path one day." – Lee Jihoon

Chapter 1: Introduction

A Spectroscopic and Microscopic Study of Protein Interactions and Membrane Mimetic Systems

1.1 Membrane Proteins

Membrane proteins make up approximately 30% of the human genome and are responsible for a variety of physiological functions.[1] These proteins are separated into classes including channels, transporters, and receptors, carrying out important functions such as cell signaling, membrane trafficking, homeostasis, and energy transduction.[2] Since these proteins are responsible for so many crucial processes, they are often associated with diseases such as diabetes and cardiac arrhythmias.[3]

Determining the structures of membrane proteins is crucial to understanding their overall function and their roles in larger systems. Collecting structural data of a membrane protein in its native environment is considerably more difficult than doing so for a soluble protein, leading to a severe deficit in the available membrane protein structures. There are approximately 1100 known 3D structures of membrane proteins as of 2020, compared to about 150 just 12 years prior, which is a small percentage of the overall structures available in the Protein Data Bank (PDB).[4,5] The difficulty of studying membrane proteins comes from a variety of sources ranging from low expression yields, insufficient solubilization, and overall instability of the protein.[6] Commonly used structural determination techniques can also be incompatible with membrane proteins. X-Ray Crystallography requires certain conditions for protein crystals to form that is vastly different from the preferred environment of the membrane protein of interest, leading it to adopt non-native conformations.[7] Solution NMR spectroscopy, which is the second most common technique, is limited by protein size.[8] Many membrane proteins and complexes are too large, resulting in broad linewidths that cannot be resolved in sufficient detail. All of these issues combined make it difficult to study membrane proteins, explaining why they so severely lag behind their soluble counterparts. More recently, Cryo-Electron Microscopy (Cryo-EM) has become a popular structural determination technique with its high resolution and fewer size constraints, but obtaining high resolution structures of small proteins remains challenging.[9]

Membrane proteins function and fold best in environments that closely resemble their native hydrophobic environment in the cell. Since structural studies require for proteins to be purified, and therefore removed from their native environment, a membrane mimetic is used to mimic the native membrane.[10] There are several types of mimetics that are in use today, that each have their

own advantages and disadvantages.[11] When working with a new protein, mimetics must be tested to determine which is best for the protein and the technique being used.

Membrane proteins are complex systems that require extensive optimization to work with in any lab setting, making them more difficult to study than soluble proteins. It is crucial for them to be in an environment that closely mimics their native environment, as structural studies require purification and cannot be accomplished without the removal of the protein from its native membrane.[10] In recent years there have been many advancements in structural studies such as Cryo-EM and EPR spectroscopy, as well as the development of new membrane mimetics like SMALPs that make it possible to purify membrane proteins with the surrounding membrane intact.[9,12,13] As a result of these recent developments, membrane protein structures are more accessible than before, making it possible for proteins that could be crucial drug targets to be sufficiently studied for the first time.

1.2 Ion Channels

Ion channels are a class of membrane protein that are responsible for the maintenance of ion gradients across cell membranes. They play a crucial role in a variety of physiological processes such as regulation of cardiac action potential, muscle contraction, neurotransmitter release, and energy transduction.[14,15] Due to their ubiquity across both species and cell types, ion channels are also linked to a number of diseases, including Cystic Fibrosis, Long QT Syndrome, congenital deafness, diabetes, and hereditary myopathies among many others.[14,16] In order to better understand these diseases, ion channels have been studied extensively mainly via electrophysiology techniques such as patch clamp.[14,17] These functional studies have been used to show how the channels behave under different conditions and with disease-state mutations, providing context that allows for a clearer understanding of the channelopathies associated with these proteins.[18]

Structurally, ion channels all have a similar architecture in that they all form a pore in the membrane bilayer. This pore contains a selectivity filter that is suited to specifically allow the passage of one or two ions based on the ion's size, valency, and hydration energy.[19] For example the selectivity filter in potassium channels contains layers of carboxyl oxygens that mimic the arrangement of water binding sites surrounding a hydrated K^+ ion, allowing it to pass through the

hydrophobic membrane.[20] Ion channels can be further classified based on their gating mechanism. This gating mechanism ensures that ion flow only occurs when the appropriate conditions are met.[3,14,19] This involves some type of stimulus, which could be a voltage change, ligand, or temperature change that signals the channel to either open or close.[14,20] Without selective permeability and gating, the delicate electrochemical gradients that control many of life's processes would be impossible to maintain. Therefore, an in depth understanding of the function and dysfunction of ion channels will be necessary to effectively treat the channelopathies associated with them.

1.3 KCNQ1 and KCNE1

KCNQ1 ($K_V7.1$) is a potassium channel that is expressed in several tissues in the human body such as the heart, intestines, and ear.[21] The role of KCNQ1 in these tissues is crucial for several physiological processes such as heartbeat regulation and homeostasis. Disruption of its function can result in disease.[15,22] Structurally, KCNQ1 contains six transmembrane helices, S1-S6. S1-S4 make up the voltage sensing domain (VSD) which is responsible for sensing voltage change and controlling channel gating, and S5-S6 makes up the pore domain which lines the pore and contains the K^+ selectivity filter.[23] The N terminal domain is short and contains a phosphorylation site and the C terminal domain has 4 helices referred to as HA, HB, HC, and HD.[22,24] HA and HB make up the calmodulin binding domain that is largely responsible for the tetramerization of the channel, which is the oligomeric state required for channel function.[24] The C terminal domain also facilitates the binding of the lipid phosphatidylinositol 4,5-bisphosphate (PIP2) which is required for normal function in the membrane.[15,24,25]

The KCNE family of proteins (KCNE1-5) are a group of single pass membrane proteins that interact with KCNQ1 to regulate channel function.[21,26] The KCNE protein that is associated with KCNQ1 is determined by the tissue in which the proteins are expressed, with KCNE1 being expressed in the heart, which is the focus of the work described here. KCNE1 is a 15.7 kDa transmembrane protein with a single transmembrane helix.[27] It forms a complex with KCNQ1 in cardiac myocytes to form the low delayed rectifier (I_{KS}) channel, slowing down the activation kinetics of the channel, and allowing for the cardiac myocytes to be repolarized with the proper timing to maintain a heartbeat.[27,28] It interacts with KCNQ1 in a cleft between the S6 of one

KCNQ1 monomer and the S1 of another at a varying molar ratio.[29–31] The nature of the interactions between the two proteins have been previously studied with crosslinking, molecular modeling, and electrophysiology.[17,26,31,32] It has been found that the N and C terminus of KCNE1 interacts more dynamically with KCNQ1 while the transmembrane region of KCNE1 forms more rigid interactions, with residues 57-59 in KCNE1 being essential for the slowing of the activation kinetics.[17,28,31]

Dysfunction of KCNQ1 as well as its ancillary proteins in the KCNE family can lead to a number of diseases such as diabetes, congenital deafness, and Long QT Syndrome.[16] Long QT syndrome is a hereditary cardiac arrhythmia that is characterized by an abnormally long QT interval, which is easily diagnosable by electrocardiogram.[33] The condition is typically aggravated by strenuous exercise since the cardiac myocytes cannot repolarize quickly enough when heart rate is elevated. This leads to fainting spells and in extreme cases sudden cardiac arrest and death. Both KCNQ1 and KCNE1 contain mutations that can lead to Long QT Syndrome.[21,26,33] By understanding the function of these proteins and how they interact, this disease can be better understood and more effective treatments could be found as a result.

1.4 TRPV1

TRPV1 is a member of the Transient Receptor Potential Vanilloid channel family, and is most widely known for its role in nociception.[34] Much like other members of the TRPV family, TRPV1 responds to a diverse range of stimuli including high temperature, low pH, and agonists such as capsaicin, the chemical found in spicy peppers that elicits a pain response in humans.[34,35] Many of the initial studies of TRPV1 focused on its role as a pain receptor, but more recently it has been found expressed in the brain and vascular systems, with links to diseases such as epilepsy, depression, schizophrenia, hypertension, and diabetes.[34,36] Therefore, it has become a more viable drug target for issues other than treating pain.

Structurally, TRPV1 is a six pass transmembrane protein with a long N-terminal region containing ankyrin repeats and a short C-terminal region.[37] In the membrane it forms a tetramer much like other channels in the TRP and K_v families.[23,37] The channel also contains a region that mirrors the voltage sensing domain of K_v channels comprised of helices S1-S4, and has been found via Cryo-EM to contain the binding pockets of many ligands including capsaicin.[36,37]

The S1-S4 region of TRPV1, also referred to as the Voltage Sensing Like Domain (VSLD), has also been found to contribute to the thermosensitivity of the channel.[36] As mentioned above, not only is TRPV1 a ligand activated channel, but it can also be activated by high temperatures.[34] Recently using electrophysiology and NMR, the role of the VSLD in thermosensing has been confirmed, with the temperature dependent conformational changes being observed for the first time.[36] This result highlights the broad functionality of TRPV1, and how a further understanding of its mechanism of activation could tie into treatments for a number of diseases.

1.5 Tau

Alzheimer's Disease (AD) is the most frequently diagnosed neurodegenerative disease, affecting millions of patients globally, most commonly in the aged population.[38,39] It is characterized by the formation of amyloid beta plaques and tau neurofibrillary tangles (NFTs). While much of the previous AD research has focused on amyloid beta, recently more attention has turned towards tau, as the formation of NFTs is found universally in every AD patient, while amyloid beta plaques form later as the disease progresses.[39]

Tau protein is a member of the microtubule-associated protein (MAP) family, where it is responsible for stabilizing microtubule bundles in the axonal region of neurons.[40,41] Tau microtubule binding and aggregation are both affected by mutations and post translational modifications, particularly hyperphosphorylation, which has been found to be strongly linked to an increase in aggregation and cell death.[40,42] Structurally, tau is considered to be an intrinsically disordered protein (IDP), but it does have some local secondary structures such as beta sheets found in the microtubule binding region (MTBR).[40] The MTBR contains four repeat domains (R1-R4) that have been found to be the location of the aggregate core in AD fibrils, making it both the most functionally important region of the protein.[40,43,44]

Tau is the most thoroughly studied of the MAPs due to its association with neurodegenerative diseases.[38,40] There is an entire class of diseases that are associated with tau aggregation referred to as tauopathies. These diseases include AD, Parkinson's, and Pick's Disease among others.[39,43,44] In each of these diseases tau aggregates and forms lesions in the brain.[38] Recently it has been found through Cryo-EM imaging of tau isolated from the brains of patients that tau adopts different aggregate structures for different diseases, which implies that

the structure of the protein monomer in the aggregate is linked to the pathology.[43,44] In a lab setting, aggregates are typically formed via an inducer or seeding method.[45–47] The structure of the heparin induced aggregate has also recently been solved via Cryo-EM and was found to have a unique structure when compared to the AD filament.[43,44] Therefore, the structure of the aggregate seems to be dependent on the method used, which could mean that the structure of disease state aggregates could provide clues for the mechanism by which aggregation begins in patients with these tauopathies. The aggregate structure of each *in vitro* method should be resolved to determine the physiological relevance of each aggregation method.

1.6 Site Directed Spin Labeling

Site Directed Spin Labeling (SDSL) is a technique that is used to study proteins via Electron Paramagnetic Resonance (EPR) Spectroscopy by the introduction of a free electron.[48] In some cases, the addition of a free electron is not necessary, such as certain metalloproteins or proteins that have radical cofactors.[49] When these prerequisites are not met, a free electron can be introduced into the protein by the addition of a spin label.

There are a variety of spin labels available for use, the most common being nitroxide spin labels such as the ones used in this work, S-(1-oxyl-2,2,5,5-tetramethyl-2,5-dihydro-1H-pyrrol-3-yl)methyl methanesulfonothioate (MTSL) and 3-maleimido-PROXYL (MSL).[50] Each of these spin labels bind specifically with cysteine, either through a disulfide bond for MTSL (shown in **Figure 1.1**) and a maleimide bond for MSL.[48,51] In order to use these spin labels, site directed mutagenesis must be used to remove native cysteines and place cysteines in sites of interest, taking into account that mutations made do not disrupt the structure of the protein, or the function if it is crucial to the study.[12,48,50]

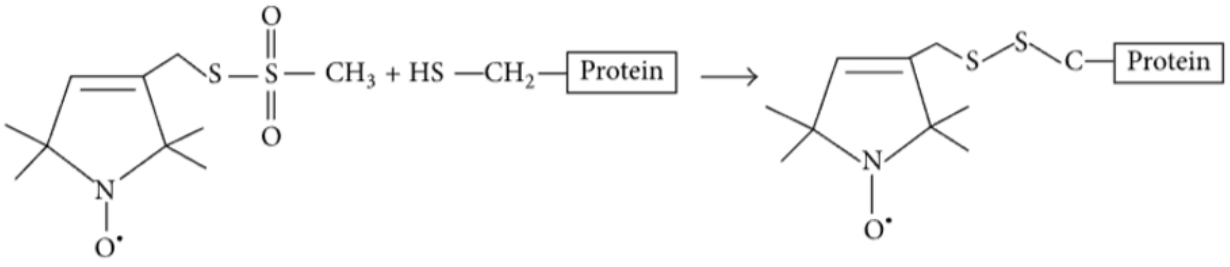

Figure 1.1: Structure of MTSL spin label including the disulfide attachment to cysteine.[48]

1.7 Electron Paramagnetic Resonance Spectroscopy

EPR Spectroscopy is a magnetic resonance technique that can be used to gain information on the local environment surrounding a paramagnetic center. Protein samples that are not EPR active can be made active by the addition of a spin label. EPR techniques can either be continuous wave (CW) or pulsed. Some of the information gathered from CW techniques can be dynamics or membrane depth.[50] Pulsed techniques can be used to measure the nuclear environment surrounding the spin label or the distances between multiple spin labels.[52]

EPR spectroscopy makes use of an electromagnet to apply a magnetic field to a sample

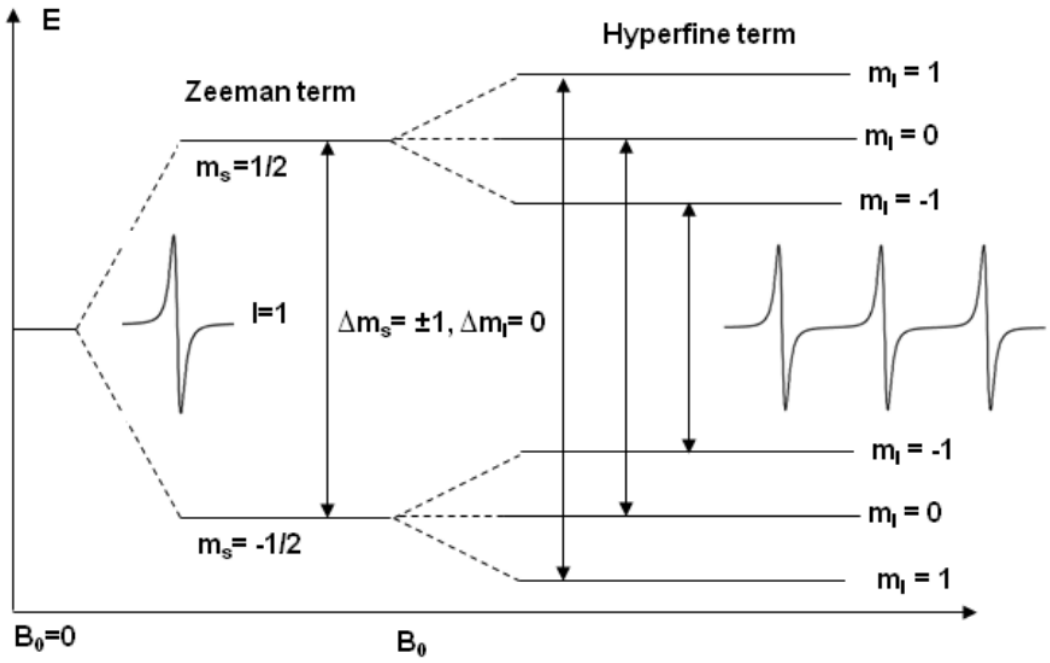

Figure 1.2: Energy level diagram of the MTSL spin label with a representative spectrum.[54]

containing free electrons with M_s quantum states of -1/2 and +1/2.[50,53] These two states are degenerate until a magnetic field is applied. The energy difference between these two levels is represented by the equation $\Delta E = h\nu = g\beta_e B_o$ where h is Planck's constant, ν is the microwave frequency, g is the g-factor of the electron, β_e is the Bohr Magneton, and Bo is the static magnetic field value in Gauss (G).[53] When $h\nu = g\beta_e B_o$ the energy level difference generated by the microwave frequency is the same as the energy level difference generated by the magnetic

field, and an EPR signal is observed.[53] The energy level diagram that illustrates this principle is shown in **Figure 1.2**.

1.8 Continuous Wave EPR Spectroscopy

Continuous Wave (CW) EPR spectroscopy is a commonly used EPR technique that involves the microwave frequency being applied continuously at a constant value and the magnetic field swept across a set range. CW EPR spectroscopy is typically performed at X-Band or 9.5 GHz, and the magnetic field value is determined by the g factor of the unpaired electron. For nitroxide spin labels, that magnetic field value is ~3300 G.[50,54,55]

The spectrum that is generated during data collection is a field modulated derivative spectrum, with the number of peaks dependent on the nuclear environment surrounding the free electron, following the 2nI + 1 rule.[50,53] In the case of nitroxide spin labels, the ^{14}N near the free electron has a nuclear spin of 1, resulting in a spectrum with 3 peaks.[50,53] The shape of these peaks is determined by the spin label's mobility, with peak broadening occurring as the motion of the spin label is restricted. Representative spectrum can be seen in **Figure 1.2**.

1.9 Double Electron Electron Resonance Spectroscopy

Double Electron Electron Resonance (DEER) Spectroscopy is a pulsed EPR technique that is used to determine the distance between two paramagnetic centers with a detection range of 20-70 Å.[56] In this work, a nitroxide spin label is used, which is the most commonly used spin label for studying the structure of proteins using DEER.[48] The value that is being measured during DEER data collection is the dipolar coupling of the two spin labels, which is dependent on the distance between the labels and the angle of the labels relative to the applied magnetic field.[57] The commonly used four pulse sequence is shown in **Figure 1.3**. Using this pulse sequence, one set of spins is excited at a probe frequency (ν_1) using a Hahn Echo Sequence to produce an echo, followed by an additional π pulse to refocus the echo.[58] The second set of spins is inverted by a single π pulse at the pump frequency (ν_2) with a position that varies between the two π pulses at ν_1.[48] The sign of the echo changes as the pump pulse changes position, producing time domain data where the periodicity of the echo is related to the intensity of the interactions between spins.[52,57]

The sensitivity of DEER is mainly dependent on the concentration of spin label in the sample, microwave frequency, temperature, and deuteration.[52] Having an optimal spin concentration and microwave frequency will improve your signal to noise ratio, with the optimal range of spin concentration being 30-100 μM for nitroxide labels, and most DEER data being collected at Q Band (34 GHz).[52] The length of data collection depends on the relaxation times of the spin labels. The spin-spin relaxation time (T_2) is the time it takes for the spins to relax by diffusing energy through the surrounding spins, and is largely influenced by temperature and deuteration.[56] The spin-lattice relaxation time (T_1), which is the amount of time it takes the spins to relax by diffusing energy through the surrounding matrix, can also be increased by the same means.[56] At lower temperatures most of the relaxation is through proton diffusion, so by removing many of those protons through deuteration, the length of data collection can be increased and longer distances can be observed.[52,56] To convert this time domain into a distance

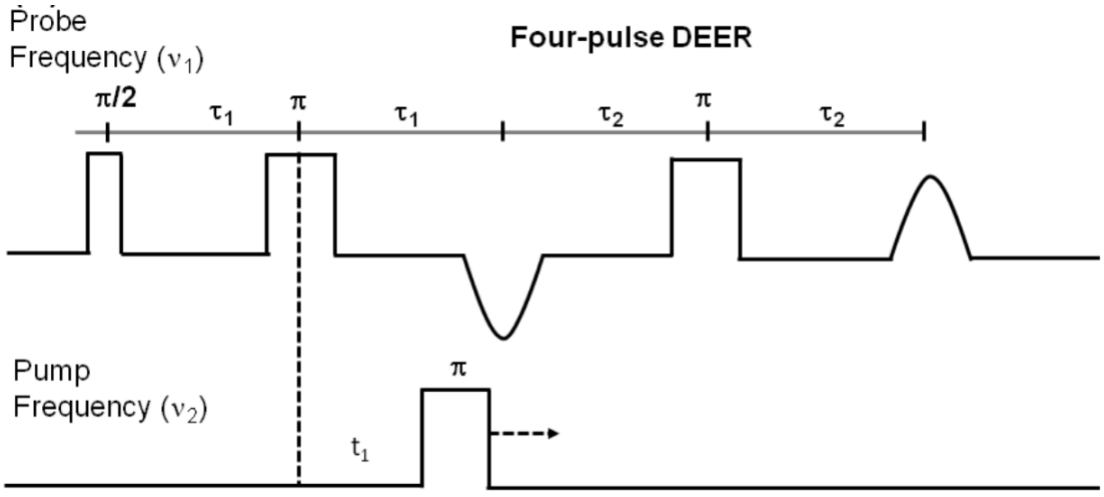

Figure 1.3: Diagram of the typical four-pulse DEER pulse sequence.[54]

distribution a Tikhonov regularization is used that yields a distance distribution that represents the weighted average of distances with a standard deviation.[52,56,57]

1.10 Membrane Mimetics

One of the main challenges of working with membrane proteins is selecting the appropriate membrane mimetic system that suits both the protein and the technique being used. There are a

variety of membrane mimetic systems available, while those discussed in this work are depicted in **Figure 1.4**.

Detergent micelles are the simplest and one of the most common membrane mimetics used.[11] They do not form bilayers, instead the single acyl chains surround the hydrophobic region of the protein, leaving the soluble regions solvent exposed.[11] Since they do not form bilayers, detergent micelles are not used when the goal is to mimic the native membrane more accurately. The advantage of detergent is that they are cheaper than lipid containing mimetics and take less work to prepare. Detergent selection is an important step in the process of method development when working with an unfamiliar protein. Some detergents can be quite harsh, even to the point of denaturing the protein, such as sodium dodecyl sulfate.[11,59] Others are gentler surfactants due to their structures closely resembling lipids or being zwitterionic.[59,60] These detergents are more likely to promote near native conformations and are often used for solution NMR determination of smaller membrane proteins.[28]

Liposomes are a commonly used bilayer forming membrane mimetic. They can be unilamellar or multilamellar, vary in size, and can be made up of a single type or multiple types of lipids.[10] A protein can be incorporated into them either during or after their formation to form proteoliposomes, which are useful for studying the dynamics and membrane interactions of proteins in their native environments via EPR and solid state NMR spectroscopy.[60,61] In this work, liposomes are formed using the thin film method, which involves dissolving lipids in chloroform then evaporating it off, leaving a thin film of lipid behind that is then put through several freeze thaw cycles in the desired buffer to form vesicles.[60] This minimizes the use of detergent and makes it a faster process to incorporate a protein than the lipid slurry method, which requires the removal of a large amount of SDS during vesicle formation.[61]

Bicelles are a disc shaped membrane mimetic that is made up of specific combinations of lipids and detergents.[62] The lipids form a bilayer and the detergents surround the ends of the bilayer, giving it a disc-like shape to which a protein can be incorporated. Unlike liposomes, both ends of the protein are exposed to the same solvent. This mimetic is limited by the lipid and detergent combinations that are available for use.[63] The combinations have to have the appropriate difference in acyl chain length to properly form the bicelle shape, which is defined

by the ratio of long chain to short chain. Bicelles are particularly useful for magnetic alignment studies and can be aligned either mechanically or chemically.[64]

Nanodiscs made with protein have been used to create bilayer containing particles that are significantly smaller than liposomes and bicelles. The original lipid nanodiscs were made with membrane scaffold protein (MSP), which is based on truncated human apolipoprotein.[8] These nanodiscs can range in sizes from ~6 nm up to ~12 nm, so they are quite limited in the proteins that can be incorporated in them.[8,10] These nanodiscs are formed by the slow removal of detergent via dialysis or other methods from a mixture of MSP, lipid, and the protein of interest, similar to the formation of liposomes.[8] Since this still requires the presence of detergent, proteins that are very sensitive to detergents are still not compatible with this mimetic. To ensure that these proteins can be studied, a mimetic that does not require the introduction of detergent and ideally keeps the native membrane intact is required. This is achievable with polymer or peptide nanodiscs, as each of these systems are capable of inserting into a bilayer and wrapping around the lipids to "cut out" a nanodiscs due to the hydrophobic regions both on the polymer and the peptides.[10] Polymer nanodiscs have an advantage over peptide nanodiscs because they are more stable for longer periods of time and they are more amenable to functionalization of the polymer that can make them customizable to different membrane protein systems.[65,66]

Selecting a membrane mimetic is a crucial step in working with membrane proteins that requires careful consideration. Not only is the function and stability of the protein an important factor in choosing a mimetic, but the technique being used must also be considered. Recent

progress has led to many new membrane mimetics being developed that opens up the opportunity to study systems that have been previously inaccessible.

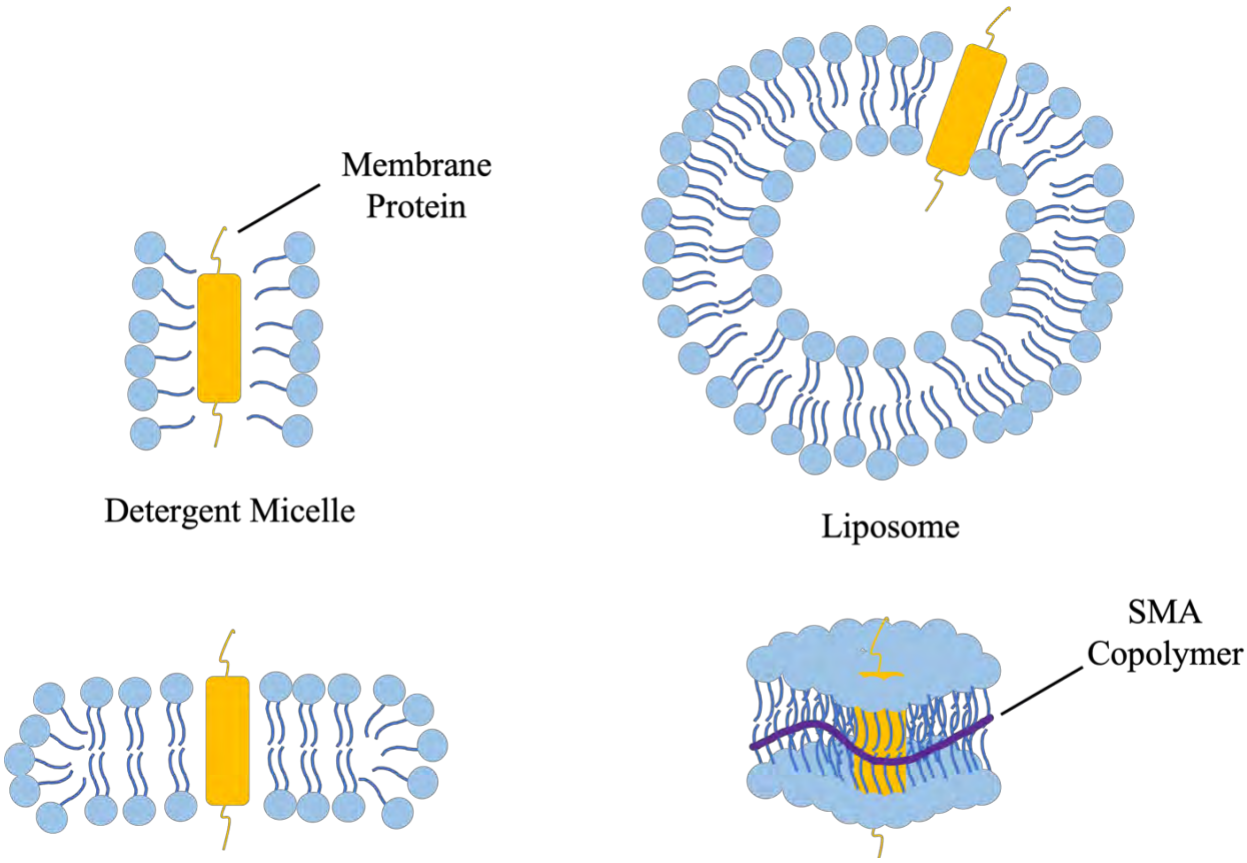

Figure 1.4: Schematic of different membrane mimetics.

1.11 SMA Synthesis

Synthesis of styrene maleic acid (SMA) copolymer makes use of the RAFT polymerization technique to synthesize a polymer chain of alternating monomers, the synthesis of which is shown in **Figure 1.5**.[67] SMA polymer can be customized to have different degrees of hydrophobicity based on the molar ratio of styrene to maleic anhydride.[13] By increasing the amount of styrene, the polymer is made more hydrophobic.[13] The typical ratios of styrene to maleic anhydride used for the formation of discs out of liposomes or native biological membranes is 2:1 or 3:1, as each of these ratios is capable of dissolving in aqueous solutions, making them suitable for use with most buffers used in these applications.[13,66] At a ratios of 4:1 or greater the polymer becomes too hydrophobic to dissolve in buffer, while at ratios of 1.5:1 or less the polymer is incapable of fully solubilizing membranes.[13] The molecular weight of the polymer can also be tuned by changing the amount of chain transfer agent used, which is the end group of each polymer chain.[13,68] After the initial synthesis is confirmed, the polymer can be hydrolyzed or functionalized to suit the user's needs. Hydrolysis yields the traditional SMA

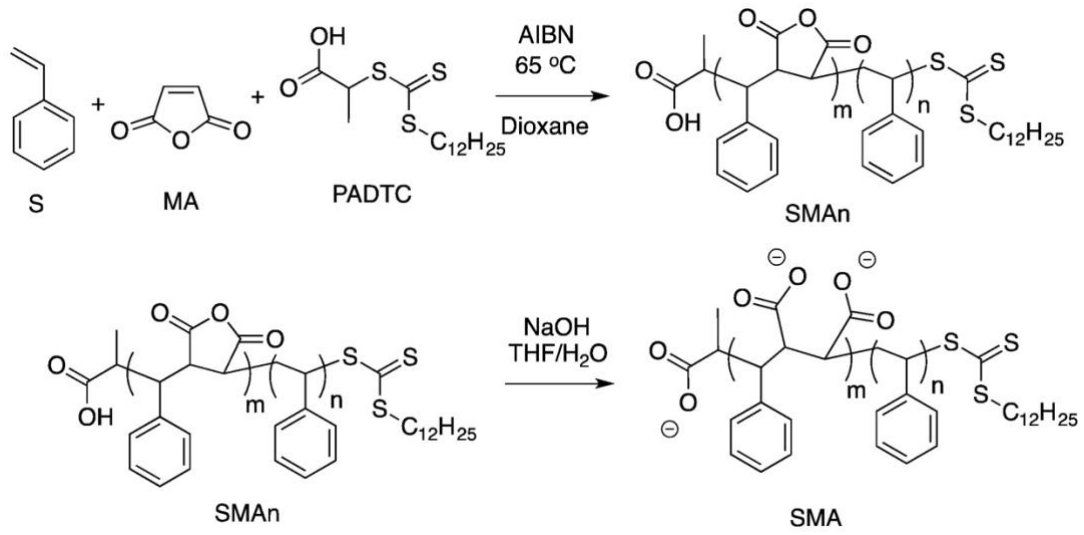

Figure 1.5: Synthesis of SMA polymer including hydrolysis to yield traditional SMA.[13]

polymer, which is compatible with many systems, but is not the gentlest surfactant so it may not effectively solubilize proteins that require more gentle surfactants when dissolved in detergent. SMA is also quite sensitive to pH values under 6 and Mg^{2+} concentrations over 10 mM, which

excludes its use in applications with proteins requiring these conditions.[66] To circumvent these issues, the polymer can be functionalized by an opening of the anhydride and addition of certain nucleophiles.[66] The ability to customize SMA to suit the needs of different systems makes it a more accessible mimetic to use with systems that are incompatible with the removal of the native lipids as well as those that cannot form nanodiscs via other means.

1.12 SMALPs

Styrene maleic acid copolymer lipid nanoparticles (SMALPs) are a new membrane mimetic used to form nanodiscs that have advantages compared to previously used MSP and peptide nanodiscs.[10] SMALPs, like peptide nanodiscs, can solubilize native membranes without the use of detergent. Unlike peptide nanodiscs, SMALPs have a much wider range of sizes that can be formed, which allows for larger membrane proteins and complexes to be solubilized in nanodiscs for the first time.[10] These advantages make them the most adaptable of all nanodisc forming mimetics.

The mechanism of SMALPs formation involves several steps, the first of which being the binding of the charged polymer to the head groups of the lipids.[65,69] The polymer is negatively charged, so a bilayer rich in anionic lipids will not form as many nanodiscs due to the repulsion between the negatively charged polymer and lipids. This can be fixed by functionalizing the polymer to have a positive charge. The next step is the insertion of the hydrophobic styrene moieties into the membrane, followed by the polymer wrapping around the lipids to form the nanodisc.[65,69] This step can be affected by the membrane fluidity, membrane thickness, and the lateral pressure that is exerted by the polymer on the membrane.[65] SMA copolymers solubilize the membrane faster above the T_m of lipids, when they are in the gel phase and packing is tighter.[69] They also solubilize saturated lipids faster and lipids that have a positive intrinsic curvature, which results in lower lateral pressure.[69] However, SMA still solubilizes the membrane when these conditions are not met, just not as efficiently.

The process of SMALPs formation is quite simple to observe, since they visibly reduce turbidity in vesicle samples once enough SMA has been added for SMALPs to form.[65,68,69] The ratio of SMA to lipid that is necessary to form SMALPs can vary based on the type of SMA and lipid being used, with a lower ratio indicating more efficient SMALPs formation.[66,69] Native membranes can also be used to form SMALPs, which is useful for detergent free purification of membrane proteins.[70,71] The size of formed SMALPs can be confirmed via Dynamic Light

Scattering (DLS) and Transmission Electron Microscopy (TEM), with typical size ranging from 10-50 nm with 10 nm being the most common.[13,69] The size of nanodiscs is not influenced by the type of lipids in the membrane, but has been found to be dependent on the molar ratio of styrene to maleic anhydride.[13]

SMALPs are a powerful new membrane mimetic that is highly customizable to suit purification of membrane proteins that could have been previously inaccessible to structural and dynamic studies. Due to their smaller size, they can be used for techniques that have size restrictions that bar the use of larger mimetics such as liposomes.[8] Due to their ability to remove proteins from their native membrane, it is now more feasible to resolve membrane protein structures in their native environment with Cryo-EM.[9] With so much diversity in their possible applications, SMALPs have the potential to help study membrane proteins structure, dynamics, interactions, and function more easily than before.

1.13 Conclusion

In the following chapters, the techniques described above are used to answer questions relating to several protein systems. The versatility of site directed spin labeling and EPR spectroscopic techniques is demonstrated in regard to both the types of protein systems it is compatible with and the information that can be gained about these protein systems. In this work the dynamics of protein-protein interactions, measurement of interhelical distances, and screening for aggregation are all highlighted as useful applications of spin labeling and EPR spectroscopic techniques.

References

(1) Hunte, C.; Richers, S. Lipids and Membrane Protein Structures. *Curr. Opin. Struct. Biol.* **2008**, *18* (4), 406–411. https://doi.org/10.1016/j.sbi.2008.03.008.

(2) Cho, W.; Stahelin, R. V. Membrane-Protein Interactions in Cell Signaling and Membrane Trafficking. *Annu. Rev. Biophys. Biomol. Struct.* **2005**, *34* (1), 119–151. https://doi.org/10.1146/annurev.biophys.33.110502.133337.

(3) Dworakowska, B.; Do, K. Ion Channels-Related Diseases*. *Ion Channels* **2000**, *47*.

(4) White, S. H. The Progress of Membrane Protein Structure Determination. *Protein Sci.* **2004**, *13* (7), 1948–1949. https://doi.org/10.1110/ps.04712004.

(5) Birch, J.; Cheruvara, H.; Gamage, N.; Harrison, P. J.; Lithgo, R.; Quigley, A. Changes in Membrane Protein Structural Biology. *Biology* **2020**, *9* (11), 401. https://doi.org/10.3390/biology9110401.

(6) Bill, R. M.; Henderson, P. J. F.; Iwata, S.; Kunji, E. R. S.; Michel, H.; Neutze, R.; Newstead, S.; Poolman, B.; Tate, C. G.; Vogel, H. Overcoming Barriers to Membrane Protein Structure Determination. *Nat. Biotechnol.* **2011**, *29* (4), 335–340. https://doi.org/10.1038/nbt.1833.

(7) Birch, J.; Axford, D.; Foadi, J.; Meyer, A.; Eckhardt, A.; Thielmann, Y.; Moraes, I. The Fine Art of Integral Membrane Protein Crystallisation. *Methods* **2018**, *147*, 150–162. https://doi.org/10.1016/j.ymeth.2018.05.014.

(8) Günsel, U.; Hagn, F. Lipid Nanodiscs for High-Resolution NMR Studies of Membrane Proteins. *Chem. Rev.* **2022**, *122* (10), 9395–9421. https://doi.org/10.1021/acs.chemrev.1c00702.

(9) Cheng, Y. Membrane Protein Structural Biology in the Era of Single Particle Cryo-EM. *Curr. Opin. Struct. Biol.* **2018**, *52*, 58–63. https://doi.org/10.1016/j.sbi.2018.08.008.

(10) Thoma, J.; Burmann, B. M. Fake It 'Till You Make It—The Pursuit of Suitable Membrane Mimetics for Membrane Protein Biophysics. *Int. J. Mol. Sci.* **2020**, *22* (1), 50. https://doi.org/10.3390/ijms22010050.

(11) Seddon, A. M.; Curnow, P.; Booth, P. J. Membrane Proteins, Lipids and Detergents: Not Just a Soap Opera. *Biochim. Biophys. Acta BBA - Biomembr.* **2004**, *1666* (1–2), 105–117. https://doi.org/10.1016/j.bbamem.2004.04.011.

(12) García-Rubio, I. EPR of Site-Directed Spin-Labeled Proteins: A Powerful Tool to Study Structural Flexibility. *Arch. Biochem. Biophys.* **2020**, *684*, 108323. https://doi.org/10.1016/j.abb.2020.108323.

(13) Craig, A. F.; Clark, E. E.; Sahu, I. D.; Zhang, R.; Frantz, N. D.; Al-Abdul-Wahid, M. S.; Dabney-Smith, C.; Konkolewicz, D.; Lorigan, G. A. Tuning the Size of Styrene-Maleic Acid Copolymer-Lipid Nanoparticles (SMALPs) Using RAFT Polymerization for Biophysical Studies. *Biochim. Biophys. Acta BBA - Biomembr.* **2016**, *1858* (11), 2931–2939. https://doi.org/10.1016/j.bbamem.2016.08.004.

(14) Ackerman, M. J.; Clapham, D. E. Ion Channels — Basic Science and Clinical Disease. *N. Engl. J. Med.* **1997**.

(15) Dixit, G.; Dabney-Smith, C.; Lorigan, G. A. The Membrane Protein KCNQ1 Potassium Ion Channel: Functional Diversity and Current Structural Insights. *Biochim. Biophys. Acta BBA - Biomembr.* **2020**, *1862* (5), 183148. https://doi.org/10.1016/j.bbamem.2019.183148.

(16) Maljevic, S.; Wuttke, T. V.; Seebohm, G.; Lerche, H. KV7 Channelopathies. *Pflüg. Arch. - Eur. J. Physiol.* **2010**, *460* (2), 277–288. https://doi.org/10.1007/s00424-010-0831-3.

(17) Chung, D. Y.; Chan, P. J.; Bankston, J. R.; Yang, L.; Liu, G.; Marx, S. O.; Karlin, A.; Kass, R. S. Location of KCNE1 Relative to KCNQ1 in the I_{KS} Potassium Channel by Disulfide Cross-Linking of Substituted Cysteines. *Proc. Natl. Acad. Sci.* **2009**, *106* (3), 743–748. https://doi.org/10.1073/pnas.0811897106.

(18) Huang, H.; Kuenze, G.; Smith, J. A.; Taylor, K. C.; Duran, A. M.; Hadziselimovic, A.; Meiler, J.; Vanoye, C. G.; Jr, A. L. G.; Sanders, C. R. Mechanisms of KCNQ1 Channel

Dysfunction in Long QT Syndrome Involving Voltage Sensor Domain Mutations. *Sci. Adv.* **2018**, 12.

(19) Grant, A. O. Cardiac Ion Channels. *Circ. Arrhythm. Electrophysiol.* **2009**, *2* (2), 185–194. https://doi.org/10.1161/CIRCEP.108.789081.

(20) MacKinnon, R. Potassium Channels. *FEBS Lett.* **2003**, *555* (1), 62–65. https://doi.org/10.1016/S0014-5793(03)01104-9.

(21) Abbott, G. W. Biology of the KCNQ1 Potassium Channel. *New J. Sci.* **2014**, *2014*, 1–26. https://doi.org/10.1155/2014/237431.

(22) Jespersen, T.; Grunnet, M.; Olesen, S.-P. The KCNQ1 Potassium Channel: From Gene to Physiological Function. *Physiology* **2005**, *20* (6), 408–416. https://doi.org/10.1152/physiol.00031.2005.

(23) Smith, J. A.; Vanoye, C. G.; George, A. L.; Meiler, J.; Sanders, C. R. Structural Models for the KCNQ1 Voltage-Gated Potassium Channel. *Biochemistry* **2007**, *46* (49), 14141–14152. https://doi.org/10.1021/bi701597s.

(24) Wiener, R.; Haitin, Y.; Shamgar, L.; Fernández-Alonso, M. C.; Martos, A.; Chomsky-Hecht, O.; Rivas, G.; Attali, B.; Hirsch, J. A. The KCNQ1 (Kv7.1) COOH Terminus, a Multitiered Scaffold for Subunit Assembly and Protein Interaction. *J. Biol. Chem.* **2008**, *283* (9), 5815–5830. https://doi.org/10.1074/jbc.M707541200.

(25) Royal, A. A.; Tinker, A.; Harmer, S. C. Phosphatidylinositol-4,5-Bisphosphate Is Required for KCNQ1/KCNE1 Channel Function but Not Anterograde Trafficking. *PLOS ONE* **2017**, *12* (10), e0186293. https://doi.org/10.1371/journal.pone.0186293.

(26) Nakajo, K.; Kubo, Y. KCNQ1 Channel Modulation by KCNE Proteins via the Voltage-Sensing Domain: KCNQ1 Channel Modulation by KCNE. *J. Physiol.* **2015**, *593* (12), 2617–2625. https://doi.org/10.1113/jphysiol.2014.287672.

(27) Gofman, Y.; Shats, S.; Attali, B.; Haliloglu, T.; Ben-Tal, N. How Does KCNE1 Regulate the Kv7.1 Potassium Channel? Model-Structure, Mutations, and Dynamics of the Kv7.1-KCNE1 Complex. *Structure* **2012**, *20* (8), 1343–1352. https://doi.org/10.1016/j.str.2012.05.016.

(28) Kang, C.; Tian, C.; Sönnichsen, F. D.; Smith, J. A.; Meiler, J.; George, A. L.; Vanoye, C. G.; Kim, H. J.; Sanders, C. R. Structure of KCNE1 and Implications for How It Modulates the KCNQ1 Potassium Channel † ‡. *Biochemistry* **2008**, *47* (31), 7999–8006. https://doi.org/10.1021/bi800875q.

(29) Nakajo, K.; Ulbrich, M. H.; Kubo, Y.; Isacoff, E. Y. Stoichiometry of the KCNQ1 - KCNE1 Ion Channel Complex. *Proc. Natl. Acad. Sci.* **2010**, *107* (44), 18862–18867. https://doi.org/10.1073/pnas.1010354107.

(30) Plant, L. D.; Xiong, D.; Dai, H.; Goldstein, S. A. N. Individual IKs Channels at the Surface of Mammalian Cells Contain Two KCNE1 Accessory Subunits. *Proc. Natl. Acad. Sci.* **2014**, *111* (14), E1438–E1446. https://doi.org/10.1073/pnas.1323548111.

(31) Kuenze, G.; Vanoye, C. G.; Desai, R. R.; Adusumilli, S.; Brewer, K. R.; Woods, H.; McDonald, E. F.; Sanders, C. R.; George, A. L.; Meiler, J. Allosteric Mechanism for KCNE1 Modulation of KCNQ1 Potassium Channel Activation. *eLife* **2020**, *9*, e57680. https://doi.org/10.7554/eLife.57680.

(32) Lvov, A.; Gage, S. D.; Berrios, V. M.; Kobertz, W. R. Identification of a Protein–Protein Interaction between KCNE1 and the Activation Gate Machinery of KCNQ1. *J. Gen. Physiol.* **2010**, *135* (6), 607–618. https://doi.org/10.1085/jgp.200910386.

(33) Peroz, D.; Rodriguez, N.; Choveau, F.; Baró, I.; Mérot, J.; Loussouarn, G. Kv7.1 (KCNQ1) Properties and Channelopathies: Kv7.1 (KCNQ1) Properties and Channelopathies. *J. Physiol.* **2008**, *586* (7), 1785–1789. https://doi.org/10.1113/jphysiol.2007.148254.

(34) Storozhuk, M. V.; Moroz, O. F.; Zholos, A. V. Multifunctional TRPV1 Ion Channels in Physiology and Pathology with Focus on the Brain, Vasculature, and Some Visceral Systems. *BioMed Res. Int.* **2019**, *2019*, 1–12. https://doi.org/10.1155/2019/5806321.

(35) Yang, F.; Xiao, X.; Lee, B. H.; Vu, S.; Yang, W.; Yarov-Yarovoy, V.; Zheng, J. The Conformational Wave in Capsaicin Activation of Transient Receptor Potential Vanilloid 1 Ion Channel. *Nat. Commun.* **2018**, *9* (1), 2879. https://doi.org/10.1038/s41467-018-05339-6.

(36) Kim, M.; Sisco, N. J.; Hilton, J. K.; Montano, C. M.; Castro, M. A.; Cherry, B. R.; Levitus, M.; Van Horn, W. D. Evidence That the TRPV1 S1-S4 Membrane Domain Contributes to Thermosensing. *Nat. Commun.* **2020**, *11* (1), 4169. https://doi.org/10.1038/s41467-020-18026-2.

(37) Benítez-Angeles, M.; Morales-Lázaro, S. L.; Juárez-González, E.; Rosenbaum, T. TRPV1: Structure, Endogenous Agonists, and Mechanisms. *Int. J. Mol. Sci.* **2020**, *21* (10), 3421. https://doi.org/10.3390/ijms21103421.

(38) Pîr, D. F. V.; Pirici, I.; Tudoric, V. Tau Protein in Neurodegenerative Diseases – a Review.

(39) Falcon, B.; Zhang, W.; Schweighauser, M.; Murzin, A. G.; Vidal, R.; Garringer, H. J.; Ghetti, B.; Scheres, S. H. W.; Goedert, M. Tau Filaments from Multiple Cases of Sporadic and Inherited Alzheimer's Disease Adopt a Common Fold. *Acta Neuropathol. (Berl.)* **2018**, *136* (5), 699–708. https://doi.org/10.1007/s00401-018-1914-z.

(40) Barbier, P.; Zejneli, O.; Martinho, M.; Lasorsa, A.; Belle, V.; Smet-Nocca, C.; Tsvetkov, P. O.; Devred, F.; Landrieu, I. Role of Tau as a Microtubule-Associated Protein: Structural and Functional Aspects. *Front. Aging Neurosci.* **2019**, *11*, 204. https://doi.org/10.3389/fnagi.2019.00204.

(41) Morris, M.; Maeda, S.; Vossel, K.; Mucke, L. The Many Faces of Tau. *Neuron* **2011**, *70* (3), 410–426. https://doi.org/10.1016/j.neuron.2011.04.009.

(42) Liu, M.; Sui, D.; Dexheimer, T.; Hovde, S.; Deng, X.; Wang, K.-W.; Lin, H. L.; Chien, H.-T.; Kweon, H. K.; Kuo, N. S.; Ayoub, C. A.; Jimenez-Harrison, D.; Andrews, P. C.; Kwok, R.; Bochar, D. A.; Kuret, J.; Fortin, J.; Tsay, Y.-G.; Kuo, M.-H. Hyperphosphorylation Renders Tau Prone to Aggregate and to Cause Cell Death. *Mol. Neurobiol.* **2020**, *57* (11), 4704–4719. https://doi.org/10.1007/s12035-020-02034-w.

(43) Fichou, Y.; Vigers, M.; Goring, A. K.; Eschmann, N. A.; Han, S. Heparin-Induced Tau Filaments Are Structurally Heterogeneous and Differ from Alzheimer's Disease Filaments. *Chem. Commun.* **2018**, *54* (36), 4573–4576. https://doi.org/10.1039/C8CC01355A.

(44) Zhang, W.; Falcon, B.; Murzin, A. G.; Fan, J.; Crowther, R. A.; Goedert, M.; Scheres, S. H. Heparin-Induced Tau Filaments Are Polymorphic and Differ from Those in Alzheimer's and Pick's Diseases. *eLife* **2019**, *8*, e43584. https://doi.org/10.7554/eLife.43584.

(45) Margittai, M.; Langen, R. Template-Assisted Filament Growth by Parallel Stacking of Tau. *Proc. Natl. Acad. Sci.* **2004**, *101* (28), 10278–10283. https://doi.org/10.1073/pnas.0401911101.

(46) *Tau Protein: Methods and Protocols*; Smet-Nocca, C., Ed.; Methods in Molecular Biology; Springer New York: New York, NY, 2017; Vol. 1523. https://doi.org/10.1007/978-1-4939-6598-4.

(47) Carmel, G.; Mager, E. M.; Binder, L. I.; Kuret, J. The Structural Basis of Monoclonal Antibody Alz50's Selectivity for Alzheimer's Disease Pathology. *J. Biol. Chem.* **1996**, *271* (51), 32789–32795. https://doi.org/10.1074/jbc.271.51.32789.

(48) Sahu, I. D.; Lorigan, G. A. Site-Directed Spin Labeling EPR for Studying Membrane Proteins. *BioMed Res. Int.* **2018**, *2018*, 1–13. https://doi.org/10.1155/2018/3248289.

(49) Osborne, M. J.; Crowe, D.; Davy, S. L.; Macdonald, C.; Moore, G. R. NMR of Paramagnetic Proteins. In *Protein NMR Techniques*; Humana Press: New Jersey, 1997; Vol. 60, pp 233–270. https://doi.org/10.1385/0-89603-309-0:233.

(50) Klug, C. S.; Feix, J. B. Methods and Applications of Site-Directed Spin Labeling EPR Spectroscopy. In *Methods in Cell Biology*; Elsevier, 2008; Vol. 84, pp 617–658. https://doi.org/10.1016/S0091-679X(07)84020-9.

(51) Torricella, F.; Pierro, A.; Mileo, E.; Belle, V.; Bonucci, A. Nitroxide Spin Labels and EPR Spectroscopy: A Powerful Association for Protein Dynamics Studies. *Biochim. Biophys. Acta BBA - Proteins Proteomics* **2021**, *1869* (7), 140653. https://doi.org/10.1016/j.bbapap.2021.140653.

(52) Jeschke, G. DEER Distance Measurements on Proteins. *Annu. Rev. Phys. Chem.* **2012**, *63* (1), 419–446. https://doi.org/10.1146/annurev-physchem-032511-143716.

(53) Roessler, M. M.; Salvadori, E. Principles and Applications of EPR Spectroscopy in the Chemical Sciences. *Chem. Soc. Rev.* **2018**, *47* (8), 2534–2553. https://doi.org/10.1039/C6CS00565A.

(54) Sahu, I. D.; Zhang, R.; Dunagan, M. M.; Craig, A. F.; Lorigan, G. A. Characterization of KCNE1 inside Lipodisq Nanoparticles for EPR Spectroscopic Studies of Membrane Proteins. *J. Phys. Chem. B* **2017**, *121* (21), 5312–5321. https://doi.org/10.1021/acs.jpcb.7b01705.

(55) Sahu, I. D.; Dixit, G.; Reynolds, W. D.; Kaplevatsky, R.; Harding, B. D.; Jaycox, C. K.; McCarrick, R. M.; Lorigan, G. A. Characterization of the Human KCNQ1 Voltage Sensing Domain (VSD) in Lipodisq Nanoparticles for Electron Paramagnetic Resonance (EPR) Spectroscopic Studies of Membrane Proteins. *J. Phys. Chem. B* **2020**, *124* (12), 2331–2342. https://doi.org/10.1021/acs.jpcb.9b11506.

(56) Jeschke, G.; Polyhach, Y. Distance Measurements on Spin-Labelled Biomacromolecules by Pulsed Electron Paramagnetic Resonance. *Phys. Chem. Chem. Phys.* **2007**, *9* (16), 1895. https://doi.org/10.1039/b614920k.

(57) Sahu, I. D.; Lorigan, G. A. EPR Techniques, Spin Labeling, and Spin Trapping. In *Reference Module in Chemistry, Molecular Sciences and Chemical Engineering*; Elsevier, 2018; p B9780124095472140000. https://doi.org/10.1016/B978-0-12-409547-2.14080-6.

(58) Sahu, I. D.; Lorigan, G. A. Electron Paramagnetic Resonance as a Tool for Studying Membrane Proteins. *Biomolecules* **2020**, *10* (5), 763. https://doi.org/10.3390/biom10050763.

(59) Rath, A.; Glibowicka, M.; Nadeau, V. G.; Chen, G.; Deber, C. M. Detergent Binding Explains Anomalous SDS-PAGE Migration of Membrane Proteins. *Proc. Natl. Acad. Sci.* **2009**, *106* (6), 1760–1765. https://doi.org/10.1073/pnas.0813167106.

(60) Dixit, G.; Stowe, R. B.; Bates, A.; Jaycox, C. K.; Escobar, J. R.; Harding, B. D.; Drew, D. L.; New, C. P.; Sahu, I. D.; Edelmann, R. E.; Dabney-Smith, C.; Sanders, C. R.; Lorigan, G. A. Purification and Membrane Interactions of Human KCNQ1100–370 Potassium Ion Channel.

Biochim. Biophys. Acta BBA - Biomembr. **2022**, *1864* (11), 184010. https://doi.org/10.1016/j.bbamem.2022.184010.

(61) Dixit, G.; Sahu, I. D.; Reynolds, W. D.; Wadsworth, T. M.; Harding, B. D.; Jaycox, C. K.; Dabney-Smith, C.; Sanders, C. R.; Lorigan, G. A. Probing the Dynamics and Structural Topology of the Reconstituted Human KCNQ1 Voltage Sensor Domain (Q1-VSD) in Lipid Bilayers Using Electron Paramagnetic Resonance Spectroscopy. *Biochemistry* **2019**, *58* (7), 965–973. https://doi.org/10.1021/acs.biochem.8b01042.

(62) Duc, N. M.; Du, Y.; Thorsen, T. S.; Lee, S. Y.; Zhang, C.; Kato, H.; Kobilka, B. K.; Chung, K. Y. Effective Application of Bicelles for Conformational Analysis of G Protein-Coupled Receptors by Hydrogen/Deuterium Exchange Mass Spectrometry. *J. Am. Soc. Mass Spectrom.* **2015**, *26* (5), 808–817. https://doi.org/10.1007/s13361-015-1083-4.

(63) Morrison, E. A.; Henzler-Wildman, K. A. Reconstitution of Integral Membrane Proteins into Isotropic Bicelles with Improved Sample Stability and Expanded Lipid Composition Profile. *Biochim. Biophys. Acta BBA - Biomembr.* **2012**, *1818* (3), 814–820. https://doi.org/10.1016/j.bbamem.2011.12.020.

(64) Sahu, I. D.; Mayo, D. J.; Subbaraman, N.; Inbaraj, J. J.; McCarrick, R. M.; Lorigan, G. A. Probing Topology and Dynamics of the Second Transmembrane Domain (M2δ) of the Acetyl Choline Receptor Using Magnetically Aligned Lipid Bilayers (Bicelles) and EPR Spectroscopy. *Chem. Phys. Lipids* **2017**, *206*, 9–15. https://doi.org/10.1016/j.chemphyslip.2017.05.010.

(65) Xue, M.; Cheng, L.; Faustino, I.; Guo, W.; Marrink, S. J. Molecular Mechanism of Lipid Nanodisk Formation by Styrene-Maleic Acid Copolymers. *Biophys. J.* **2018**, *115* (3), 494–502. https://doi.org/10.1016/j.bpj.2018.06.018.

(66) Burridge, K. M.; Harding, B. D.; Sahu, I. D.; Kearns, M. M.; Stowe, R. B.; Dolan, M. T.; Edelmann, R. E.; Dabney-Smith, C.; Page, R. C.; Konkolewicz, D.; Lorigan, G. A. Simple Derivatization of RAFT-Synthesized Styrene–Maleic Anhydride Copolymers for Lipid Disk Formulations. *Biomacromolecules* **2020**, *21* (3), 1274–1284. https://doi.org/10.1021/acs.biomac.0c00041.

(67) Huang, J.; Turner, S. R. Recent Advances in Alternating Copolymers: The Synthesis, Modification, and Applications of Precision Polymers. *Polymer* **2017**, *116*, 572–586. https://doi.org/10.1016/j.polymer.2017.01.020.

(68) Dörr, J. M.; Scheidelaar, S.; Koorengevel, M. C.; Dominguez, J. J.; Schäfer, M.; van Walree, C. A.; Killian, J. A. The Styrene–Maleic Acid Copolymer: A Versatile Tool in Membrane Research. *Eur. Biophys. J.* **2016**, *45* (1), 3–21. https://doi.org/10.1007/s00249-015-1093-y.

(69) Scheidelaar, S.; Koorengevel, M. C.; Pardo, J. D.; Meeldijk, J. D.; Breukink, E.; Killian, J. A. Molecular Model for the Solubilization of Membranes into Nanodisks by Styrene Maleic Acid Copolymers. *Biophys. J.* **2015**, *108* (2), 279–290. https://doi.org/10.1016/j.bpj.2014.11.3464.

(70) Lee, S. C.; Knowles, T. J.; Postis, V. L. G.; Jamshad, M.; Parslow, R. A.; Lin, Y.; Goldman, A.; Sridhar, P.; Overduin, M.; Muench, S. P.; Dafforn, T. R. A Method for Detergent-Free Isolation of Membrane Proteins in Their Local Lipid Environment. *Nat. Protoc.* **2016**, *11* (7), 1149–1162. https://doi.org/10.1038/nprot.2016.070.

(71) Dörr, J. M.; Koorengevel, M. C.; Schäfer, M.; Prokofyev, A. V.; Scheidelaar, S.; van der Cruijsen, E. A. W.; Dafforn, T. R.; Baldus, M.; Killian, J. A. Detergent-Free Isolation, Characterization, and Functional Reconstitution of a Tetrameric K^+ Channel: The Power of Native Nanodiscs. *Proc. Natl. Acad. Sci.* **2014**, *111* (52), 18607–18612. https://doi.org/10.1073/pnas.1416205112.

Chapter 2

Oligomerization of the KCNQ1$_{100\text{-}370}$ Construct Confirmed via Native PAGE Gel Analysis

Gunjan Dixit [a,b,1], Rebecca B. Stowe [a,1], Alison Bates [a], Colleen K. Jaycox [a], Jorge R. Escobar [a,b], Benjamin D. Harding [a], Daniel L. Drew Jr. [a], Christopher P. New [a,b], Indra D. Sahu [a], Richard E. Edelmann [c], Carole Dabney-Smith [a,b], Charles R. Sanders [d], Gary A. Lorigan [a,b,*]

a *Department of Chemistry and Biochemistry, Miami University, 651 E. High Street, Oxford, OH 45056, USA*

b *Cell, Molecular and Structural Biology Program, Department of Chemistry & Biochemistry, Miami University, Oxford, OH 45056, USA*

c *Center for Advanced Microscopy and Imaging, Miami University, Oxford, OH 45056, USA*

d *Department of Biochemistry and Center for Structural Biology, Vanderbilt University, Nashville, TN 37240, USA*

This work has been published in BBA Biomembranes.

Purification and membrane interactions of human KCNQ1$_{100–370}$ potassium ion channel

BBA Biomembranes, 2022. Work in this chapter was contributed by RBS.

2.1 Abstract

KCNQ1 has been traditionally thought to form a homotetramer by the interactions of the C termini of the monomer with other monomers as well as calmodulin. While this interaction does play a major role in the tetramerization of the channel, it is not the only contributor. Other interactions that lead KCNQ1 to oligomerize have not been studied in depth due to the focus on the C terminus and the difficulty in expressing and purifying KCNQ1 for the purpose of structural studies. In this study a truncated construct of KCNQ1 containing only the residues 100-370 that make up the transmembrane domain was expressed and purified using a bacterial expression vector system and affinity chromatography. This construct was found to form higher order oligomers including the tetramer that is natively formed in the membrane of cardiac myocytes and other tissues. By confirming that this oligomerization does happen without the C terminus present, this study shows that more information is needed to have a full understanding on how the KCNQ1 potassium channel forms its native quaternary structure.

2.2 Introduction

KCNQ1 (Kv7.1) is a member of the voltage gated potassium channel (Kv) family that is expressed in a variety of tissues including the heart, intestines, and ear.[1–4] When KCNQ1 associates with KCNE1(minK) it forms the slow delayed rectifier (I_{KS}) channel that is responsible for the repolarization of cardiac myocytes.[5–9] Mutations in KCNQ1 and its accessory proteins can lead to a number of diseases such as diabetes, atrial fibrillation, congenital deafness, and Long QT Syndrome.[10–15]

The human KCNQ1 protein is made up of 676 residues, with a six helix transmembrane region, flanked by the cytoplasmic N and C terminal regions.[16] The transmembrane domain is made up of the voltage sensing domain (VSD) (helices S1-S4) and the pore domain (PD) (S5-S6).[3,16] To form a channel KCNQ1 tetramerizes in a domain swapped structure, with the VSD of one monomer coupled with the PD of an adjacent monomer.[17] The mechanism for tetramer formation has largely been attributed to the interaction between the C-terminal helix HA with calmodulin.[18] While there is sufficient evidence to suggest that this interaction is the main driving force behind the formation of the channel, the role that other domains play in this process has not been studied as thoroughly.

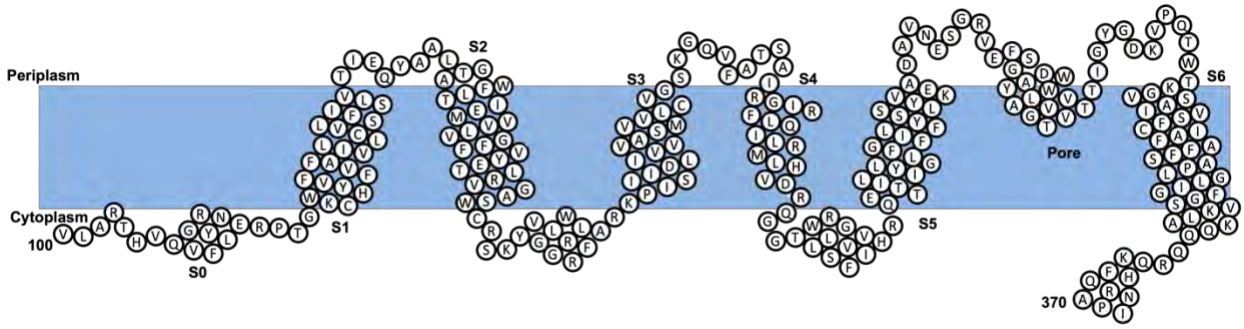

Figure 2.1. Membrane topology diagram of KCNQ1$_{100\text{-}370}$.

In this study, a truncated construct of KCNQ1 containing residues 100-370, shown in **Figure 2.1,** which makes up all six transmembrane helices, was expressed and purified, and was found to form a tetramer while solubilized in a non-denaturing detergent. This is the first time that the full transmembrane region of human KCNQ1 has been expressed and purified using a

bacterial expression vector system, as well as the first time it has been shown to form a tetramer in the absence of the C-terminus.

2.3 Materials and Methods

2.3.1 KCNQ1$_{100-370}$ Expression

The expression vector (pET 21-b) containing His tagged KCNQ1$_{100-370}$ was transformed into BL21 DE3 Codon Plus RP cells. The transformed cells were cultured in Terrific Broth (TB) media containing chloramphenicol and ampicillin and induced at and OD_{600} of ~0.6 with 1 mM IPTG at 25 C overnight.

2.3.2 KCNQ1$_{100-370}$ Purification

The cells were harvested by centrifugation at 5400xg for 10 minutes at 4 C and resuspended in 20x lysis buffer (75 mM Tris base, 300 mM NaCl, 0.2 M EDTA, pH 7.5), LDR stock (0.2 mg/mL lysosyme, 0.02 mg/mL RNAse, 0.02 mg/mL DNAse) phenylmethylsulfonylfluoride (PMSF) (0.2 mg/mL), 2 mM tris(2-carboxyethyl)phosphine (TCEP), and 5 mM $Mg(AC)_2$. The lysis mixture was incubated with agitation for 30 minutes at room temperature then sonicated using the Fisher Scientific Sonic Dismembrator Model 550 with a ¼ inch tip for 6 and a half minutes with a 5 second pulse on/off cycle and 40% amplitude on ice. After lysis Empigen BB detergent was added at 3% v/v to the cell lysate and incubated with agitation overnight at 4 C. The insolubilized membranes were pelleted via centrifugation and the supernatant was incubated with pre-equilibrated Ni(II)-NTA Superflow resin (Qiagen) at 4 C for 30 minutes. The resin supernatant mixture was centrifuged at 1300 xg for 10 minutes to collect the protein bound resin. The supernatant was transferred to a column and rinsed with cold Buffer A (40 mM HEPES, 300 mM NaCl, pH 7.5) with 2mM TCEP and 1% Empigen. The column was washed with Buffer A + 50 mM Imidazole + 2 mM TCEP + 1% Empigen, followed by a detergent exchange of Buffer A + 2mM TCEP + 0.05% w/v DPC. The protein was eluted with Buffer A + 2mM TCEP + 250 mM Imidazole + 0.5% w/v DPC and concentrated in an Amicon filter tube. The final protein concentration was collected via Nanodrop, and purity was confirmed with SDS PAGE gel analysis. The oligomerization was confirmed with SDS PAGE and silver staining.

2.3.3 Immunoblot Verification of Recombinant KCNQ1$_{100\text{-}370}$ Expression

The expressed KCNQ1$_{100\text{-}370}$ protein solubilized in 0.05% DPC was immunoblotted with 6×-His Tag Polyclonal Antibody (Fischer Scientific) followed by Horse radish peroxidase (HRP) as the secondary anti-body (Dabney-Smith lab) to confirm its expression and purity. Different samples corresponding to serial dilutions of purified KCNQ1$_{100–370}$ were run in Blue Native PAGE for 120 min at 100 V then another 120 min at 70 V. The protein was transferred on to nitrocellulose membrane in a fully submerged western blot set up. The transfer ran for 1 h at 100 V at room temperature. The membrane was then blocked in 5 % powdered milk in tris buffered saline with tween 20 (TBST), for 60 min at room temperature. The blocked membrane was treated with anti-His tag antibody (Invitrogen, titer 1:8000) for 60 min at room temperature. The membrane was then washed with TBST twice followed by the addition of the secondary HRP coupled antibody (Kindly provided by the Dr. Dabney-Smith Lab, titer 1:10,000). The blot is then washed with TBST 2 more times before the addition of substrate. The Protein blot was then treated with enhanced chemiluminescence (ECL) substrate (Bio-Rad) and imaged using a BioRad chemiluminescence image system.

2.4 Results and Discussion

KCNQ1$_{100\text{-}370}$ was confirmed to form higher order oligomers according to SDS PAGE and immunoblotting. This is the first time that a construct containing only the transmembrane region of KCNQ1 was observed to oligomerize, including the formation of the native tetramer. Up until this point it has been thought that the C terminus plays a major role in the formation of the tetrameric channel, to the point where the role of other regions has been largely ignored or only briefly mentioned. The data presented here shows that the transmembrane region alone is capable of forming the native tetramer.

KCNQ1$_{100-370}$ was first observed to form higher order oligomers using SDS PAGE and Coomassie Blue stain, but due to the low protein concentration, the higher molecular weight bands were too faint to properly visualize. SDS PAGE is known to disrupt native contacts due to the SDS in the gel and running buffer denaturing the proteins so that they are separated with a high resolution. To increase the intensity of the higher molecular weight bands and encourage any native contacts that may be partially disrupted by SDS, Blue Native PAGE was used instead. Since native contacts are encouraged with Blue Native PAGE, it was also used to determine if the addition of TCEP during purification disrupts aggregation, as TCEP is typically used to prevent aggregation via disulfide bonding. A sample of KCNQ1$_{100-370}$ was prepared without the usual 2mM TCEP and run on the Blue Native Gel for the purpose of determining if the lack of reducing agent would encourage aggregation, specifically at the molecular weights of the higher

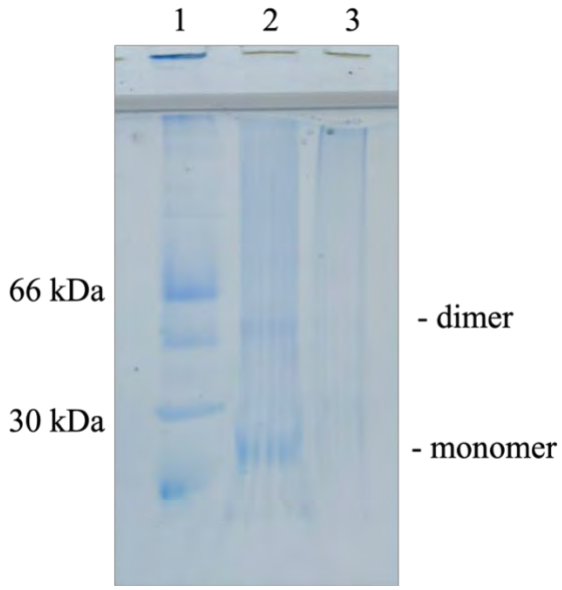

Figure 2.2. A Blue Native PAGE gel of purified KCNQ1$_{100-370}$ under different reducing conditions. Lane 1 is the marker, lane 2 is KCNQ1$_{100-370}$ +TCEP, and lane 3 is KCNQ1$_{100-370}$ -TCEP. The absence of TCEP did not increase the intensity of the higher molecular weight bands, therefore the potential formation of disulfide bonds did not lead to aggregation in the sample, so any higher order bands are true oligomers and not aggregates.

order oligomers. This would provide a clue as to whether the cysteines would form disulfide bonds that would result in oligomerization. As shown in **Figure 2.2** both samples with and

without TCEP have faintly visible bands around the proper molecular weights for the monomer and dimer, but the sample with TCEP is slightly more intense and each lacked a visible tetramer band. There is also no protein left behind in the wells of either sample, so there are no large aggregates under both reducing and non-reducing conditions. While this confirms that higher molecular weight bands are not the result of aggregation, the appearance of the bands could be improved in both resolution and intensity, as the native tetramer was not visible with this technique.

Due to its higher sensitivity silver staining was used with SDS PAGE to improve both the resolution and intensity of the oligomer bands.[19] **Figure 2.3** depicts a silver stained SDS PAGE gel with lanes containing both 1 ug and 2 ug of $KCNQ1_{100\text{-}370}$ with the monomer and tetramer bands appearing at the appropriate molecular weights of ~26 kDa and ~100 kDa respectively. The slight streaking that is visible in the lanes containing KCNQ1 has been attributed to the presence of detergent, as it improved once the concentration of detergent was lowered from 0.5% DPC to 0.05% DPC, which is still above the critical micelle concentration.[20] This gel greatly improved the appearance of the oligomer bands, and to confirm that these bands were the protein of interest, immunoblotting was performed.

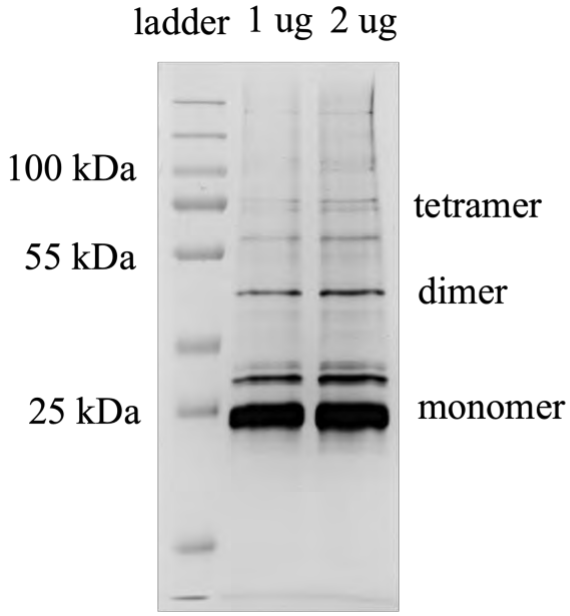

Figure 2.3. Silver stained SDS-PAGE gel of $KCNQ1_{100\text{-}370}$.

For immunoblotting, Blue Native PAGE was used for the final gel as SDS PAGE disrupted the tetramerization too much to be detectable with this technique.[21,22] **Figure 2.4** shows the immunoblot gel with $KCNQ1_{100\text{-}370}$ loaded into five lanes as a serial dilution starting with 0.66 ug and decreasing by a factor of two each time. The monomer and tetramer band are both clearly visible at the molecular weights of ~30 kDa and ~125 kDa respectively, according to the chemiluminescent marker. These molecular weights do differ slightly from the SDS PAGE gel, but this is not unusual as Blue Native PAGE gels have lower resolution. The detergent streaking can also be seen on this gel, but as stated before this was improved by reducing the detergent concentration.[20] The tetramer band also appears warped which is a common phenomenon with Blue Native PAGE gels as they are sensitive to heat, but as this band appears in each lane and decreases in intensity as would be expected from a serial dilution, the warping of the band does not call into question whether it is $KCNQ1_{100\text{-}370,}$ which confirms that the transmembrane region of KCNQ1 is capable of forming the native tetramer without the aid of the C-terminus.

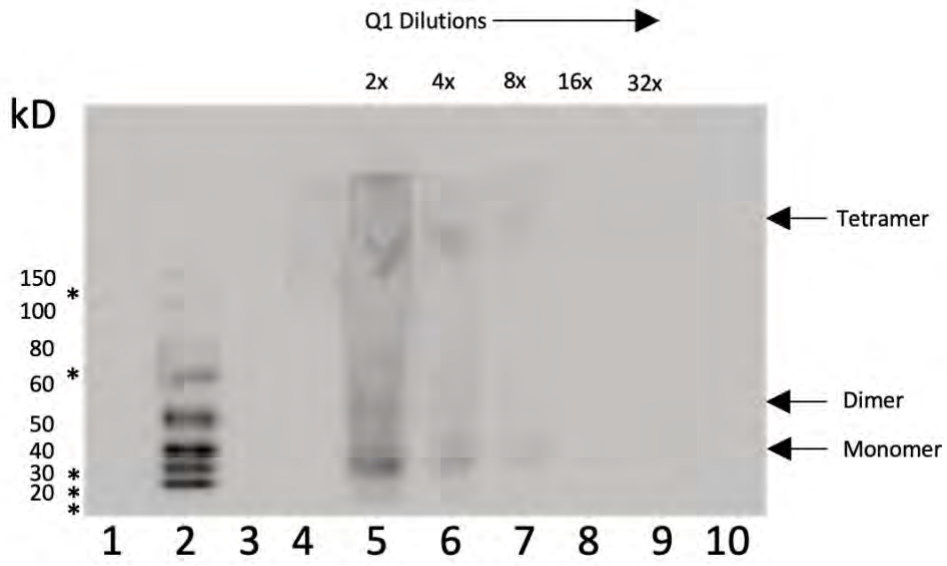

Figure 2.4. Western blot analysis of the purification profile using anti-His tag antibody. The lanes are as follows, 1) empty, 2) prestained Western marker, 3) empty, 4) Native marker (location denoted by *) non-chemiluminescent so did not appear on transfer, 5-9) $KCNQ1_{100\text{-}370}$, 10) empty. The lanes containing Q1 are serial dilutions of a 0.66 mg/mL stock.

2.5 Conclusions

This study showed that the KCNQ1 channel can tetramerize with only the transmembrane domain present. Based on this finding, it can be concluded that while the C-terminus drives the formation of the tetramer, there must be interactions involved between the monomers in the transmembrane region that stabilize the native quaternary structure. Structural studies of this construct could determine what those interactions are and how they allow the tetramer to form.

2.6 Acknowledgements

This work was generously supported by an NIGMS/NIH Maximizing Investigator's Research Award (MIRA) R35 GM126935 grant to G.A.L.

References

(1) Abbott, G. W. Biology of the KCNQ1 Potassium Channel. *New J. Sci.* **2014**, *2014*, 1–26. https://doi.org/10.1155/2014/237431.

(2) MacKinnon, R. Potassium Channels. *FEBS Lett.* **2003**, *555* (1), 62–65. https://doi.org/10.1016/S0014-5793(03)01104-9.

(3) Catterall, W. A. STRUCTURE AND FUNCTION OF VOLTAGE-GATED ION CHANNELS.

(4) Jespersen, T.; Grunnet, M.; Olesen, S.-P. The KCNQ1 Potassium Channel: From Gene to Physiological Function. *Physiology* **2005**, *20* (6), 408–416. https://doi.org/10.1152/physiol.00031.2005.

(5) Gofman, Y.; Shats, S.; Attali, B.; Haliloglu, T.; Ben-Tal, N. How Does KCNE1 Regulate the Kv7.1 Potassium Channel? Model-Structure, Mutations, and Dynamics of the Kv7.1-KCNE1 Complex. *Structure* **2012**, *20* (8), 1343–1352. https://doi.org/10.1016/j.str.2012.05.016.

(6) Kang, C.; Tian, C.; Sönnichsen, F. D.; Smith, J. A.; Meiler, J.; George, A. L.; Vanoye, C. G.; Kim, H. J.; Sanders, C. R. Structure of KCNE1 and Implications for How It Modulates the KCNQ1 Potassium Channel † ‡. *Biochemistry* **2008**, *47* (31), 7999–8006. https://doi.org/10.1021/bi800875q.

(7) Wang, K.-W.; Tai, K.-K.; Goldstein, S. A. N. MinK Residues Line a Potassium Channel Pore. *Neuron* **1996**, *16* (3), 571–577. https://doi.org/10.1016/S0896-6273(00)80076-8.

(8) Xu, Y.; Wang, Y.; Meng, X.-Y.; Zhang, M.; Jiang, M.; Cui, M.; Tseng, G.-N. Building KCNQ1/KCNE1 Channel Models and Probing Their Interactions by Molecular-Dynamics Simulations. *Biophys. J.* **2013**, *105* (11), 2461–2473. https://doi.org/10.1016/j.bpj.2013.09.058.

(9) Kuenze, G.; Vanoye, C. G.; Desai, R. R.; Adusumilli, S.; Brewer, K. R.; Woods, H.; McDonald, E. F.; Sanders, C. R.; George, A. L.; Meiler, J. Allosteric Mechanism for KCNE1 Modulation of KCNQ1 Potassium Channel Activation. *eLife* **2020**, *9*, e57680. https://doi.org/10.7554/eLife.57680.

(10) Maljevic, S.; Wuttke, T. V.; Seebohm, G.; Lerche, H. KV7 Channelopathies. *Pflüg. Arch. - Eur. J. Physiol.* **2010**, *460* (2), 277–288. https://doi.org/10.1007/s00424-010-0831-3.

(11) Tiron, C.; Campuzano, O.; Pérez-Serra, A.; Mademont, I.; Coll, M.; Allegue, C.; Iglesias, A.; Partemi, S.; Striano, P.; Oliva, A.; Brugada, R. Further Evidence of the Association between LQT Syndrome and Epilepsy in a Family with KCNQ1 Pathogenic Variant. *Seizure* **2015**, *25*, 65–67. https://doi.org/10.1016/j.seizure.2015.01.003.

(12) Dworakowska, B.; Do, K. Ion Channels-Related Diseases*. *Ion Channels* **2000**, *47*.

(13) Niemeyer, B. A.; Mery, L.; Zawar, C.; Suckow, A.; Monje, F.; Pardo, L. A.; Stühmer, W.; Flockerzi, V.; Hoth, M. Ion Channels in Health and Disease: 83 rd Boehringer Ingelheim Fonds International Titisee Conference. *EMBO Rep.* **2001**, *2* (7), 568–573. https://doi.org/10.1093/embo-reports/kve145.

(14) Peroz, D.; Rodriguez, N.; Choveau, F.; Baró, I.; Mérot, J.; Loussouarn, G. Kv7.1 (KCNQ1) Properties and Channelopathies: Kv7.1 (KCNQ1) Properties and Channelopathies. *J. Physiol.* **2008**, *586* (7), 1785–1789. https://doi.org/10.1113/jphysiol.2007.148254.

(15) Huang, H.; Kuenze, G.; Smith, J. A.; Taylor, K. C.; Duran, A. M.; Hadziselimovic, A.; Meiler, J.; Vanoye, C. G.; Jr, A. L. G.; Sanders, C. R. Mechanisms of KCNQ1 Channel Dysfunction in Long QT Syndrome Involving Voltage Sensor Domain Mutations. *Sci. Adv.* **2018**, 12.

(16) Smith, J. A.; Vanoye, C. G.; George, A. L.; Meiler, J.; Sanders, C. R. Structural Models for the KCNQ1 Voltage-Gated Potassium Channel. *Biochemistry* **2007**, *46* (49), 14141–14152. https://doi.org/10.1021/bi701597s.

(17) Zaydman, M. A.; Kasimova, M. A.; McFarland, K.; Beller, Z.; Hou, P.; Kinser, H. E.; Liang, H.; Zhang, G.; Shi, J.; Tarek, M.; Cui, J. Domain–Domain Interactions Determine the Gating, Permeation, Pharmacology, and Subunit Modulation of the IKs Ion Channel. *eLife* **2014**, *3*, e03606. https://doi.org/10.7554/eLife.03606.

(18) Wiener, R.; Haitin, Y.; Shamgar, L.; Fernández-Alonso, M. C.; Martos, A.; Chomsky-Hecht, O.; Rivas, G.; Attali, B.; Hirsch, J. A. The KCNQ1 (Kv7.1) COOH Terminus, a

Multitiered Scaffold for Subunit Assembly and Protein Interaction. *J. Biol. Chem.* **2008**, *283* (9), 5815–5830. https://doi.org/10.1074/jbc.M707541200.

(19) Chevallet, M.; Luche, S.; Rabilloud, T. Silver Staining of Proteins in Polyacrylamide Gels. *Nat. Protoc.* **2006**, *1* (4), 1852–1858. https://doi.org/10.1038/nprot.2006.288.

(20) Rath, A.; Glibowicka, M.; Nadeau, V. G.; Chen, G.; Deber, C. M. Detergent Binding Explains Anomalous SDS-PAGE Migration of Membrane Proteins. *Proc. Natl. Acad. Sci.* **2009**, *106* (6), 1760–1765. https://doi.org/10.1073/pnas.0813167106.

(21) Van Coster, R.; Smet, J.; George, E.; De Meirleir, L.; Seneca, S.; Van Hove, J.; Sebire, G.; Verhelst, H.; De Bleecker, J.; Van Vlem, B.; Verloo, P.; Leroy, J. Blue Native Polyacrylamide Gel Electrophoresis: A Powerful Tool in Diagnosis of Oxidative Phosphorylation Defects. *Pediatr. Res.* **2001**, *50* (5), 658–665. https://doi.org/10.1203/00006450-200111000-00020.

(22) Wittig, I.; Schägger, H. Features and Applications of Blue-Native and Clear-Native Electrophoresis. *PROTEOMICS* **2008**, *8* (19), 3974–3990. https://doi.org/10.1002/pmic.200800017.

Chapter 3

Detergent Free Purification of His_{6x}-KCNE1 Using Functionalized SMALPS

Rebecca B. Stowe, Emma A. Gordon, Yazmyne Richardson, Kevin M. Burridge, Muhammed Zeeshan Shah, Lauryn E. Cook, Dominik Konkolewicz, Carole Dabney-Smith, Gary A. Lorigan*

Department of Chemistry and Biochemistry, Miami University, 651 E. High Street, Oxford, OH 45056, USA

Project conceived by DK, GAL, KMG, and RBS. Sample preparation by RBS. Data collection by RBS and EAG. Data analysis by RBS, EAG, DK, MZS, CDS, and DAL. Manuscript written by RBS. Manuscript edited by GAL, CDS, and DK.

3.1 Abstract

Styrene maleic acid copolymer lipid nanoparticles (SMALPs) have gained popularity in recent years due to their ability to purify membrane proteins directly from the native membrane. There are many benefits to studying a protein in its native environment since many proteins rely on the presence of specific lipids to fold and function properly. SMA is not compatible with every membrane protein because it tends to precipitate out of solution under acidic pH conditions and in the presence of divalent cations. In this study, a derivative referred to as SMA-Neut was synthesized at a lower molecular weight than is typical to optimize the efficiency of SMA with the SMALPs. The functionalization of SMA to SMA-Neut allows for the polymer to be used to purify the His_{6x}-KCNE1 protein, which requires Mg^{2+} during cell lysis. The reduction in molecular weight makes SDS-PAGE analysis more easily accessible for confirming the purification of smaller membrane proteins such as His_{6x}-KCNE1.

3.2 Introduction

Membrane proteins play a critical role in many biological processes such as photosynthesis, signal transduction, transport, and more while also making up over a quarter of all encoded proteins.[1,2,3] Despite their biological significance they have been much less thoroughly studied than soluble proteins. One reason for this is the challenge of effectively mimicking the native membrane environment during isolation and purification in the presence of detergents. In many cases, components of the native membrane not only stabilize the protein, but also facilitate the protein's function.[1,4] Therefore, the study of membrane proteins could be greatly improved by the ability to study proteins of interest in their native environments.

Currently, there are a variety of membrane mimetic systems available to choose from such as micelles, liposomes, bicelles, and membrane scaffold protein (MSP) nanodiscs.[2] Each of these mimetics requires the protein to be removed from the native membrane environment using detergent before being reconstituted into the bilayer.[5,6] Likewise, the protein may be characterized while in detergent without reconstitution into a bilayer. While there are many detergents to choose from and each will have their own unique effect on different proteins, it is often the case that a protein is unstable and inactive in a detergent micelle.[7]

When micelles are not sufficient, reconstitution into a bilayer forming mimetic is typically better suited for stabilizing certain proteins. While liposomes, bicelles, and MSP nanodiscs are more like a native membrane environment than a detergent micelle, there are disadvantages. For example, liposomes and MSP nanodiscs are too large for solution NMR structural studies due to slow tumbling times caused by their large size.[5] Additionally, depending on the experiments, the MSP protein can interfere with the signal of the membrane protein to be studied. Bicelles are also known to be less stable than nanodiscs and they only work with a relatively narrow range of lipid and surfactant combinations.[5]

Styrene maleic acid copolymer lipid nanoparticles (SMALPs) are one of the only membrane mimetics capable of forming nanodiscs out of the native lipid bilayer without the use of detergent solubilization.[8,9] SMALPs have been used previously to create nanodiscs from liposomes formed from traditional methods, both with and without protein present.[10,11] SMALPs form through the hydrophobic interaction of the styrene moiety with the acyl chain of the lipids,

allowing the polymer to insert into the hydrophobic core of the membrane and create nanodiscs out of the bilayer **(Figure 3.1)**.[12] The method of forming SMALPs from liposomes has been successful for several proteins, however challenges remain unresolved.[10] The diacids in SMA are sensitive to their environment and can be protonated or bound to divalent cations such as Ca^{2+} and Mg^{2+}, which are common cofactors for membrane proteins.[13] Binding to divalent cations will typically cause the SMA to precipitate rendering them suboptimal for characterization of the solubilized protein. SMA-Neut is a derivative of SMA, forming lipid particles named SMADLPs, that is zwitterionic within the pH range of ~6.4-10.4.[13] It has been found to be less sensitive to pH or divalent ions than the original SMA, as it was not found to precipitate during acid/base titration nor when high concentrations of Mg^{2+} are added.[13] This allows for a wider range of proteins to be solubilized using SMALPS. In this study, we combine the use of a functionalized SMA copolymer known as SMA-Neut with a detergent free purification protocol to show that the membrane protein His_{6x}-KCNE1 can be easily purified directly from the cell membrane into functionalized SMALPs, hereby referred to as styrene maleic acid derivative lipid nanoparticles (SMADLPs). This will allow for His_{6x}-KCNE1 to be studied in a near native environment and will open avenues for other smaller membrane proteins to be studied with this method.

3.3 Methods

3.3.1 SMAn Synthesis

All materials were obtained from commercial suppliers and used as directed. The synthesis of SMAn was carried out from a previously described protocol.[10] Styrene (1.727g, 16.58 mmol), maleic anhydride (809 mg, 8.25 mmol), and 2-

(dodecylthiocarbonothioylthio)propionic acid (325 mg, 0.927 mmol) were combined in a 50 mL round bottom flask and dissolved with 2.9 g dry 1,4-dioxane. 1,1-Azobis(cyclohexanecarbonitrile) (7.9 mg, 0.032 mmol) was added to the mixture and dissolved. A small aliquot of solution was set aside. The flask was capped with a rubber septum and sparged with nitrogen for 15 minutes. The solution was heated to 90 °C and stirred for 24 hours. The conversion was tracked using NMR spectroscopy. Once the conversion reached at least 80% when compared to the aliquot that was previously set aside the polymer was purified from THF

into a large excess of cold hexanes and allowed to dry at ambient temperature. A typical yield from the starting material was ~2.4g of yellow powder. The targeted molecular weight of ~3 kDa was confirmed with Gel Permeation Chromatography (GPC).

3.3.2 Synthesis of 2-1 SMA Neut

In a 10 mL round bottom flask, 400 mg of SMAn was added, containing 2.75 mmol/g anhydride, for a total of 1.1 mmol anhydride. The polymer was dissolved in minimal dry DMF. To the flask, N,N-dimethylethylenediamine (617 mg, 6.9 mmol) was added. The solution was stirred at room temperature for 30 minutes, then purified from THF by precipitating in an excess of cold ether. The ether was decanted and the polymer was freeze dried, yielding 190 mg of off-white powder. Conversion of the anhydride was confirmed with infrared spectroscopy **(Supplementary Figure 3.1)**. The polymer was dissolved in cell lysis buffer (70 mM Tris-HCl, 300 mM NaCl, pH 8.0) at 2.5% w/v for use in protein purification.

3.3.3 His_{6x}-KCNE1 Expression and Purification

The His_{6x}-KCNE1 mutant I2C was overexpressed in BL21 DE3 *E. Coli* cells grown in Terrific Broth (TB) media with 50 ug/mL chloramphenicol and 50 ug/mL ampicillin. The cell cultures were incubated with shaking at 250 rpm and 37 °C until an OD_{600} of 0.6 was reached the cells were induced with 1 mM IPTG (isopropyl-1-thio-D-galactopyranoside). Purification of His_{6x}-KCNE1 protein was carried out using a previously described protocol adapted for SMA.[14] Briefly, the cells were harvested by centrifugation at 10000 xg and the pellet was resuspended in lysis buffer with LDR stock (100 mg/mL lysozyme,10 mg/mL DNAse, 10 mg/mL RNAse), and Tris (2-carboxyethyl) phosphine (TCEP). The mixture was lysed with a Fisherbrand Sonic Dismembrator 505 and ¼" tip for 1 minute total with pulse 5s on, 5s off at 40% amplitude. The lysate was centrifuged at 17000 X *g* to separate the inclusion bodies. The pellet was resuspended and split into two tubes containing Urea-Tris Salt buffer (Urea-TS; 8M Urea, 20 mM Tris-HCl, 150 mM NaCl, pH 8.0) and 2 mM TCEP. One tube contained 2% SDS and the other contained 0.05% SMA-Neut, so that the polymer purification could be directly compared to the original purification protocol. SMA-Neut was also added to the supernatant from this centrifugation step to compare the abundance of purified protein to the inclusion body fraction. The samples were rotated overnight at 4 °C and the insolubilized membranes were removed the next day by

centrifugation at 17000 X *g* for 30 minutes. The supernatants were then incubated with Ni^{2+}-NTA resin overnight. The resin was transferred to a gravity column and rinsed with TS buffer (20 mM Tris-HCl, 150 mM NaCl, pH 8.0) and washed with TS buffer with 50 mM Imidazole. Fractions originally solubilized with SDS were rinsed and washed with buffers containing 0.05% DPC. The pure protein was eluted with TS buffer, 250 mM Imidazole, ±0.5% DPC, and concentrated using a Microcon YM-3 filter (molecular weight cutoff, 3000 Da; Amicon). His_{6x}-KCNE1 protein purity was confirmed with sodium dodecyl sulfate polyacrylamide gel electrophoresis (SDS-PAGE). The presence of nanodiscs was confirmed by transmission electron microscopy (TEM) and dynamic light scattering (DLS).

3.3.4 Transmission Electron Microscopy

All TEM samples were examined on a JEOL JEM-1200EX II TEM instrument. A 2 µL droplet of sample was placed on a Formvar-carbon coated copper grid for about 30 seconds to allow the sample to adsorb onto the surface of the grid. Excess sample was blotted off and the grid was allowed to dry before imaging. All images were taken at 120 keV. Sample preparation and TEM imaging were completed at the Center for Advanced Microscopy and Imaging at Miami University.

3.3.5 Gel Permeation Chromatography (GPC)

GPC was performed using an Agilent 1260 GPC system equipped with an isocratic pump, autosampler, column oven and refractive index detector, using tetrahydrofuran as an eluent at 1 mL/min at 30 °C. The system was calibrated with poly(methyl methacrylate) standards in the molecular weight range of 1010-617,000. All samples were filtered through a 200 nm PTFE filter.

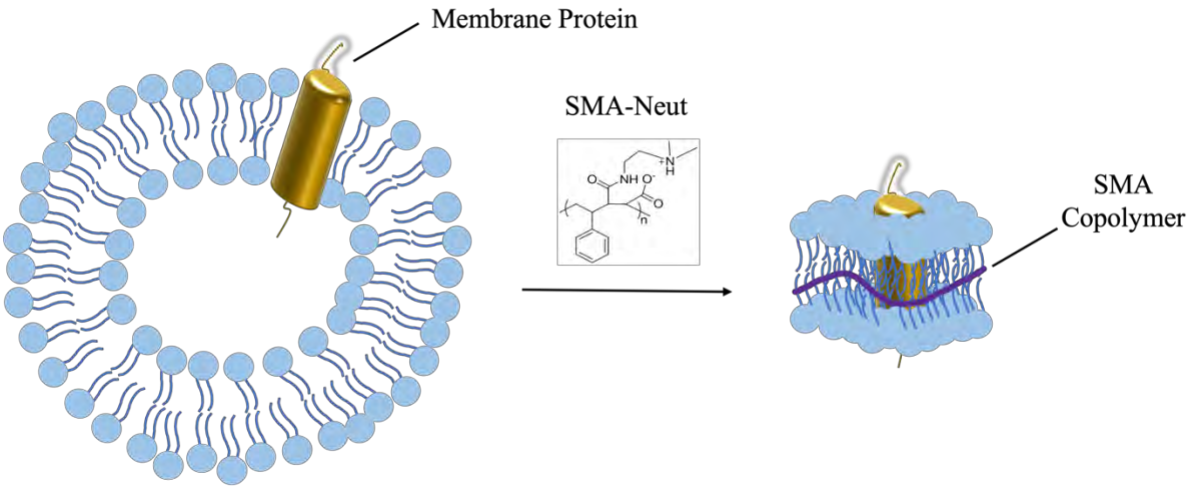

Figure 3.1. Schematic of the formation of SMADLPs from a lipid bilayer upon the addition of SMA-Neut. Polymer shown in black. The His_{6x}-KCNE1 protein begins solubilized in the native membrane before the addition of SMA-Neut. Upon addition of SMA-Neut the protein and surrounding lipids are encased in SMADLPs.

3.4 Results and Discussion

3.4.1 Tuning the Molecular Weight of SMA-Neut

SMA copolymers are traditionally synthesized with a target molecular weight of approximately 10 kDa. This is acceptable for larger proteins, but when purifying smaller proteins of 15 kDa or less there is the risk of the SMA obscuring the protein band on SDS-PAGE, which ideally should not occur if the excess polymer is successfully removed during purification. SMA polymers are charged, so they will migrate in an electrophoretic field, and they are susceptible to stain. Therefore, the size of the polymer compared to the size of the protein must be accounted for. Because His_{6x}-KCNE1 has a molecular weight of 15.7 kDa, a polymer with a lower molecular weight was synthesized. The GPC data showed that the synthesized SMA polymer had a number averaged molecular weight (M_n) of 3600 with a dispersity (M_w/M_n) of 1.4 **(Figure**

3.2). The dispersity of the polymer achieved by this method indicates a relatively uniform polymer, since values closer to 1 meaning a more homogenous size distribution, and values closer to 2 indicate a relatively poorly controlled polymer typical of conventional radical polymerization.[15] This will decrease streaking on SDS-PAGE compared to the commercial polymer made by conventional radical polymerization that typically has a dispersity >2. Synthesis of shorter SMA copolymers with low dispersity will allow for detergent free purification to be used with smaller membrane proteins without having to sacrifice the ability to use traditional purification verification methods such as PAGE analysis. This synthesis also allows the functionalized polymer to be used with a wider variety of systems. In addition to the accommodation of smaller membranes proteins due to the shorter length, the functionalization of the polymer reduces sensitivity towards divalent cations and allows use over a wider pH range.

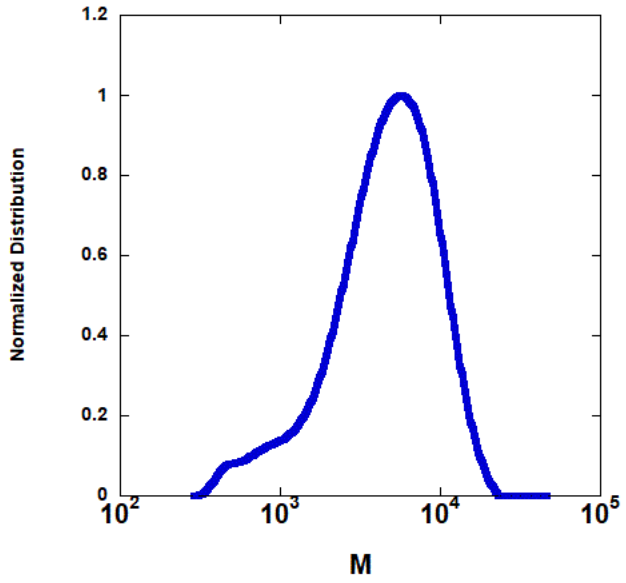

Figure 3.2. GPC trace of SMA-Neut. Maximum intensity was normalized to 1. The peak is centered around 3600 kDa, which is our target molecular weight.

3.4.2 Purification of His_{6x}-KCNE1 Monitored via Dynamic Light Scattering (DLS) and Transmission Electron Microscopy (TEM)

TEM and DLS were used to confirm the formation of nanodiscs after the purification process. DLS data of intact cells and purified SMADLPS were collected to compare the overall sizes of the particles in solution **(Figure 3.3)**. The DLS data were represented as particle size vs volume (%), which shows the percentage of the total volume that is occupied by particles of the indicated size. The SMADLPs were found to be in the range of 40 nm in diameter, with intact *E. coli* cells at 1 μm. The reduction in size observed from intact cells to purified SMADLPs as well as the homogeneity of the SMADLPs particle size is consistent with formation of SMADLPs. This was further confirmed by TEM images taken at each step in the purification process **(Figure 3.4)**. The SMADLPs were not clearly visible on the TEM grid until after purification with Ni-NTA affinity chromatography. This is expected due to cellular debris produced by lysis

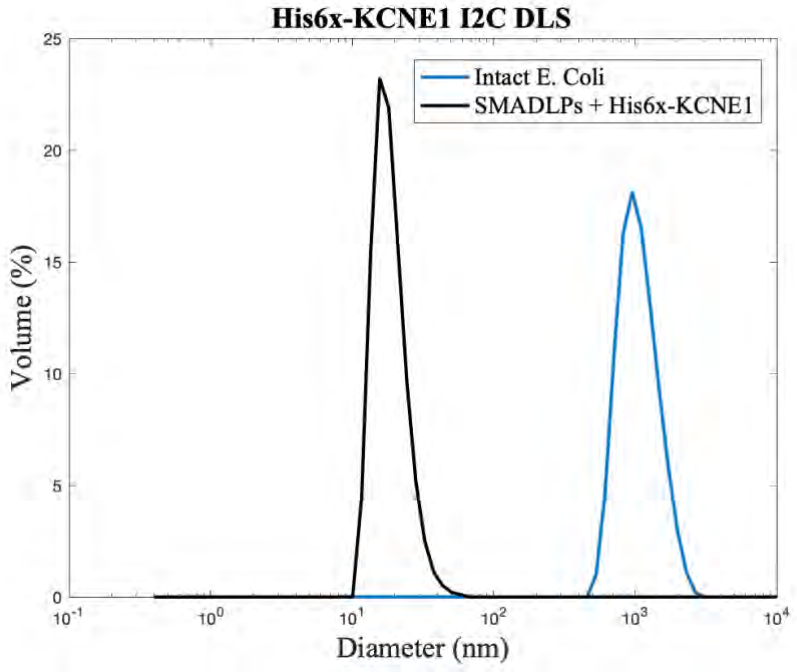

Figure 3.3. DLS curves of intact E. Coli cells and purified SMADLPs containing His_{6x}-KCNE1. The intact cells are significantly larger than the cell lysate or SMADLPs at around 1000 nm in diameter. The SMADLPs used to collect DLS data were purified from the same intact cells shown here.

and protein aggregates that would be present before purification and obscuring the view of smaller particles like SMADLPs. The column wash and the purified SMADLPs both showed particles of the appropriate size and shape for nanodisc formation that was also consistent with the DLS data. It is to be expected that the column wash would also have SMADLPs in it since the SMA-Neut copolymer forms SMADLPs in the presence of any lipid bilayer regardless of the presence of protein.

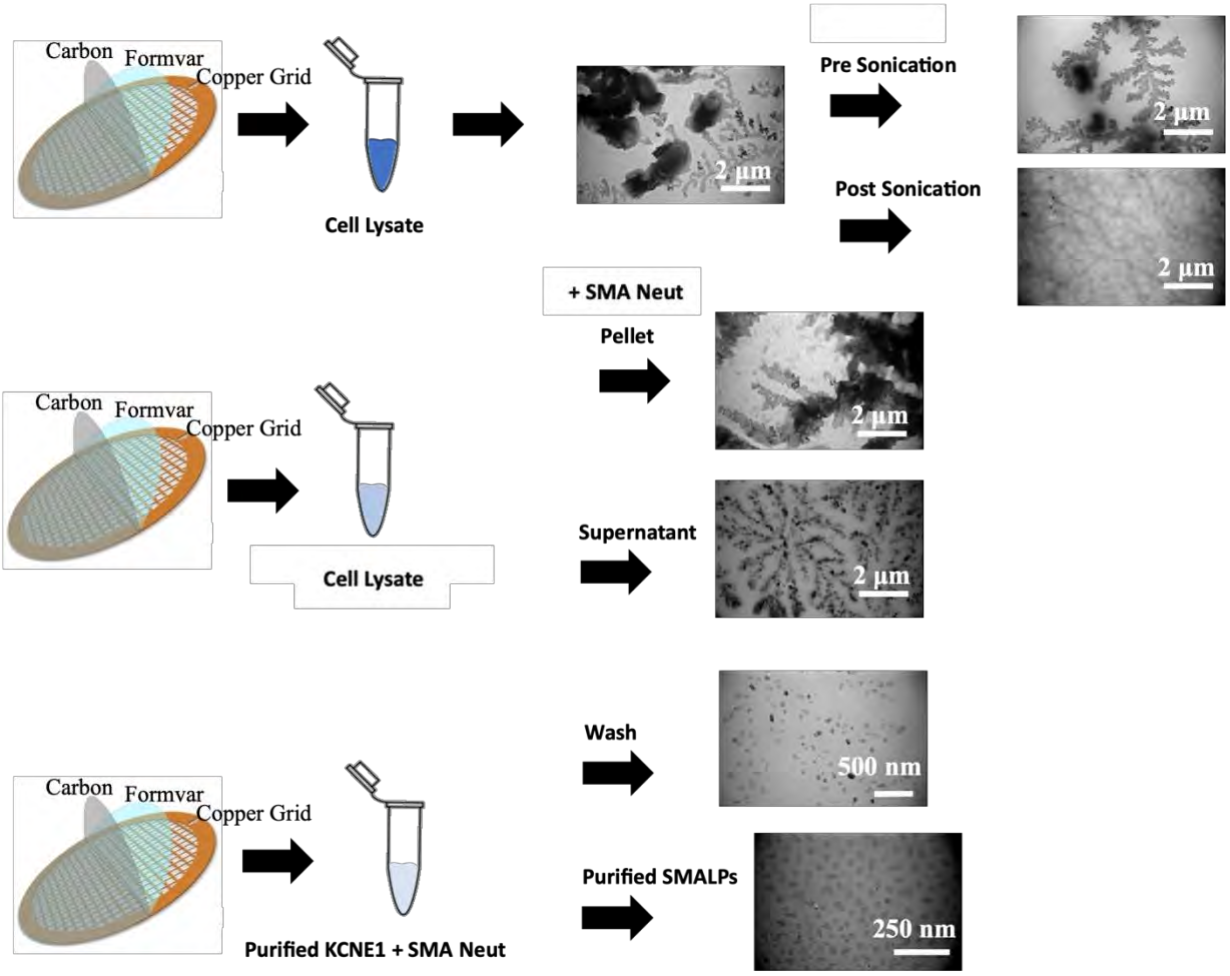

Figure 3.4. TEM images of each step in the purification process. The difference in size between the lysed cell material and the SMADLPs can be seen clearly due to the differences between the scale bars.

3.4.3 SDS PAGE Confirms Detergent Free Purification of His_{6x}-KCNE1

. In addition to investigating the ability of the polymer to solubilize inclusion bodies, we tested to see how much soluble protein in the supernatant could be incorporated into nanodiscs. To confirm the presence and purity of our protein of interest, silver stained SDS PAGE was used. A band that was not present in the lanes containing SMA-Neut or lipid was observed just above

the 15 kDa marker in the lanes where His_{6x}-KCNE1 was purified with detergent and from inclusion bodies with SMA-Neut **(Figure 3.5)**. This agrees with the 15.7 kDa molecular weight of His_{6x}-KCNE1 Testing each fraction for incorporation of protein into nanodiscs would give us an idea of how efficient generation of KCNE1-His nanodiscs would be from crude cell lysate.The overexpression involves formation of inclusion bodies, so we initially added the SMA-Neut after inclusion body purification to confirm that the purified protein was coming from the inclusion bodies and not the supernatant, because the supernatant would likely have a much lower abundance of protein and therefore would not yield enough to be useful for further studies. The supernatant + SMA-Neut fraction contains some bands visible at higher molecular weights (**Figure 3.5, lane 7)**, the monomer band at ~15 kDa is not visible, and the bands are much fainter than in lane 6, which contains the protein purified from the inclusion body pellet. The smear characteristic of excess polymer is also not observed in lanes 6 or 7, indicating that the column washing and subsequent concentration by filtration successfully removed the excess polymer from the purified protein samples. His_{6x}-KCNE1 was also purified using sodium dodecyl sulfate (SDS) and dodecylphosphorylcholine (DPC), to compare the yield of protein purified with SMA-Neut to a previously established protocol.[16] It was found that the SMA-Neut purification protocol produces slightly less protein, but with a similar level of purity, thus confirming that SMA-Neut can purify His_{6x}-KCNE1 from inclusion bodies without the use of detergents suggesting this method could be adapted to suit other membrane proteins that are typically overexpressed in inclusion bodies, further broadening the applications of SMA copolymers.

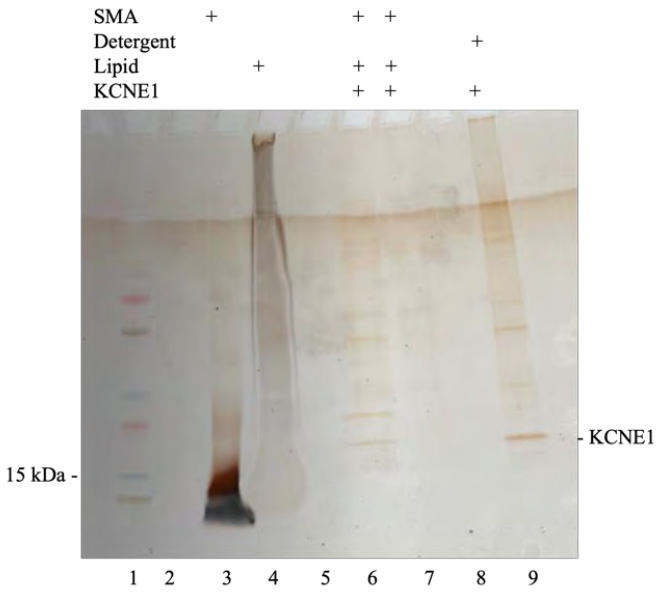

Figure 3.5. Silver stained SDS PAGE gel of purified His_{6x}-KCNE1 in SMADLPs of SMA-Neut. Lanes are as follows (1) ladder, (2) blank, (3) SMA-Neut, (4) lipid, (5) blank, (6) His_{6x}-KCNE1 + SMA-Neut from inlusion body pellet, (7) His_{6x}-KCNE1 + SMA-Neut from supernatant, (8) blank, (9) His_{6x}-KCNE1 purified with detergent.

3.5 Conclusions

SMA derivative polymers are a powerful tool for detergent free purification of membrane proteins that have allowed some of the hurdles associated with SMA such as pH and divalent cation sensitivity have been overcome. SMA-Neut was used to purify membrane proteins that require divalent cations directly from the cell membrane. The versatility of the SMA derivatives has also been expanded with this method by demonstrating that it can also be used to purify proteins overexpressed in inclusion bodies. Compatibility with SDS PAGE is an advantage to this method as it is a common and accessible method for confirming protein purity. In further studies this method can be improved by scaling up the synthesis for proteins that do not express as highly as His_{6x}-KCNE1 or for purifying larger quantities of proteins for techniques that require milligram quantities of protein. This method could also be adapted for use with other

SMA derivatives for membrane proteins that are not compatible with traditional SMA or SMA-Neut. Overall, the use of SMA derivatives will further expand the capabilities of SMA to solubilize membrane proteins in a near native environment.

3.6 Acknowledgements

GAL acknowledges generous supported by a NIGMS/NIH Maximizing Investigator's Research Award (MIRA) R35 GM126935 for membrane protein and lipid biochemistry. DK acknowledges support from NIGMS/NIH under award number R15GM144907 for polymer chemistry.

References

(1) Hunte, C.; Richers, S. Lipids and Membrane Protein Structures. *Curr. Opin. Struct. Biol.* **2008**, *18* (4), 406–411. https://doi.org/10.1016/j.sbi.2008.03.008.

(2) Majeed, S.; Ahmad, A. B.; Sehar, U.; Georgieva, E. R. Lipid Membrane Mimetics in Functional and Structural Studies of Integral Membrane Proteins. *Membranes* **2021**, *11* (9), 685. https://doi.org/10.3390/membranes11090685.

(3) Thoma, J.; Burmann, B. M. Fake It 'Till You Make It—The Pursuit of Suitable Membrane Mimetics for Membrane Protein Biophysics. *Int. J. Mol. Sci.* **2020**, *22* (1), 50. https://doi.org/10.3390/ijms22010050.

(4) Royal, A. A.; Tinker, A.; Harmer, S. C. Phosphatidylinositol-4,5-Bisphosphate Is Required for KCNQ1/KCNE1 Channel Function but Not Anterograde Trafficking. *PLOS ONE* **2017**, *12* (10), e0186293. https://doi.org/10.1371/journal.pone.0186293.

(5) Morrison, E. A.; Henzler-Wildman, K. A. Reconstitution of Integral Membrane Proteins into Isotropic Bicelles with Improved Sample Stability and Expanded Lipid Composition Profile. *Biochim. Biophys. Acta BBA - Biomembr.* **2012**, *1818* (3), 814–820. https://doi.org/10.1016/j.bbamem.2011.12.020.

(6) Shen, H.-H.; Lithgow, T.; Martin, L. Reconstitution of Membrane Proteins into Model Membranes: Seeking Better Ways to Retain Protein Activities. *Int. J. Mol. Sci.* **2013**, *14* (1), 1589–1607. https://doi.org/10.3390/ijms14011589.

(7) Seddon, A. M.; Curnow, P.; Booth, P. J. Membrane Proteins, Lipids and Detergents: Not Just a Soap Opera. *Biochim. Biophys. Acta BBA - Biomembr.* **2004**, *1666* (1–2), 105–117. https://doi.org/10.1016/j.bbamem.2004.04.011.

(8) Günsel, U.; Hagn, F. Lipid Nanodiscs for High-Resolution NMR Studies of Membrane Proteins. *Chem. Rev.* **2022**, *122* (10), 9395–9421. https://doi.org/10.1021/acs.chemrev.1c00702.

(9) Lee, S. C.; Knowles, T. J.; Postis, V. L. G.; Jamshad, M.; Parslow, R. A.; Lin, Y.; Goldman, A.; Sridhar, P.; Overduin, M.; Muench, S. P.; Dafforn, T. R. A Method for Detergent-

Free Isolation of Membrane Proteins in Their Local Lipid Environment. *Nat. Protoc.* **2016**, *11* (7), 1149–1162. https://doi.org/10.1038/nprot.2016.070.

(10) Craig, A. F.; Clark, E. E.; Sahu, I. D.; Zhang, R.; Frantz, N. D.; Al-Abdul-Wahid, M. S.; Dabney-Smith, C.; Konkolewicz, D.; Lorigan, G. A. Tuning the Size of Styrene-Maleic Acid Copolymer-Lipid Nanoparticles (SMALPs) Using RAFT Polymerization for Biophysical Studies. *Biochim. Biophys. Acta BBA - Biomembr.* **2016**, *1858* (11), 2931–2939. https://doi.org/10.1016/j.bbamem.2016.08.004.

(11) Vargas, C.; Arenas, R. C.; Frotscher, E.; Keller, S. Nanoparticle Self-Assembly in Mixtures of Phospholipids with Styrene/Maleic Acid Copolymers or Fluorinated Surfactants. *Nanoscale* **2015**, *7* (48), 20685–20696. https://doi.org/10.1039/C5NR06353A.

(12) Xue, M.; Cheng, L.; Faustino, I.; Guo, W.; Marrink, S. J. Molecular Mechanism of Lipid Nanodisk Formation by Styrene-Maleic Acid Copolymers. *Biophys. J.* **2018**, *115* (3), 494–502. https://doi.org/10.1016/j.bpj.2018.06.018.

(13) Burridge, K. M.; Harding, B. D.; Sahu, I. D.; Kearns, M. M.; Stowe, R. B.; Dolan, M. T.; Edelmann, R. E.; Dabney-Smith, C.; Page, R. C.; Konkolewicz, D.; Lorigan, G. A. Simple Derivatization of RAFT-Synthesized Styrene–Maleic Anhydride Copolymers for Lipid Disk Formulations. *Biomacromolecules* **2020**, *21* (3), 1274–1284. https://doi.org/10.1021/acs.biomac.0c00041.

(14) Tian, C.; Vanoye, C. G.; Kang, C.; Welch, R. C.; Kim, H. J.; George, A. L.; Sanders, C. R. Preparation, Functional Characterization, and NMR Studies of Human KCNE1, a Voltage-Gated Potassium Channel Accessory Subunit Associated with Deafness and Long QT Syndrome †, ‡. *Biochemistry* **2007**, *46* (41), 11459–11472. https://doi.org/10.1021/bi700705j.

(15) O'Shaughnessy, B.; Yu, J. Autoacceleration in Free Radical Polymerization. *Phys. Rev. Lett.* **1994**, *73* (12), 1723–1726. https://doi.org/10.1103/PhysRevLett.73.1723.

(16) Sahu, I. D.; Craig, A. F.; Dunagan, M. M.; Troxel, K. R.; Zhang, R.; Meiberg, A. G.; Harmon, C. N.; McCarrick, R. M.; Kroncke, B. M.; Sanders, C. R.; Lorigan, G. A. Probing Structural Dynamics and Topology of the KCNE1 Membrane Protein in Lipid Bilayers via Site-

Directed Spin Labeling and Electron Paramagnetic Resonance Spectroscopy. *Biochemistry* **2015**, *54* (41), 6402–6412. https://doi.org/10.1021/acs.biochem.5b00505.

Supplementary Figures

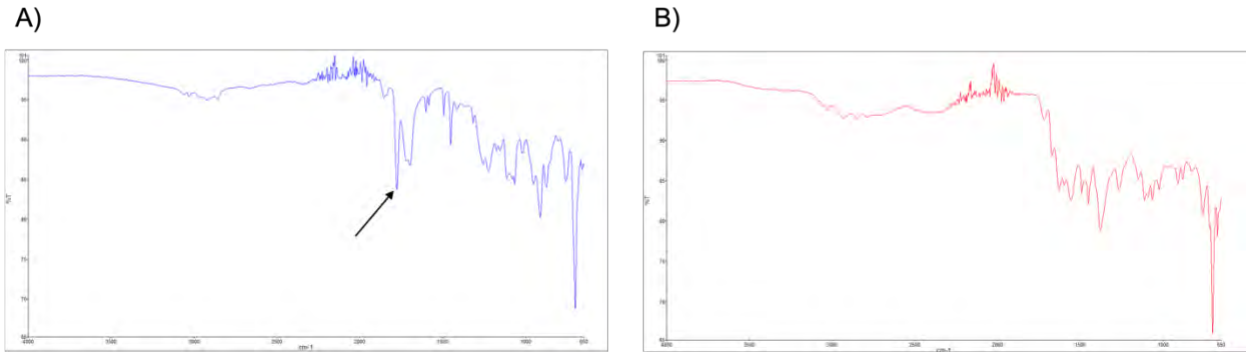

Supplementary Figure 3.1: IR spectra of SMAn (A), and SMA-Neut (B), showing successful functionalization of the polymer. The arrow in panel A indicates the peak at ~1800 cm^{-1} that is not present in panel B, indicating that the maleic acid ring has been opened and the functionalization was successful.

Chapter 4

Dynamic Protein-Protein Interactions of KCNQ1 and KCNE1 Measured by EPR Line Shape Analysis

Rebecca B. Stowe[1], Alison M. Bates[1], Lauryn E. Cook[1], Gunjan Dixit[4], Indra D. Sahu[2], Charles R. Sanders[3], Carole Dabney-Smith[1], Gary A. Lorigan[1]

[1]Department of Chemistry and Biochemistry, Miami University, 651 E. High Street, Oxford, Ohio 45056, USA.

[2]Division of Natural Sciences, Campbellsville University, Campbellsville, Kentucky 42718, USA.

[3]Department of Biochemistry and Center for Structural Biology, Vanderbilt University, Nashville, Tennessee 37240, USA.

[4]Cell, Molecular and Structural Biology Program, Department of Chemistry & Biochemistry, Miami University, Oxford, OH 45056, USA.

Project conceived by GAL, CRS, GD, and RBS. Sample preparation and data collection by RBS, AMB, and LEC. Data analysis by RBS and CDS. Manuscript written by RBS. Manuscript edited by RBS, GAL, and CDS.

4.1 Abstract

KCNQ1, also known as Kv7.1, is a voltage gated potassium channel that associates with the KCNE protein family. Mutations in this protein has been found to cause a variety of diseases including Long QT syndrome, a type of cardiac arrythmia where the QT interval observed on an electrocardiogram is longer than normal. This condition is often aggravated during strenuous exercise and can cause fainting spells or sudden death. KCNE1 is an ancillary protein that interacts with KCNQ1 in the membrane at varying molar ratios. This interaction allows for the flow of potassium ions to be modulated to facilitate repolarization of the heart. The interaction between these two proteins has been studied previously with methods such as cysteine crosslinking. Electron paramagnetic resonance (EPR) spectroscopy line shape analysis in tandem with site directed spin labeling (SDSL) was used to observe changes in spin label mobility as KCNE1 interacts with KCNQ1. KCNE1 was labeled at different sites that were found to interact with KCNQ1 based on previous literature, along with sites outside of that range as a control. Once labeled KCNE1 was incorporated into 3:1 PC:PG vesicles, KCNQ1 (helices S1-S6) was titrated into the vesicles. The line shape differences observed upon addition of KCNQ1 are indicative of an interaction between the two proteins.

4.2 Introduction

The KCNQ1 ($K_V7.1$) channel is a member of the voltage gated potassium (K_V) channel family and it is responsible for regulating the passage of potassium across the lipid bilayer in many areas of the body including the heart, ear, lung, and intestines.[1–4] In cardiac myocytes KCNQ1 associates with its ancillary protein KCNE1 (MinK), forming the slow delayed rectifier (I_{KS}) channel, which causes an increase in current amplitude and slowing down of activation kinetics of the channel.[5–8] Mutations in either of these proteins protein leads to a variety of pathologies including Long QT Syndrome, deafness, and diabetes.[9–14]

KCNQ1 has the standard topology of K_V channels, six transmembrane helices flanked by a cytoplasmic N-terminal and C-terminal region.[15–18] The functional KCNQ1 channel is a domain swapped tetramer in the membrane with each monomer containing two distinct domains, the voltage sensing domain (VSD) made up of helices S1-S4, and the pore domain (PD) made up of helices S5-S6.[19–22] In cardiac myocytes, KCNE1 binds in a cleft between two KCNQ1 VSDs and one PD, in a position that allows it to modulate S4 and the gating of the channel.[5,23,24] The stoichiometry of the channel complex has not been found to conform to a strict molar ratio of KCNE1:KCNQ1, and has been found to function with any ratio between 1:4 and 1:1.[25,26]

In this study, the dynamics of the interactions between KCNQ1 and KCNE1 was investigated using site directed spin labeling (SDSL) and continuous wave electron paramagnetic resonance (CW-EPR) spectroscopy line shape analysis. A selection of KCNE1 cysteine mutations were chosen based on previous cross linking, functional studies, and molecular modeling.[5,23,27,28] These KCNE1 mutants were spin labeled and reconstituted into vesicles both in the absence and presence of KCNQ1 to determine the effect of the protein-protein interaction on the dynamics of each residue. The results presented in this study provide site-specific patterns for the dynamics of KCNE1 when it associates with KCNQ1 in its native environment.

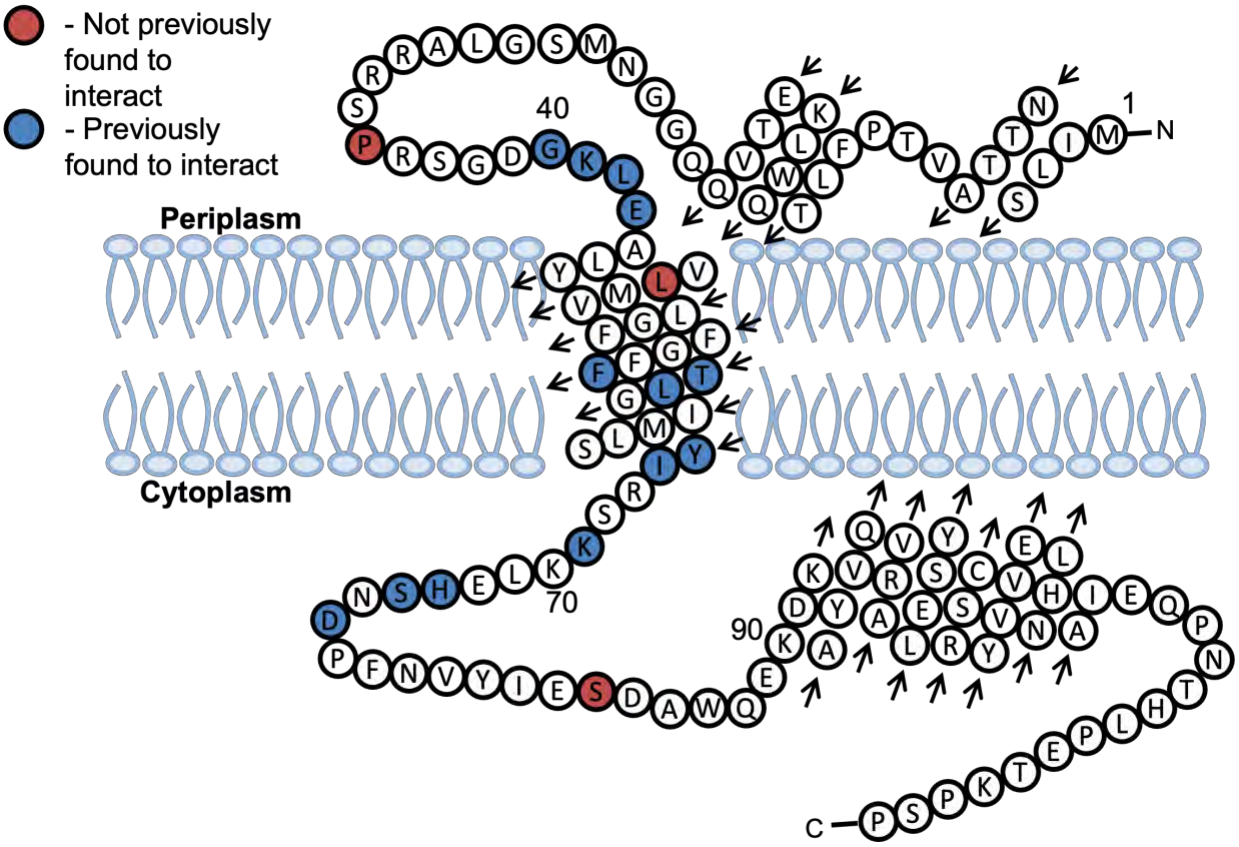

Figure 4.1. A membrane topology diagram of KCNE1. Residues chosen for EPR spectroscopic measurements are color coded according to whether they have previously been found to interact through other methods.

4.3 Methods

4.3.1 KCNE1 Overexpression and Purification

The KCNE1 mutants were overexpressed in BL21 DE3 *E. Coli* cells grown in LB minimal media with 50 ug/mL ampicillin. The cell cultures were incubated at 250 rpm and 37 ºC until an OD_{600} of 0.6 was reached the cells were induced with 1 mM IPTG (isopropyl-1-thio-D-galactopyranoside). Purification of KCNE1 protein was carried out using a previously described protocol.[12] The pure protein was eluted in 0.5% DPC (Dodecylphosphocholine) detergent and concentrated using a Microcon YM-3 (molecular weight cutoff, 3000 Da) filter (Amicon). The protein concentration was determined from A_{280} using a molecular extinction coefficient of

19940 M^{-1} cm^{-1} on a Nanodrop 200c (Thermo Scientific). Protein purity was confirmed with sodium dodecyl sulfate polyacrylamide gel electrophoresis (SDS-PAGE).

4.3.2 KCNQ1 Overexpression and Purification

KCNQ1 was overexpressed with plasmid pET-21b in BL21 DE3 Codon Plus RP cells grown in TB minimal media with 50 ug/mL chloramphenicol and 100 ug/mL ampicillin. The cell cultures were incubated at 250 rpm and 37C until an OD_{600} of 0.6 was reached and the cells were induced with 1mM IPTG. The incubation temperature was then changed to 25 C and left to incubate for 12-18 hours overnight. Purification of KCNQ1 protein was carried out using a previously described protocol.[29] The pure protein was eluted in 0.5 % DPC and concentrated using a Microcon YM-3 (molecular weight cutoff, 10 kDa) filter (Amicon). The protein concentration was determined from A_{280} using a molecular extinction coefficient of 58900 M^{-} cm^{-} on a Nanodrop 200c (Thermo Scientific). Protein purity was determined with SDS-PAGE.

4.3.3 KCNE1 Spin Labeling

The protein sample was reduced with 2.5 mM DTT, with gentle agitation at room temperature for 24 h. The MTSL spin label was added in 10x molar excess to KCNE1 solution, incubated at room temperature 30 min, followed by agitation at 37 C for 3h then agitation at room temperature for the remainder of 24 h. The sample was then buffer exchanged into 50 mM phosphate, 0.05% DPC, pH 7.0. After buffer exchange, samples were bound to NiNTA resin in a gravity column which was washed with 300 mL 50 mM phosphate, 0.05% DPC, pH 7.0 to remove excess spin label. Spin labeled KCNE1 was eluted in 50 mM phosphate, 250 mM Imidazole, 0.5% DPC, pH 7.0.

4.3.4 Reconstitution into Liposomes

Liposomes were prepared using the thin film method. POPC and POPG were measured out to a 3:1 molar ratio with a final concentration of 100 mM. The powder lipid was dissolved in minimal chloroform then the chloroform was evaporated off with nitrogen. The flask was rotated during evaporation to form a thin film of lipids on the surface of the flask. The lipids were desiccated overnight to ensure complete removal of solvent. The lipids were solubilized in 50

mM phosphate buffer pH 7.0 and subjected to freeze-thaw with sonication for three cycles to form liposomes.

The concentrated spin labeled KCNE1 protein was mixed with the liposomes to a 1:400 protein to lipid molar ratio. The sample underwent three freeze thaw cycles to ensure incorporation of the protein into the liposome. The sample then underwent dialysis for 48 h in 4 L of dialysis buffer (10 mM Imidazole and 0.1 mM EDTA at pH 7.0) with buffer changed twice daily. The completion of detergent removal was determined when the KCNE1-liposome sample became turbid and viscous when compared to pre-dialysis. This was further confirmed by CW-EPR line shape broadening.

For liposomes that include KCNQ1, the overall protein to lipid ratio of 1:400 and the final KCNE1 concentration were kept constant with the liposomes containing only KCNE1. Purified KCNQ1 was mixed with KCNE1 at a 2:1 and 4:1 E1:Q1 molar ratio. After addition of lipids theses samples underwent the same treatment as the liposomes with KCNE1.

4.3.5 Crosslinking

Crosslinking was performed with AMAS (4.4 Å). The linker was dissolved to a 10 mM stock in DMSO. The crosslinker was incubated with KCNQ1 at a 10x molar excess for 30 minutes at room temperature. Excess linker was removed from solution by spin filtration. KCNQ1 was mixed with each KCNE1 mutant to achieve a 4:1 KCNE1:KCNQ1 molar ratio and incubated at room temperature for 30 minutes. SDS PAGE gel analysis was used to confirm crosslinking.

4.4 Results and Discussion

4.4.1 CW-EPR Line Shape Analysis Reveals a Dynamic Interaction Between KCNE1 and KCNQ1$_{100\text{-}370}$

Each KCNE1 mutation was chosen based on potential interaction sites or areas of close proximity found in previous literature.[23,27,28] As a control, sites that have not been found to previously interact or come in close proximity were used, with the exception of the transmembrane region, as all residues can be assumed to be in close proximity. F57, T58, and

L59 are known to have functional importance, while others were found to interact based on previous crosslinking experiments or modeling studies.[6,24,27,28] CW EPR spectra were collected for each sample in replicate to ensure that any observed line shape changes were reproducible.

For the outer membrane flanking region of KCNE1, prior studies indicated that residues 40-43 could interact with KCNQ1 and they were studied here as well. KCNE1-P35 selected as a control as it has been shown not to interact with KCNQ1 previously.[23,27] Overall, the trends observed in this region were that the spin label mobility increased, which can mainly be seen in the low field line (Figure 2). Spectra from spin label at positions G40C, L42C, and E43C showed more dramatic changes than K41C, with residues 40-43 all showing some increase in the fast motion component. Residue E43 was previously shown to strongly interact with the S3-S4 linker of Q1.[27] As can be seen in the CW spectra, comparing residues 40-43 to the control P35C, there is a marked decrease in the rigid component in the low field line, with the majority of the spin population shifting to the fast motion component (Figure 2). Typically, it is expected that upon interaction with another large mass like a protein or a membrane, that the mobility of the spin label would decrease due to new obstacles surrounding the spin label, but these spectral features have been observed before in the interactions of exoenzyme U (ExoU) with its cofactors.[30] It is also worth noting that upon interaction with another protein, the area around the spin label could undergo a conformational change or change in dynamics. Therefore, the spectral features observed for residues G40C, L42C, and E43C would be consistent with some type of conformational change occurring in this region upon association with Q1. This region is unstructured so movement occurring in this region would lead to narrower linewidths. Residues 40-42 were previously found to be in close proximity to Q1 according to distance constraints from *in vivo* crosslinking.[27] Since they follow the same spectral patterns overall as residue E43C, these CW spectra support proposed conformational changes driven by the interactions between 43 and Q1's S3-S4 linker. A potential explanation for why residue K41C does not appear to interact with Q1 could be that the mutation is simply not favorable for allowing interactions between Q1 and E1, as cysteine is not charged and smaller than lysine. There are four Q1 residues (T144C, I145C, Q147C, V324C) that favorably form disulfide crosslinks with K41C *in vivo,* with I145C favoring the open state of the channel and the other three favoring the closed state of the channel.[23,24,27] Using that technique, both E1 and Q1 have cysteine mutations

introduced at those residues. It is possible that when E1 is mutated at position K41 this interaction cannot be visualized via CW EPR.

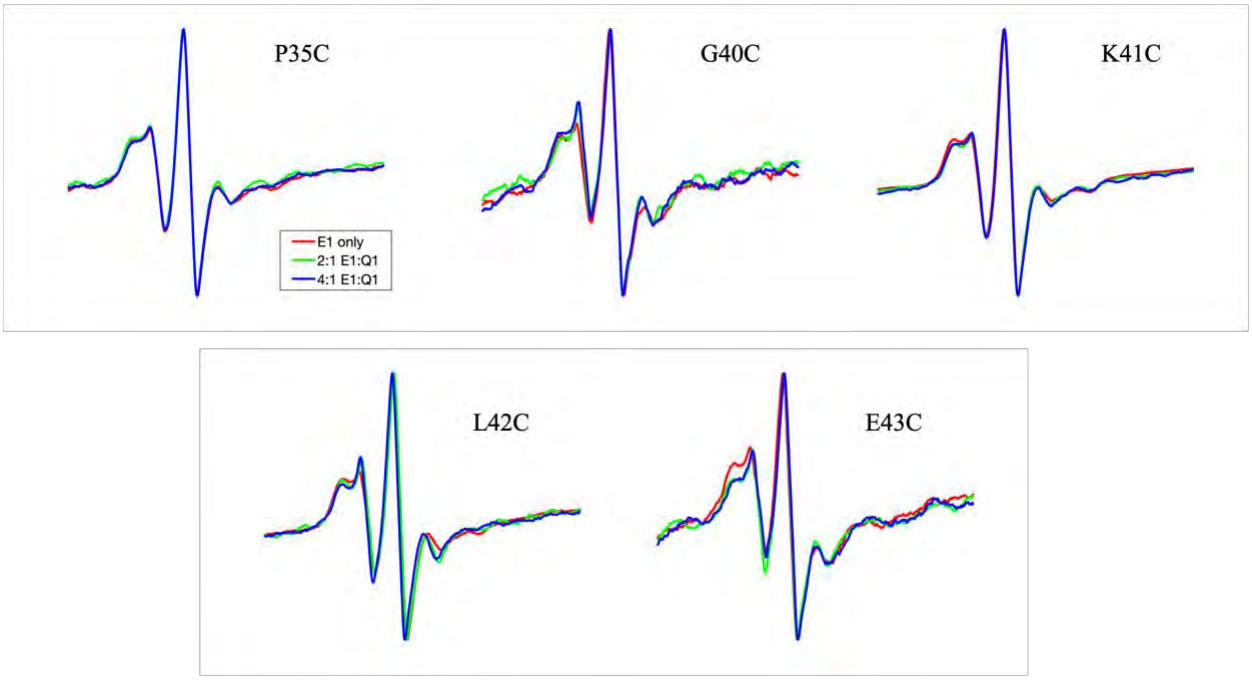

Figure 4.2. CW EPR traces of the N-terminal KCNE1 mutations. For each spectrum, red is KCNE1 alone, green is 2:1 E1:Q1, and blue is 4:1 E1:Q1.

The transmembrane region of KCNE1 contains residues 57-59, which are crucial to Kv7.1 channel function, as it is crucial for the slow activation of the I_{KS} channels.[1,3,7,12,23] When F57, T58, and L59 residues are swapped out with KCNE3 (E3) equivalents, the channel behaves as if it is bound to E3 instead of E1, adopting a constitutively open state.[12] Therefore, it is unlikely that Q1 would be able to interact with E1 properly when residues F57, T58, and L59 are mutated. This is supported by the dramatic increase in the fast motion component of the low field line for all three residues (Figure 3). Since these residues are in the membrane, it would be expected that interaction with a partner protein would lead to further restriction of the mobility of the spin label, or at least a similar spectrum with subtle broadening. For a control in this region L48C was chosen as it has been found to be in proximity to KCNQ1.[23] CW EPR spectra of L48C showed some broadening when KCNQ1 was incorporated into vesicles, which is consistent with

motional restriction imposed on the spin label as the transmembrane region of KCNE1 resides in a cleft between the S1 and S6 of Q1.

Residues Y65, I66, and K69 were chosen based on a computational study that found those residues to make close contact with KCNQ1.[23] Overall, the CW EPR spectra after cysteine substitution and spin labeling of those residues showed subtle broadening, especially in the high field line. As mentioned above, that pattern that would be expected upon the addition of a protein that comes into close proximity with the labeled residue. Models have shown that I66 and K69 interact with Q1 in the activated open state, while Y65 makes contact with Q1 in both the open and closed states. In this study, the Q1 construct used contains residues 100-370, for which the preferred conformation is not known. The interaction observed with E1 residues I66C and K69C suggests that there could be some channels in the activated open state.[23]

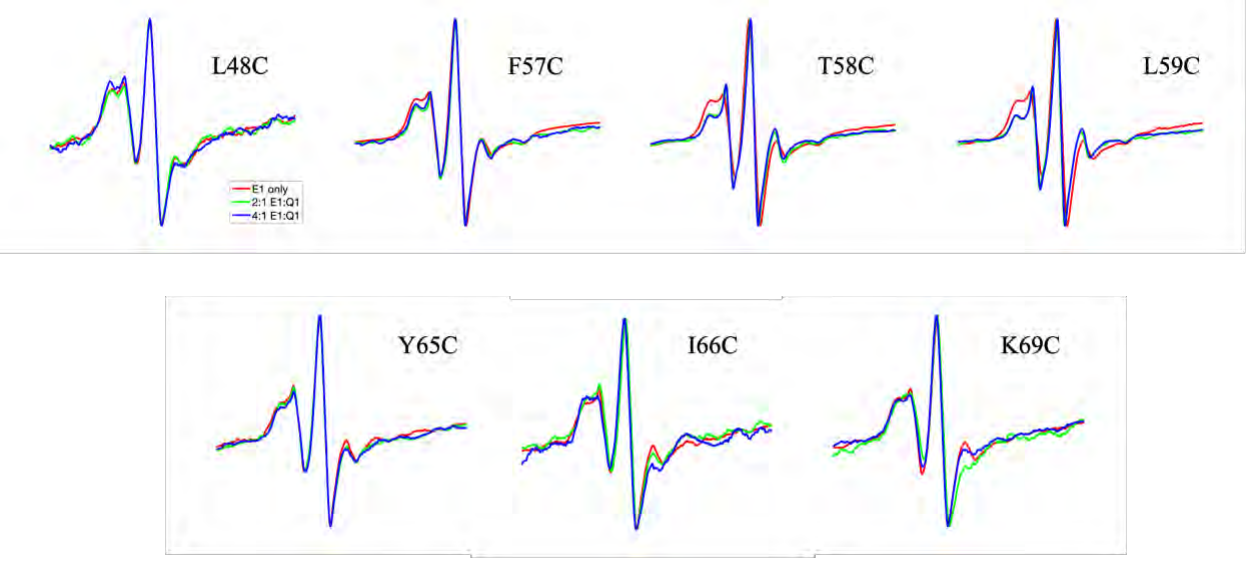

Figure 4.3. CW EPR traces of the transmembrane KCNE1 mutants. In each spectrum red is KCNE1 alone, green is 2:1 E1:Q1, and blue is 4:1 E1:Q1.

For the C terminal region of the protein, residues H73C, S74C, and D76C were chosen as they have been found to interact with the cytoplasmic side of KCNQ1 S6 helix.[6] Overall, there was not a drastic change seen in the line shapes with these mutations upon addition of KCNQ1. In previous studies, interaction between these three KCNE1 residues and KCNQ1 was found to

occur when the channel was in a closed state.[6] Interactions between I66C and K69C with Q1 suggest Q1 could potentially be in an open state with the 100-370 construct. Since interactions between I66C and K69C with Q1 were observed, this would support the hypothesis that $KCNQ1_{100\text{-}370}$ exists in an open state. Residue S84C was chosen as a control for the C-terminus as it has not been found to previously interact and it was in close proximity to the interacting residues.[6]

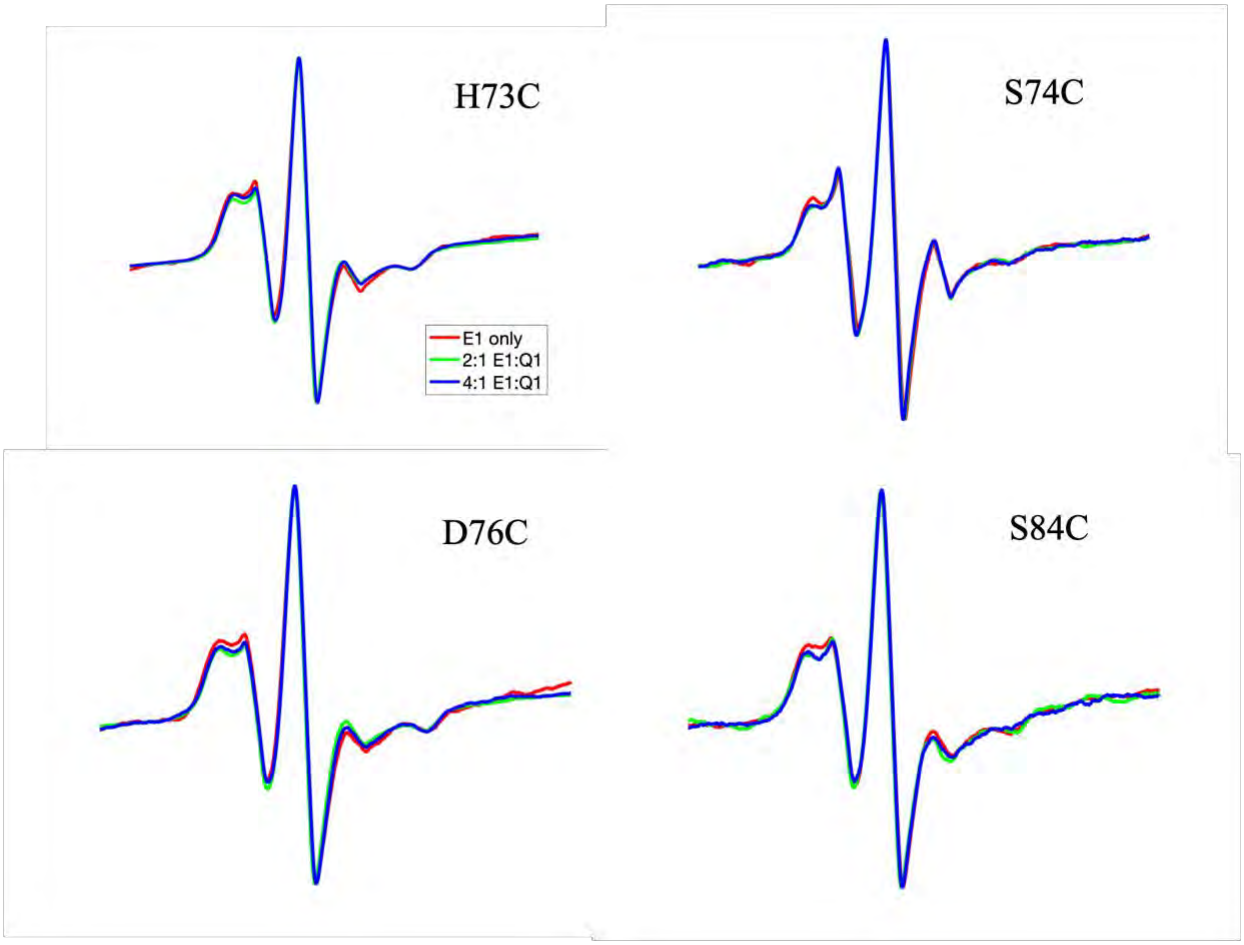

Figure 4.4. CW EPR traces of the C-terminal KCNE1 mutants. In each spectrum red is KCNE1 alone, green is 2:1 E1:Q1, and blue is 4:1 E1:Q1.

4.4.2 Crosslinking Validates KCNE1 Interaction with Truncated $KCNQ1_{100\text{-}370}$

In this study, crosslinking was used to confirm that KCNE1 and $KCNQ1_{100\text{-}370}$ come into close enough proximity to interact in a way that is detectable via CW EPR despite not using the full length KCNQ1 protein. Free amine to sulfhydryl linkers were chosen for this study since

KCNE1 single cysteine mutants were used with WT KCNQ1$_{100-370}$. Removal of native cysteines from KCNQ1 has been attempted in a previous study with no success, so a more commonly used sulfhydryl to sulfhydryl linker was not a feasible option for this pair of proteins.[27]

A KCNE1 mutant containing no cysteine was used to establish if there is any visible background interaction between KCNE1 and KCNQ1 under the conditions used for crosslinking. The complex of a KCNE1 protein with a KCNQ1 monomer would weigh approximately 42.7 kDa, which can be seen faintly in the lane containing Cys-less KCNE1 (Figure 5). This confirms that there is some background interaction between the two proteins under these conditions.

The only KCNE1 mutants that visibly crosslinked were residues F57C, T58C, L59C, Y65C, I66C, and K69C. These residues are either inside the membrane or near the membrane surface. The residues F57, T58, and L59 are known to be functionally important to the I_{KS} channel and are the main site of interaction between the two subunits. These residues had the most intense KCNE1+KCNQ1 band out of all the residues, which supports the known significance of these residues. The residues Y65, I66, and K69 have previously been found in computational studies to make a significant number of contacts with residues in KCNQ1, which is further supported by the links formed here, especially considering the length of the crosslinker is 4.4 A.

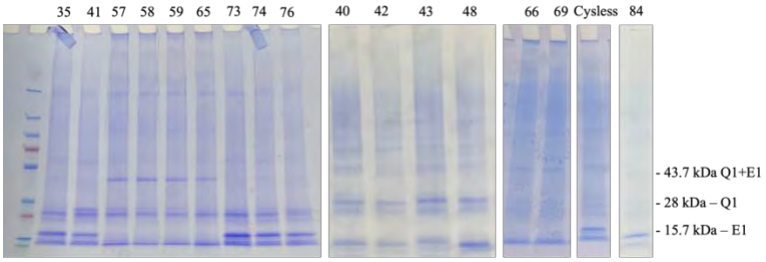

Figure 4.5. SDS-PAGE gels showing the crosslinking of each KCNE1 mutant used for CW EPR line shape analysis with KCNQ1. In each gel, the left lane is the same ladder.

4.5 Conclusions

The interactions between the KCNQ1 and KCNE1 proteins have previously been studied via functional and structural studies, as well as with computational modeling. Spin labeling and EPR spectroscopy was used to observe the interactions between E1 and Q1 from the perspective of

dynamics in the complex's native environment. This method could be used on other similar systems, such as the other KCNE's or the full length KCNQ1 channel to determine the dynamics of protein-protein interactions in those systems.

4.6 Acknowledgements

This work was generously supported by an NIGMS/NIH Maximizing Investigator's Research Award (MIRA) R35 GM126935 grant to G.A.L.

References

(1) Dixit, G.; Dabney-Smith, C.; Lorigan, G. A. The Membrane Protein KCNQ1 Potassium Ion Channel: Functional Diversity and Current Structural Insights. *Biochim. Biophys. Acta BBA - Biomembr.* **2020**, *1862* (5), 183148. https://doi.org/10.1016/j.bbamem.2019.183148.

(2) Silva, J. R.; Pan, H.; Wu, D.; Nekouzadeh, A.; Decker, K. F.; Cui, J.; Baker, N. A.; Sept, D.; Rudy, Y. A Multiscale Model Linking Ion-Channel Molecular Dynamics and Electrostatics to the Cardiac Action Potential. *Proc. Natl. Acad. Sci.* **2009**, *106* (27), 11102–11106. https://doi.org/10.1073/pnas.0904505106.

(3) Abbott, G. W. Biology of the KCNQ1 Potassium Channel. *New J. Sci.* **2014**, *2014*, 1–26. https://doi.org/10.1155/2014/237431.

(4) Jespersen, T.; Grunnet, M.; Olesen, S.-P. The KCNQ1 Potassium Channel: From Gene to Physiological Function. *Physiology* **2005**, *20* (6), 408–416. https://doi.org/10.1152/physiol.00031.2005.

(5) Gofman, Y.; Shats, S.; Attali, B.; Haliloglu, T.; Ben-Tal, N. How Does KCNE1 Regulate the Kv7.1 Potassium Channel? Model-Structure, Mutations, and Dynamics of the Kv7.1-KCNE1 Complex. *Structure* **2012**, *20* (8), 1343–1352. https://doi.org/10.1016/j.str.2012.05.016.

(6) Lvov, A.; Gage, S. D.; Berrios, V. M.; Kobertz, W. R. Identification of a Protein–Protein Interaction between KCNE1 and the Activation Gate Machinery of KCNQ1. *J. Gen. Physiol.* **2010**, *135* (6), 607–618. https://doi.org/10.1085/jgp.200910386.

(7) Nakajo, K.; Kubo, Y. KCNQ1 Channel Modulation by KCNE Proteins via the Voltage-Sensing Domain: KCNQ1 Channel Modulation by KCNE. *J. Physiol.* **2015**, *593* (12), 2617–2625. https://doi.org/10.1113/jphysiol.2014.287672.

(8) Wang, K.-W.; Tai, K.-K.; Goldstein, S. A. N. MinK Residues Line a Potassium Channel Pore. *Neuron* **1996**, *16* (3), 571–577. https://doi.org/10.1016/S0896-6273(00)80076-8.

(9) Maljevic, S.; Wuttke, T. V.; Seebohm, G.; Lerche, H. KV7 Channelopathies. *Pflüg. Arch. - Eur. J. Physiol.* **2010**, *460* (2), 277–288. https://doi.org/10.1007/s00424-010-0831-3.

(10) Peroz, D.; Rodriguez, N.; Choveau, F.; Baró, I.; Mérot, J.; Loussouarn, G. Kv7.1 (KCNQ1) Properties and Channelopathies: Kv7.1 (KCNQ1) Properties and Channelopathies. *J. Physiol.* **2008**, *586* (7), 1785–1789. https://doi.org/10.1113/jphysiol.2007.148254.

(11) Tiron, C.; Campuzano, O.; Pérez-Serra, A.; Mademont, I.; Coll, M.; Allegue, C.; Iglesias, A.; Partemi, S.; Striano, P.; Oliva, A.; Brugada, R. Further Evidence of the Association between LQT Syndrome and Epilepsy in a Family with KCNQ1 Pathogenic Variant. *Seizure* **2015**, *25*, 65–67. https://doi.org/10.1016/j.seizure.2015.01.003.

(12) Tian, C.; Vanoye, C. G.; Kang, C.; Welch, R. C.; Kim, H. J.; George, A. L.; Sanders, C. R. Preparation, Functional Characterization, and NMR Studies of Human KCNE1, a Voltage-Gated Potassium Channel Accessory Subunit Associated with Deafness and Long QT Syndrome †, ‡. *Biochemistry* **2007**, *46* (41), 11459–11472. https://doi.org/10.1021/bi700705j.

(13) Dworakowska, B.; Do, K. Ion Channels-Related Diseases*. *Ion Channels* **2000**, *47*.

(14) Niemeyer, B. A.; Mery, L.; Zawar, C.; Suckow, A.; Monje, F.; Pardo, L. A.; Stühmer, W.; Flockerzi, V.; Hoth, M. Ion Channels in Health and Disease: 83 rd Boehringer Ingelheim Fonds International Titisee Conference. *EMBO Rep.* **2001**, *2* (7), 568–573. https://doi.org/10.1093/embo-reports/kve145.

(15) Catterall, W. A. STRUCTURE AND FUNCTION OF VOLTAGE-GATED ION CHANNELS.

(16) MacKinnon, R. Potassium Channels. *FEBS Lett.* **2003**, *555* (1), 62–65. https://doi.org/10.1016/S0014-5793(03)01104-9.

(17) Peng, D.; Kim, J.-H.; Kroncke, B. M.; Law, C. L.; Xia, Y.; Droege, K. D.; Van Horn, W. D.; Vanoye, C. G.; Sanders, C. R. Purification and Structural Study of the Voltage-Sensor Domain of the Human KCNQ1 Potassium Ion Channel. *Biochemistry* **2014**, *53* (12), 2032–2042. https://doi.org/10.1021/bi500102w.

(18) Smith, J. A.; Vanoye, C. G.; George, A. L.; Meiler, J.; Sanders, C. R. Structural Models for the KCNQ1 Voltage-Gated Potassium Channel. *Biochemistry* **2007**, *46* (49), 14141–14152. https://doi.org/10.1021/bi701597s.

(19) Haitin, Y.; Yisharel, I.; Malka, E.; Shamgar, L.; Schottelndreier, H.; Peretz, A.; Paas, Y.; Attali, B. S1 Constrains S4 in the Voltage Sensor Domain of Kv7.1 K+ Channels. *PLoS ONE* **2008**, *3* (4), e1935. https://doi.org/10.1371/journal.pone.0001935.

(20) Osteen, J. D.; Barro-Soria, R.; Robey, S.; Sampson, K. J.; Kass, R. S.; Larsson, H. P. Allosteric Gating Mechanism Underlies the Flexible Gating of KCNQ1 Potassium Channels. *Proc. Natl. Acad. Sci.* **2012**, *109* (18), 7103–7108. https://doi.org/10.1073/pnas.1201582109.

(21) Zaydman, M. A.; Kasimova, M. A.; McFarland, K.; Beller, Z.; Hou, P.; Kinser, H. E.; Liang, H.; Zhang, G.; Shi, J.; Tarek, M.; Cui, J. Domain–Domain Interactions Determine the Gating, Permeation, Pharmacology, and Subunit Modulation of the IKs Ion Channel. *eLife* **2014**, *3*, e03606. https://doi.org/10.7554/eLife.03606.

(22) Wiener, R.; Haitin, Y.; Shamgar, L.; Fernández-Alonso, M. C.; Martos, A.; Chomsky-Hecht, O.; Rivas, G.; Attali, B.; Hirsch, J. A. The KCNQ1 (Kv7.1) COOH Terminus, a Multitiered Scaffold for Subunit Assembly and Protein Interaction. *J. Biol. Chem.* **2008**, *283* (9), 5815–5830. https://doi.org/10.1074/jbc.M707541200.

(23) Kuenze, G.; Vanoye, C. G.; Desai, R. R.; Adusumilli, S.; Brewer, K. R.; Woods, H.; McDonald, E. F.; Sanders, C. R.; George, A. L.; Meiler, J. Allosteric Mechanism for KCNE1 Modulation of KCNQ1 Potassium Channel Activation. *eLife* **2020**, *9*, e57680. https://doi.org/10.7554/eLife.57680.

(24) Xu, Y.; Wang, Y.; Meng, X.-Y.; Zhang, M.; Jiang, M.; Cui, M.; Tseng, G.-N. Building KCNQ1/KCNE1 Channel Models and Probing Their Interactions by Molecular-Dynamics Simulations. *Biophys. J.* **2013**, *105* (11), 2461–2473. https://doi.org/10.1016/j.bpj.2013.09.058.

(25) Nakajo, K.; Ulbrich, M. H.; Kubo, Y.; Isacoff, E. Y. Stoichiometry of the KCNQ1 - KCNE1 Ion Channel Complex. *Proc. Natl. Acad. Sci.* **2010**, *107* (44), 18862–18867. https://doi.org/10.1073/pnas.1010354107.

(26) Plant, L. D.; Xiong, D.; Dai, H.; Goldstein, S. A. N. Individual IKs Channels at the Surface of Mammalian Cells Contain Two KCNE1 Accessory Subunits. *Proc. Natl. Acad. Sci.* **2014**, *111* (14), E1438–E1446. https://doi.org/10.1073/pnas.1323548111.

(27) Chung, D. Y.; Chan, P. J.; Bankston, J. R.; Yang, L.; Liu, G.; Marx, S. O.; Karlin, A.; Kass, R. S. Location of KCNE1 Relative to KCNQ1 in the I_{KS} Potassium Channel by Disulfide Cross-Linking of Substituted Cysteines. *Proc. Natl. Acad. Sci.* **2009**, *106* (3), 743–748. https://doi.org/10.1073/pnas.0811897106.

(28) Kang, C.; Tian, C.; Sönnichsen, F. D.; Smith, J. A.; Meiler, J.; George, A. L.; Vanoye, C. G.; Kim, H. J.; Sanders, C. R. Structure of KCNE1 and Implications for How It Modulates the KCNQ1 Potassium Channel † ‡. *Biochemistry* **2008**, *47* (31), 7999–8006. https://doi.org/10.1021/bi800875q.

(29) Dixit, G.; Stowe, R. B.; Bates, A.; Jaycox, C. K.; Escobar, J. R.; Harding, B. D.; Drew, D. L.; New, C. P.; Sahu, I. D.; Edelmann, R. E.; Dabney-Smith, C.; Sanders, C. R.; Lorigan, G. A. Purification and Membrane Interactions of Human KCNQ1100–370 Potassium Ion Channel. *Biochim. Biophys. Acta BBA - Biomembr.* **2022**, *1864* (11), 184010. https://doi.org/10.1016/j.bbamem.2022.184010.

(30) Tessmer, M. H.; Anderson, D. M.; Buchaklian, A.; Frank, D. W.; Feix, J. B. Cooperative Substrate-Cofactor Interactions and Membrane Localization of the Bacterial Phospholipase A_2 (PLA_2) Enzyme, ExoU. *J. Biol. Chem.* **2017**, *292* (8), 3411–3419. https://doi.org/10.1074/jbc.M116.760074.

Chapter 5

EPR spectroscopy reveals unique polymorphism in ODS-induced tau filaments

Rebecca B. Stowe[1], Indra D. Sahu[2], Austin M. Allen[3], Christopher A. Ayoub[3], Emma A. Gordon[1], Lauryn E. Cook[1], Robert M. McCarrick[1], Jeff Kuret[3], Gary A. Lorigan[1]

[1]Department of Chemistry and Biochemistry, Miami University, Oxford, OH 45056

[2]Division of Natural Sciences, Campbellsville University, Campbellsville, KY 42718

[3]Department of Biological Chemistry and Pharmacology, The Ohio State University, Columbus, OH 43210

Project conceived by JK, GAL, IDS, and RBS. Sample preparation by RBS, CAA, AMA, and LEC. Data collection and analysis by RBS, EAG and RMM. Manuscript written by RBS. Manuscript edited by JK, GAL, AMA, and RBS.

5.1 Abstract

Alzheimer's Disease is the most frequently diagnosed neurodegenerative disease. This disease, along with several others such as Parkinson's, are characterized by the aggregation of Tau in the brain which leads to neuronal death. The structure of the Tau filaments that make up these aggregates has recently been resolved from a patient's brain slice using Cryo-EM. In a lab setting small molecule inducers are commonly used to produce Tau aggregates. The structure of these filaments formed by inducer must be resolved to determine their similarity to disease state filament structures. In this study, a method for site-directed spin labeling of full length 2N4R Tau was developed that can be used as a screening tool for estimation of the aggregate core location in fibrils formed via small molecule inducer. Octadecyl sulfate induced fibrils were used to confirm the compatibility of this spin labeling method with small molecule induced fibrils. Continuous Wave Electron Paramagnetic Resonance (CW-EPR) and Double Electron Electron Resonance (DEER) spectroscopy was used to determine the dynamics and distance constraints of a doubly labeled Tau 2N4R mutant under different aggregating conditions. These fibrils were found to have a unique morphology when compared to the more commonly used heparin, justifying further structural studies to fully resolve the fibril structure.

5.2 Introduction

The microtubule associated protein tau is an intrinsically disordered protein that can lead to fatal neurodegenerative diseases upon aggregation in the brain.[1] Diseases associated with the aggregation of tau are known as tauopathies, many of which are sporadic and largely affect the aged population.[1,2] Alzheimer's Disease (AD), being the most commonly diagnosed neurodegenerative disease, is characterized by the presence of neurofibrillary tangles (NFTs) of tau protein.[1] There are six tau isoforms of various length that are expressed in the human brain, which are characterized by the inclusion of 0-2 N terminal inserts and inclusion (4R) or exclusion (3R) of the R2 repeat domain **(Figure 5.1)**.[3] AD has a mixture of NFTs made of 3R and 4R Tau—which manifest as the two polymorphic structures paired helical filament (PHF) and straight filament (SF).[3,4]

Recently, the structure of PHFs and SFs has been resolved from the brain slice of an AD patient using Cryo-EM.[1] Since patient samples are inaccessible to most labs due to cost and scarcity, most Tau aggregates used in a lab setting are formed *in vitro* using either preformed aggregate seeds or small molecule inducers.[3,5,6] The most commonly used small molecule is heparin, which has been recently found to form an aggregate structure that differs from the structure of aggregates formed during AD.[5,6] This has led to a need to investigate the structures of filaments formed by other inducers such as octadecyl sulfate (ODS) to determine if the aggregates formed by these inducers can be compared to the disease state aggregates.

Electron paramagnetic resonance (EPR) spectroscopy is a powerful approach for detecting and quantifying protein conformation in aggregates. However, it does require a relatively high concentration of protein compared to electron microscopy and other structural methods. Aggregation can become variable under these conditions, especially for intrinsically disordered protein substrates such as tau.[4,7] Although the cysteine residues that contribute to nonspecific aggregation through disulfide bond formation are mostly blocked by covalent spin labels in EPR spectroscopy, remaining free sulfhydryls retain reactivity and can foster variability. For this reason, choice of reducing agent, such as dithiothreitol (DTT) or tris(2-carboxyethyl)phosphine (TCEP), is an important variable impacting aggregation propensity and polymorphism.[8,9]

Here we employed continuous-wave EPR measurements (CW EPR), double electron-electron resonance (DEER) spectroscopy, and transmission electron microscopy (TEM) to characterize the effect of micellar aggregation inducer ODS on human 2N4R tau aggregate conformation. Results provide evidence that ODS differentially affects tau polymorphism relative heparin inducer, and that the effects are maximally resolved in the presence of DTT reducing agent.

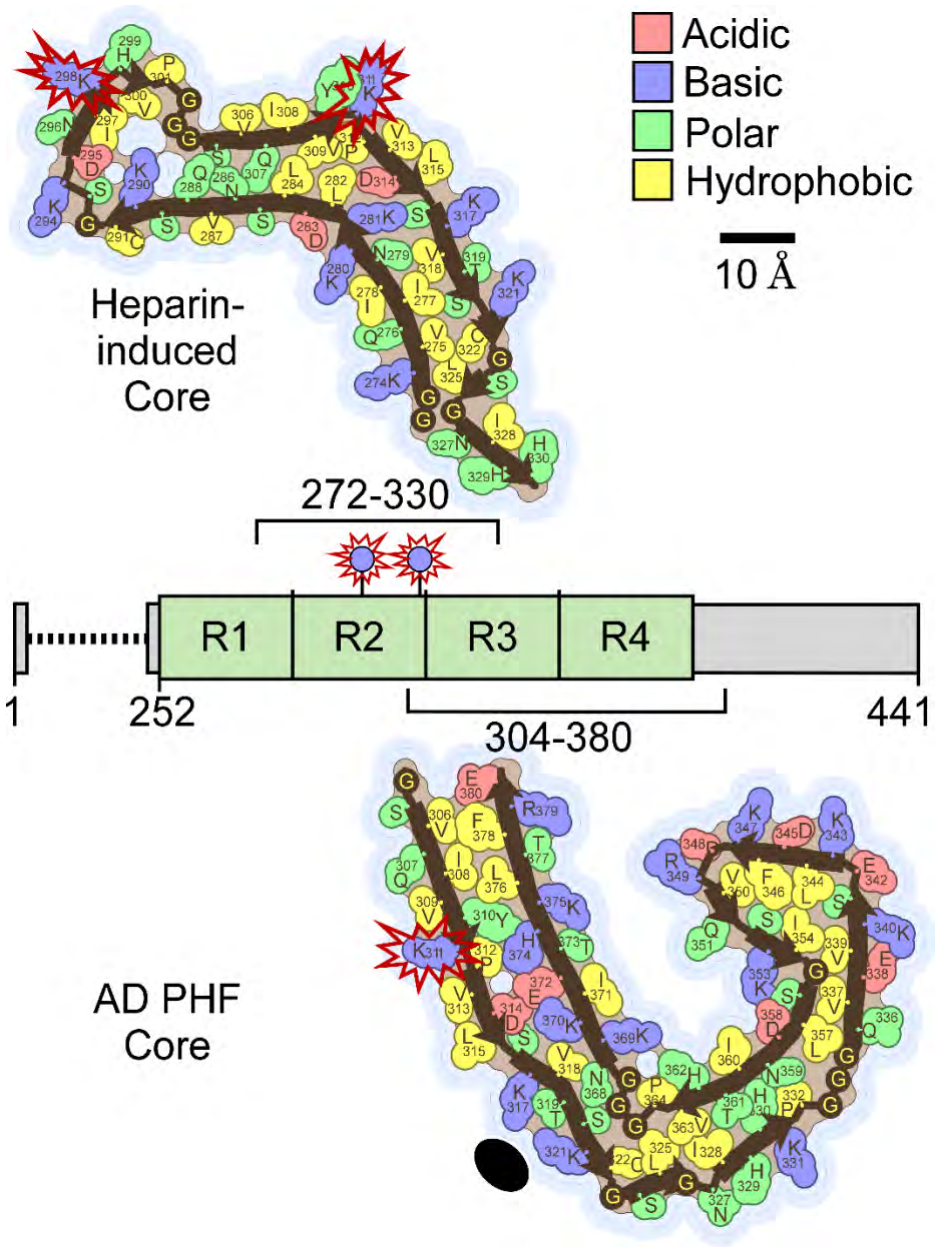

Figure 5.1. Depiction of full-length tau (human 2N4R tau isoform; 441 amino acid residues) and location of its microtubule-binding repeat region composed of four imperfect repeats (R1 – R4).[10] The cores of the AD PHF ("AD Core") and the heparin induced synthetic 2N4R tau ("heparin-induced Core" of the "snake" conformer) protofilaments are marked, along with location of the EPR spin probes used in this study (K298 and K311).[6] Location of putative anionic species associated with the AD-derived conformer is shown as a solid ellipse. The illustrated aggregate core structures were created using Amyloid Atlas Illustrator.[11]

5.3 Materials and Methods

5.3.1 Tau protein preparation

Tau expression plasmid pT7II-2N4Rtau (Addgene #177653) encoding the human 2N4R tau isoform (UniProtKB accession P10636-8) was mutagenized using the QuikChange Lightning Multi Site-Directed Mutagenesis Kit (Agilent). First, naturally occurring Cys codons were mutagenized to Ala with primers C291A (5'-TAGCAACGTCCAGTCCAAGGCTGGCTCAAAGGATAATATC-3') and C322A (5'-GCAAGGTGACCTCCAAGGCTGGCTCATTAGGCAACA-3') to create a double mutant encoding C291A/C322A. The resulting construct was then mutagenized to K298C (5'-GCTGGCTCAAAGGATAATATCTGCCACGTCCCGGGAGGC-3') and K311C (5'-ggcagtgtgcaaatagtctactgcccagttgacctgagcaaggtg-3'). The final quadruple mutant (2N4R tau-QM) was expressed in BL21(DE3) cells and purified as described previously.[12]

5.3.2 Site Directed Spin Labeling

All aqueous solutions contacting tau were treated with diethyl pyrocarbonate before use. After concentration by methanol precipitation (equal volume overnight at -20°C), tau pellets (5 min x 4000g, 10 min x 10,000g) were dissolved in Assembly Buffer (10 mM HEPES, pH 7.4, 100 mM NaCl) containing 6 M Guanidine HCl. 3-maleimido-PROXYL (MSL) spin label (250 mM in DMSO) was then mixed with the tau protein solution at a 20x molar excess and shaken at room temperature for 24 h.[13] Excess spin label was removed via gravity desalting column chromatography (10 mL; BioRad). The protein was eluted into deuterated Assembly Buffer and the fractions containing protein were confirmed via Bradford reagent and pooled. Protein concentration was determined using the bicinchoninic acid method (Thermo Scientific).

5.3.3 Tau aggregation

Spin-labeled 2N4R QM tau protein (30 μM) was aggregated in the presence of Assembly Buffer (10 mM HEPES, pH 7.4, 100 mM NaCl) and ODS inducer (150 μM) in a final volume of 300 μL as described previously, except that samples were prepared in D_2O.[14] To test the effects of reducing agents, separate samples were prepared containing 4.5 mM DTT, 4.5 mM TCEP, and no reducing agent. All aggregation samples were incubated at 37°C for 24 h.

5.3.4 Transmission Electron Microscopy (TEM)

Aliquots (2 μL) of aggregation products were adsorbed onto Formvar-carbon coated copper grids as described previously.[15] Excess sample was blotted off and the grid was allowed to dry before imaging. TEM imaging were completed at the Center for Advanced Microscopy and Imaging at Miami University using a JEOL JEM-1200EX II microscope operated at 120 keV.

5.3.5 Continuous Wave EPR Spectroscopy

CW-EPR spectroscopic measurements were collected at X-Band on a Bruker EMX CW-EPR spectrometer with a Premium X bridge and ER4119-HS cavity. All measurements were carried out at room temperature with a center field of 3318 G, a 150 G sweep width, 100 kHz modulation frequency, 1 G modulation amplitude, and a 10.02 mW microwave power. The spin label side chain motion was determined by calculating the empirical motional parameter (τ_0) for each spectrum with Equation (1), where ΔH is the central line width, is h_0 the height of the central line, and h_{-1} is the height of the high field line.[16–19] The spectra were also simulated to determine the error in the τ_0 value calculations.

$$\tau_0 = K \times \Delta H \left[\left(\frac{h_0}{h_{-1}} \right)^{\frac{1}{2}} - 1 \right] \quad (1)$$

5.3.6 Double Electron-Electron Resonance (DEER) Spectroscopy

Four-pulse DEER measurements were collected with a Bruker ELEXSYS E580 spectrometer equipped with a SuperQFT pulse Q-band system with an EN5107D2 resonator and 300 W amplifier. All DEER samples contained 10% v/v glycerol as a cryoprotectant. The samples were loaded into a 3 mm inner diameter quartz capillary (Wilmad LabGlass, Buena, NJ). DEER data were collected using a standard four-pulse sequence [(π/2)ν1 − τ1 − (π)ν1 − t − (π)ν2 − (τ1 + τ2 − t) − (π)ν1 − τ2 − echo] with probe pulse widths of 8 and 16 ns, a pump pulse width of 70 ns, 120 MHz frequency difference between the pump and probe pulses, shot repetition time determined by the spin-lattice relaxation time (T_1), 100 shots per point, and 16 step phase cycling at 80 K collected out to 2.5-3 μs determined by the spin-spin relaxation time (T_2) [30]. Each sample was allowed to signal average for 24 h. DEER data were analyzed using Matlab based DEER Analysis program 2015.[20] Tikhonov regularization was used to obtain

DEER distance distributions $P(r)$ in the distance domain with the constraint $P(r) > 0$.[21] The background correction was obtained by using a homogeneous three-dimensional model. The regularization parameter in the L curve was optimized for the best fit DEER time domain data.

5.4 Results and Discussion

To interrogate the effects of ODS inducer on tau aggregate conformation, full-length human 2N4R Tau-QM was expressed, purified and spin-labeled with MSL. This mutant was chosen for analysis because its K298C/K311C labeling sites localize to the cross-β-sheet core of heparin-induced 4-repeat tau aggregates, where they remain solvent exposed in all conformers experimentally validated through structure determination.[3,6] Moreover, spin-labeling of K311C does not interfere with its heparin-induced aggregation in vitro.[22] In contrast, while these sites also are solvent exposed in AD-derived protofilaments, only K321 overlaps with its core region (**Fig. 1**).[23] As a result, 2N4R Tau-QM is capable of distinguishing these polymorphs.

To authenticate 2N4R Tau-QM samples, the purified recombinant protein was first subjected to SDS-PAGE. In both the presence and absence of labeling, 2N4R Tau-QM samples migrated as single species between 55 – 70 KDa **(Figure 5.2)**, ,consistent with the previously established behavior of the human full-length 2N4R tau isoform.[10,24] These data indicate that full-length 2N4R tau-QM remained intact through MSL labeling, and that proteolytic fragments capable of spontaneous aggregation were not detectably generated during preparation and labeling of the protein. Second, to test whether MSL-labeled tau retained aggregation propensity, 2N4R tau-QM was incubated in the presence of ODS aggregation inducer and the products visualized by TEM.[25] In the absence of inducer, no aggregates were visible (**Figure 5.3A**), indicating that like other full-length tau constructs, 2N4R tau-QM resists spontaneous aggregation under these conditions.[26] In contrast, the addition of ODS inducer in either the presence of DTT reducing agent (**Figure 5.3B**), in the absence of reducing agent (**Figure 5.3C**), or in the presence of TCEP reducing agent (**Figure 5.3D**) all yielded filamentous aggregates. Together these data show that 2N4R tau-QM resembles full-length wild-type 2N4R tau with respect to aggregation propensity, including dependence on inducer for aggregation and in yielding the highest densities of aggregates under reducing conditions.[27]

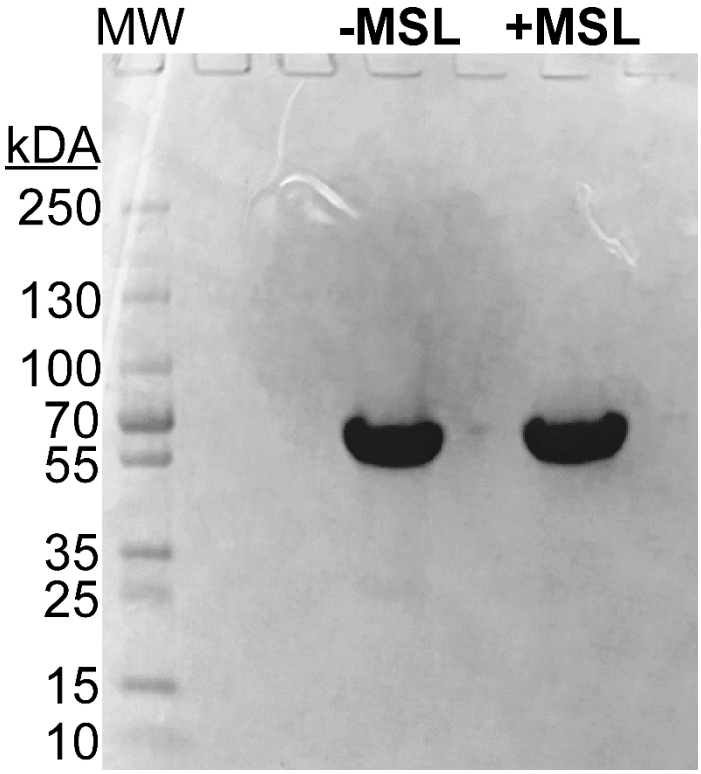

Figure 5.2. SDS-PAGE (Coomassie blue stain) of 2N4R Tau-QM with (+MSL) and without (-MSL) covalent MSL spin labelling relative to molecular weight markers (MW). Each show an intense band migrating between 55 and 70 kDa, indicating samples were highly purified and full-length.

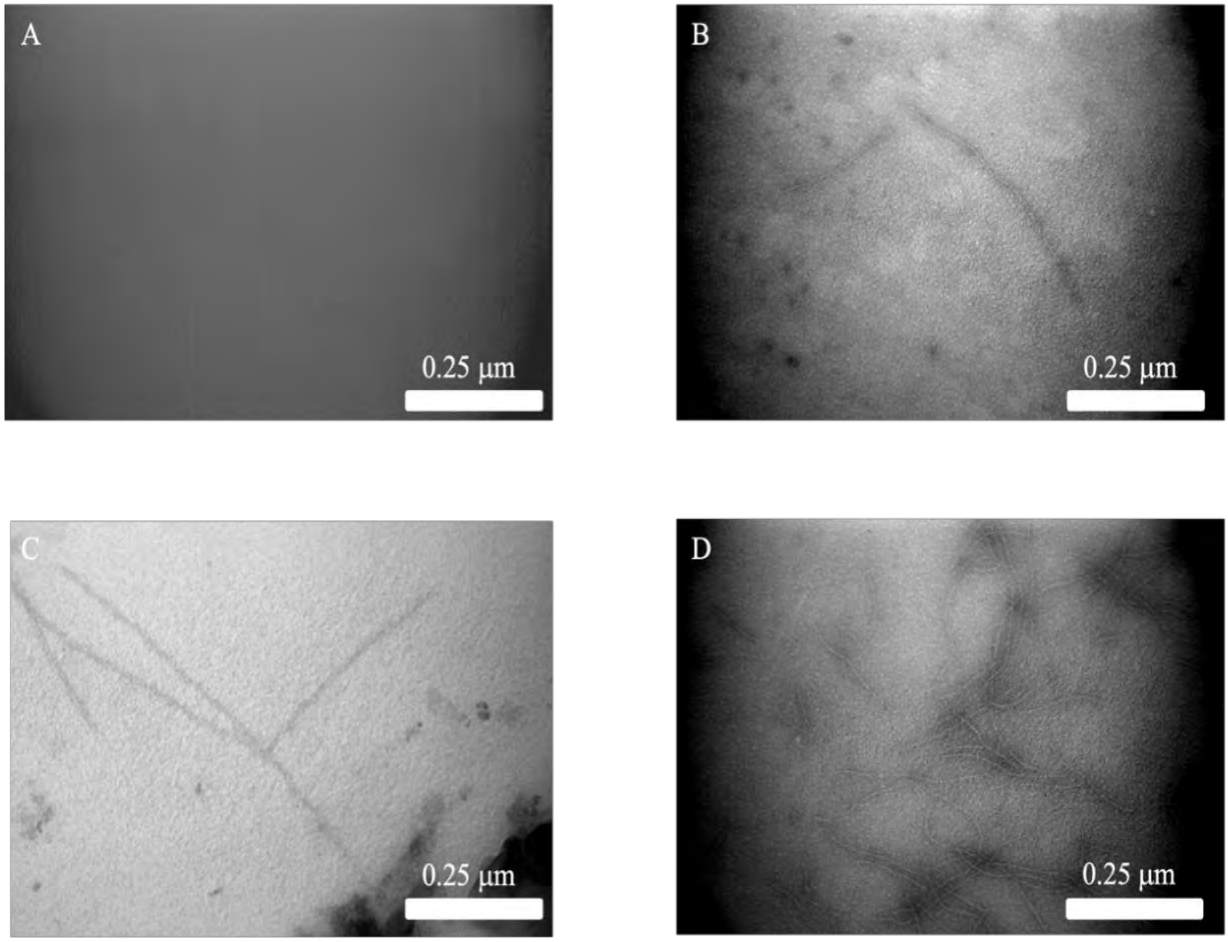

Figure 5.3. TEM images of 2N4R tau-QM aggregation products. **(A)** – ODS. (**B**) +ODS +DTT. **(C)** +ODS. **(D)** +ODS +TCEP.

To characterize the environment of MSL spin labels in 2N4R tau-QM, monomers and aggregates were subjected to CW-EPR line shape analysis (**Figure 5.4A**). The empirical motional parameter (τ_0) derived from these data is proportional to the amount of time it takes for the spin label to tumble in solution, where smaller values reflect faster motion and less rigidity.[18,19] For 2N4R tau-QM aggregates, all τ_0 values were found not to be significantly different, indicating that the presence of reducing agents has no significant effect on the spin label mobility (**Figure 5.4B**). It was also found that the spin labeling efficiency did not decrease after aggregation, except in the +DTT +ODS sample, which is likely due to reduction of the free electron on the spin label when DTT was added to the sample after the label was attached to the protein.[28] These data show that samples containing reducing agent had a shorter τ_0 than the monomer sample despite visible aggregation.

This could be due to the reducing agents' effect on the aggregate morphology, with the aggregated samples containing reducing agent adopting a conformation that puts the spin label in a more flexible local environment when compared to the aggregated sample with no reducing agent. However, the spectral linewidth seen here is much sharper than reported in previous studies using seeding and heparin as an inducer.[13,22]

2N4R Tau-QM used in this study was created with reference to the location of the core of synthetic heparin-induced fibrils. Thus, if ODS induced a similar conformer, then the linewidth should have broadened significantly—as seen previously in the presence of heparin.[13,22] These data suggest that the aggregate core formed in the presence of ODS resides in a different location compared to the heparin-induced conformer.

A:

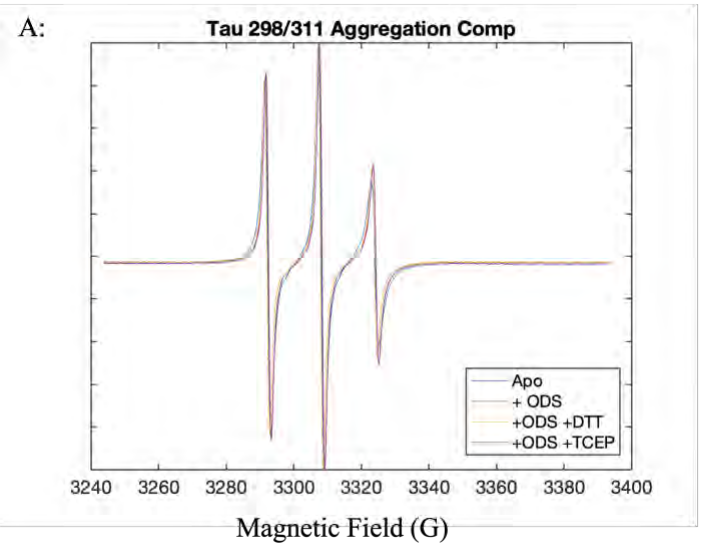

B:

Sample Name	τ_0
Apo	0.6 ± 0.2 ns
+ODS	0.5 ± 0.2 ns
+DTT +ODS	0.4 ± 0.2 ns
+TCEP +ODS	0.6 ± 0.2 ns

Figure 5.4. CW-EPR analysis of 2N4R tau-QM aggregated under different conditions. (**A**) CW-EPR spectra. (**B**) Table of calculated τ_0 values.

To test this hypothesis, samples were then subjected to DEER Spectroscopy, which provides an estimate of distance between spin labels. DEER spectra revealed a population shift away from shorter distances (i.e., ~20 Å) in all samples aggregated with ODS relative to tau monomer (**Figure**

5.5). However, the intensity of the shift varied by condition, being greatest with +ODS +DTT. Because aggregate core formation would be expected to shorten the distances between spin labels relative to intrinsically disordered monomer, these data are consistent with the K298C/K311C sites lying outside the core region of ODS-induced aggregates. Together with CW-EPR spectra, these data indicate that the location of the core region of tau aggregates induced in the presence of ODS

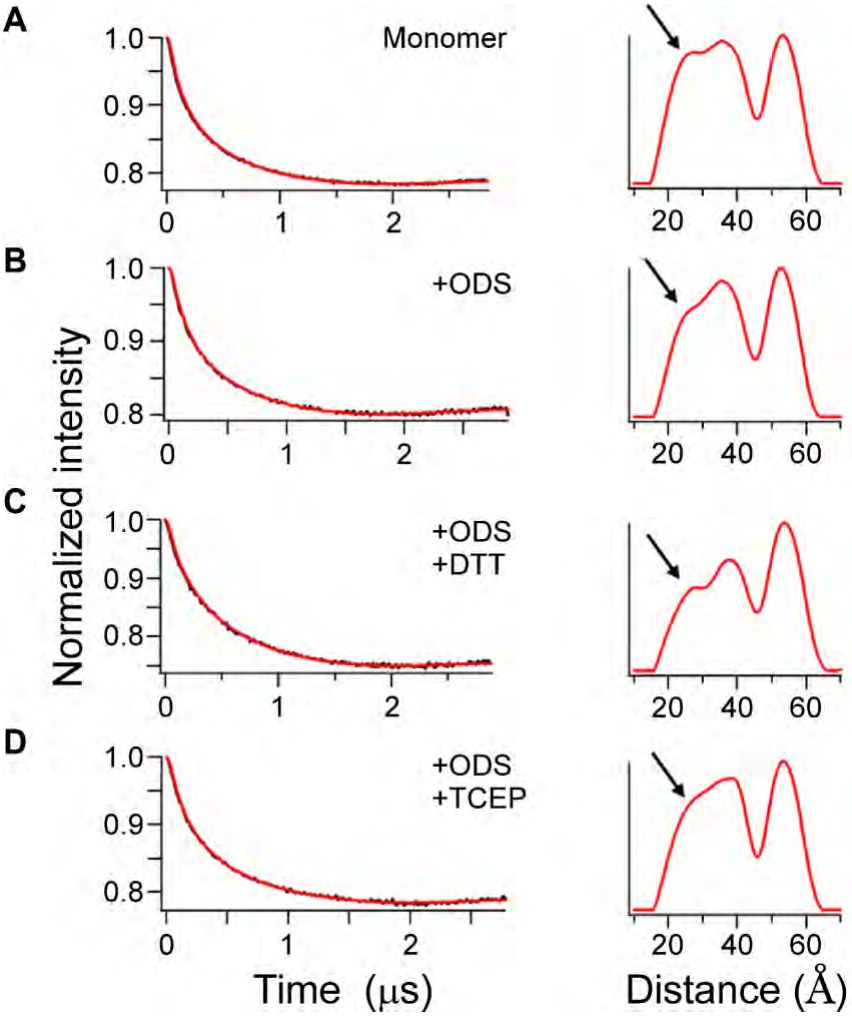

Figure 5.5. DEER spectra of 2N4R tau-QM using different reducing conditions. Left column is time domain, and right column is corresponding distance distributions. (**A**) Tau monomer, no aggregation. (**B**) Tau +ODS. (**C**) Tau +ODS +DTT. (**D**) Tau +ODS +TCEP. Arrows indicate the ~20 Å distance that varies in intensity among samples.

differs compared to aggregates induced by heparin.

5.5 Conclusion

This study has shown that full length 2N4R tau can be spin labeled and aggregated at a concentration that is suitable for EPR spectroscopy. The ODS inducer was used with mutations chosen from the heparin aggregate core, and it was found that while the protein aggregated, the core of the ODS induced aggregate is located in a different region of the protein than previously expected. This location can be elucidated by further structural studies of the ODS aggregate, which can then be further refined with DEER spectroscopy.

5.6 Acknowledgements

This work was supported by grant RF1 AG054018 (J. K. and G.A.L.) from the National Institute on Aging. The authors thank the members of the Lorigan and Kuret labs for their support in the development of this manuscript.

References

(1) Falcon, B.; Zhang, W.; Schweighauser, M.; Murzin, A. G.; Vidal, R.; Garringer, H. J.; Ghetti, B.; Scheres, S. H. W.; Goedert, M. Tau Filaments from Multiple Cases of Sporadic and Inherited Alzheimer's Disease Adopt a Common Fold. *Acta Neuropathol. (Berl.)* **2018**, *136* (5), 699–708. https://doi.org/10.1007/s00401-018-1914-z.

(2) Morris, M.; Maeda, S.; Vossel, K.; Mucke, L. The Many Faces of Tau. *Neuron* **2011**, *70* (3), 410–426. https://doi.org/10.1016/j.neuron.2011.04.009.

(3) Dregni, A. J.; Mandala, V. S.; Wu, H.; Elkins, M. R.; Wang, H. K.; Hung, I.; DeGrado, W. F.; Hong, M. In Vitro 0N4R Tau Fibrils Contain a Monomorphic β-Sheet Core Enclosed by Dynamically Heterogeneous Fuzzy Coat Segments. *Proc. Natl. Acad. Sci.* **2019**, *116* (33), 16357–16366. https://doi.org/10.1073/pnas.1906839116.

(4) Carlomagno, Y.; Manne, S.; DeTure, M.; Prudencio, M.; Zhang, Y.-J.; Hanna Al-Shaikh, R.; Dunmore, J. A.; Daughrity, L. M.; Song, Y.; Castanedes-Casey, M.; Lewis-Tuffin, L. J.; Nicholson, K. A.; Wszolek, Z. K.; Dickson, D. W.; Fitzpatrick, A. W. P.; Petrucelli, L.; Cook, C. N. The AD Tau Core Spontaneously Self-Assembles and Recruits Full-Length Tau to Filaments. *Cell Rep.* **2021**, *34* (11), 108843. https://doi.org/10.1016/j.celrep.2021.108843.

(5) Fichou, Y.; Vigers, M.; Goring, A. K.; Eschmann, N. A.; Han, S. Heparin-Induced Tau Filaments Are Structurally Heterogeneous and Differ from Alzheimer's Disease Filaments. *Chem. Commun.* **2018**, *54* (36), 4573–4576. https://doi.org/10.1039/C8CC01355A.

(6) Zhang, W.; Falcon, B.; Murzin, A. G.; Fan, J.; Crowther, R. A.; Goedert, M.; Scheres, S. H. Heparin-Induced Tau Filaments Are Polymorphic and Differ from Those in Alzheimer's and Pick's Diseases. *eLife* **2019**, *8*, e43584. https://doi.org/10.7554/eLife.43584.

(7) Xiao, S.; Wu, Q.; Yao, X.; Zhang, J.; Zhong, W.; Zhao, J.; Liu, Q.; Zhang, M. Inhibitory Effects of Isobavachalcone on Tau Protein Aggregation, Tau Phosphorylation, and Oligomeric Tau-Induced Apoptosis. *ACS Chem. Neurosci.* **2021**, *12* (1), 123–132. https://doi.org/10.1021/acschemneuro.0c00617.

(8) Huseby, C. J.; Bundschuh, R.; Kuret, J. The Role of Annealing and Fragmentation in Human Tau Aggregation Dynamics. *J. Biol. Chem.* **2019**, *294* (13), 4728–4737. https://doi.org/10.1074/jbc.RA118.006943.

(9) *Tau Protein: Methods and Protocols*; Smet-Nocca, C., Ed.; Methods in Molecular Biology; Springer New York: New York, NY, 2017; Vol. 1523. https://doi.org/10.1007/978-1-4939-6598-4.

(10) Goedert, M.; Spillantini, M. G.; Potier, M. C.; Ulrich, J.; Crowther, R. A. Cloning and Sequencing of the CDNA Encoding an Isoform of Microtubule-Associated Protein Tau Containing Four Tandem Repeats: Differential Expression of Tau Protein MRNAs in Human Brain. *EMBO J.* **1989**, *8* (2), 393–399. https://doi.org/10.1002/j.1460-2075.1989.tb03390.x.

(11) Sawaya, M. R.; Hughes, M. P.; Rodriguez, J. A.; Riek, R.; Eisenberg, D. S. The Expanding Amyloid Family: Structure, Stability, Function, and Pathogenesis. *Cell* **2021**, *184* (19), 4857–4873. https://doi.org/10.1016/j.cell.2021.08.013.

(12) Jimenez-Harrison, D.; Huseby, C. J.; Hoffman, C. N.; Sher, S.; Snyder, D.; Seal, B.; Yuan, C.; Fu, H.; Wysocki, V.; Giorgini, F.; Kuret, J. DJ-1 Molecular Chaperone Activity Depresses Tau Aggregation Propensity through Interaction with Monomers. *Biochemistry* **2023**, *62* (5), 976–988. https://doi.org/10.1021/acs.biochem.2c00581.

(13) Weismiller, H. A.; Murphy, R.; Wei, G.; Ma, B.; Nussinov, R.; Margittai, M. Structural Disorder in Four-Repeat Tau Fibrils Reveals a New Mechanism for Barriers to Cross-Seeding of Tau Isoforms. *J. Biol. Chem.* **2018**, *293* (45), 17336–17348. https://doi.org/10.1074/jbc.RA118.005316.

(14) Chirita, C. N.; Necula, M.; Kuret, J. Anionic Micelles and Vesicles Induce Tau Fibrillization in Vitro. *J. Biol. Chem.* **2003**, *278* (28), 25644–25650. https://doi.org/10.1074/jbc.M301663200.

(15) Necula, M.; Kuret, J. Electron Microscopy as a Quantitative Method for Investigating Tau Fibrillization. *Anal. Biochem.* **2004**, *329* (2), 238–246. https://doi.org/10.1016/j.ab.2004.02.023.

(16) Bates, I. R.; Boggs, J. M.; Feix, J. B.; Harauz, G. Membrane-Anchoring and Charge Effects in the Interaction of Myelin Basic Protein with Lipid Bilayers Studied by Site-Directed Spin Labeling. *J. Biol. Chem.* **2003**, *278* (31), 29041–29047. https://doi.org/10.1074/jbc.M302766200.

(17) Ishii, K.; Terauchi, S.; Murakami, R.; Valencia Swain, J.; Mutoh, R.; Mino, H.; Maki, K.; Arata, T.; Ishiura, M. Site-Directed Spin Labeling-Electron Spin Resonance Mapping of the Residues of Cyanobacterial Clock Protein KaiA That Are Affected by KaiA-KaiC Interaction. *Genes Cells* **2014**, *19* (4), 297–324. https://doi.org/10.1111/gtc.12130.

(18) Klug, C. S.; Feix, J. B. Methods and Applications of Site-Directed Spin Labeling EPR Spectroscopy. In *Methods in Cell Biology*; Elsevier, 2008; Vol. 84, pp 617–658. https://doi.org/10.1016/S0091-679X(07)84020-9.

(19) Sahu, I. D.; Craig, A. F.; Dunagan, M. M.; Troxel, K. R.; Zhang, R.; Meiberg, A. G.; Harmon, C. N.; McCarrick, R. M.; Kroncke, B. M.; Sanders, C. R.; Lorigan, G. A. Probing Structural Dynamics and Topology of the KCNE1 Membrane Protein in Lipid Bilayers via Site-Directed Spin Labeling and Electron Paramagnetic Resonance Spectroscopy. *Biochemistry* **2015**, *54* (41), 6402–6412. https://doi.org/10.1021/acs.biochem.5b00505.

(20) Jeschke, G.; Chechik, V.; Ionita, P.; Godt, A.; Zimmermann, H.; Banham, J.; Timmel, C. R.; Hilger, D.; Jung, H. DeerAnalysis2006—a Comprehensive Software Package for Analyzing Pulsed ELDOR Data. *Appl. Magn. Reson.* **2006**, *30* (3–4), 473–498. https://doi.org/10.1007/BF03166213.

(21) Chiang, Y.-W.; Borbat, P. P.; Freed, J. H. The Determination of Pair Distance Distributions by Pulsed ESR Using Tikhonov Regularization. *J. Magn. Reson.* **2005**, *172* (2), 279–295. https://doi.org/10.1016/j.jmr.2004.10.012.

(22) Margittai, M.; Langen, R. Template-Assisted Filament Growth by Parallel Stacking of Tau. *Proc. Natl. Acad. Sci.* **2004**, *101* (28), 10278–10283. https://doi.org/10.1073/pnas.0401911101.

(23) Fitzpatrick, A. W. P.; Falcon, B.; He, S.; Murzin, A. G.; Murshudov, G.; Garringer, H. J.; Crowther, R. A.; Ghetti, B.; Goedert, M.; Scheres, S. H. W. Cryo-EM Structures of Tau Filaments from Alzheimer's Disease. *Nature* **2017**, *547* (7662), 185–190. https://doi.org/10.1038/nature23002.

(24) Chirita, C. N.; Congdon, E. E.; Yin, H.; Kuret, J. Triggers of Full-Length Tau Aggregation: A Role for Partially Folded Intermediates. *Biochemistry* **2005**, *44* (15), 5862–5872. https://doi.org/10.1021/bi0500123.

(25) Rodriguez Camargo, D. C.; Sileikis, E.; Chia, S.; Axell, E.; Bernfur, K.; Cataldi, R. L.; Cohen, S. I. A.; Meisl, G.; Habchi, J.; Knowles, T. P. J.; Vendruscolo, M.; Linse, S. Proliferation of Tau 304–380 Fragment Aggregates through Autocatalytic Secondary Nucleation. *ACS Chem. Neurosci.* **2021**, *12* (23), 4406–4415. https://doi.org/10.1021/acschemneuro.1c00454.

(26) Voss, K.; Gamblin, T. C. GSK-3β Phosphorylation of Functionally Distinct Tau Isoforms Has Differential, but Mild Effects. *Mol. Neurodegener.* **2009**, *4* (1), 18. https://doi.org/10.1186/1750-1326-4-18.

(27) Barghorn, S.; Mandelkow, E. Toward a Unified Scheme for the Aggregation of Tau into Alzheimer Paired Helical Filaments. *Biochemistry* **2002**, *41* (50), 14885–14896. https://doi.org/10.1021/bi026469j.

(28) Getz, E. B.; Xiao, M.; Chakrabarty, T.; Cooke, R.; Selvin, P. R. A Comparison between the Sulfhydryl Reductants Tris(2-Carboxyethyl)Phosphine and Dithiothreitol for Use in Protein Biochemistry. *Anal. Biochem.* **1999**, *273* (1), 73–80. https://doi.org/10.1006/abio.1999.4203.

Chapter 6

Site Directed Mutagenesis, Purification, and Site Directed Spin Labeling of the Human TRPV1 Voltage Sensing Like Domain

Rebecca B. Stowe[1], Aerial Owens[2], Andrew K. Morris[1], Alison M. Bates[1], Wade Van Horn[2], Gary A. Lorigan[1]

1. Department of Chemistry and Biochemistry, Miami University, Oxford Ohio 45056
2. School of Molecular Sciences, Arizona State University, Tempe, AZ 85287

Project conceived by GAL, WVH, AO, AMB, and RBS. Sample preparation and data collection by RBS. Data analysis by RBS and AKM. Manuscript written by RBS. Manuscript edited by GAL and RBS.

6.1 Abstract

Regulation of ion flow is critical for many physiological processes. Human TRPV1 is an ion channel that is responsive to a variety of stimuli including ligands and temperature changes. TRPV1 is known for its role as a nociceptor, as well as having implications in diseases such as diabetes and depression. Recent structural studies have shown that the S1-S4 region of TRPV1 known as the voltage sensing like domain (VSLD) contains the binding pockets for a number of ligands and it is involved in the thermosensing mechanism. By using site directed spin labeling and EPR spectroscopy the structural dynamics and interhelical distances can be measured when the protein is exposed to different ligands and temperature changes. In this paper, TRPV1 VSLD was spin labeled for the first time and studied with CW EPR and DEER spectroscopic methods. It was found that the protein labels at high efficiencies and the DEER distance collected is similar to distances predicted based on Cryo-EM structures. This labeling method will allow for the protein to be studied with EPR spectroscopic techniques under different activating conditions, providing dynamic and structural information on the channel in different activation states.

6.2 Introduction

The human TRPV1 protein is an ion channel that is most well known as a pain receptor but has recently been found to play a role in diseases such as diabetes, depression, and schizophrenia.[1,2] It is a member of the Transient Receptor Potential Vanilloid family, categorized by its affinity for vanilloid ligands.[1,3] It responds to a variety of stimuli besides these ligands, including high temperature and high proton concentration. In the past it has been a drug target for pain relief, but after the recent studies confirming connections between TRPV1 and several common diseases its viability as a drug target has increased significantly.[2,4,5]

The structure of TRPV1 is like that of potassium channels such as KCNQ1, with six transmembrane helices that form a bundle comprised of two domains.[1,6–8] The voltage sensing like domain (VSLD) is made up of S1-S4 and is the location of the binding site for several ligands including capsaicin **(Figure 6.1)**.[9,10] The pore domain (PD) is comprised of helices S5-S6 and contains the selectivity filter that lines the pore in the membrane.[1,7,11] The full channel is formed when TRPV1 tetramerizes in the membrane.[1]

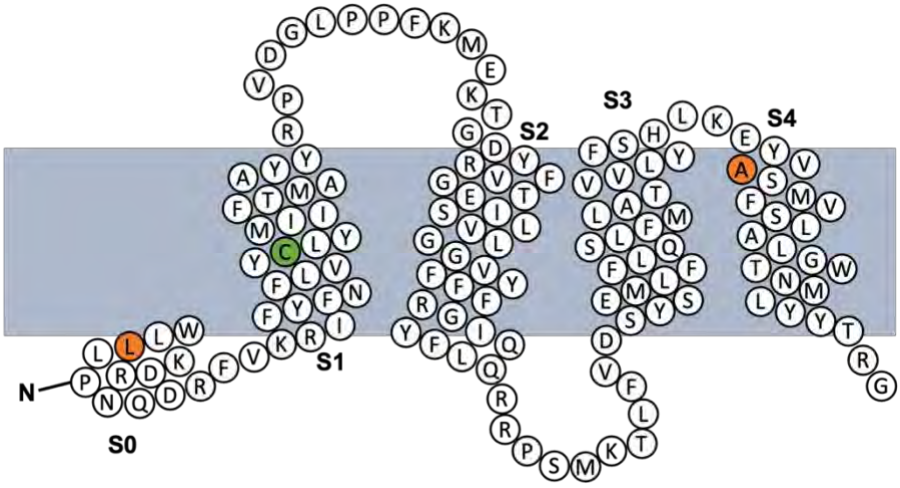

Figure 6.1. Membrane topology diagram of TRPV1 VSLD. Orange residues indicate cysteine mutations and green indicates the native cysteine C443.

Cryo-EM structures have determined that the VSLD is the location of the binding pockets for some ligands and has also recently been confirmed to play a role in thermosensing with solution NMR spectroscopy.[12] To further understand the dynamics of the protein upon ligand

binding and temperature changes, EPR spectroscopy can be used with site directed spin labeling to obtain site specific side chain mobility. DEER Spectroscopy can also be used to determine the distance between two residues under different conditions to observe larger conformational changes.

6.3 Materials and Methods

6.3.1 Site-Directed Mutagenesis

Site-Directed Mutagenesis was performed on the human TRPV1 VSLD in a pET-16b vector using pfuUltra II High Fidelity DNA Polymerase (Agilent) according to manufacturer's instructions. Primers were designed using A plasmid Editor (ApE) (University of Utah, Salt Lake City, UT). Purified plasmid DNA was extracted from transformed XL-Gold competent cell with a QIAprep Spin Miniprep Kit (Qiagen). Mutagenesis was confirmed with Sanger Sequencing (Genewiz).

6.3.2 Expression and Purification

Human TRPV1 VSLD in pET-16b vector was transformed into BL21-Codon Plus DE3-RP competent cells (Agilent). Cells were grown in M9 Minimal Media (Fisher Scientific) with 0.1 mM $CaCl_2$, 1 mM $MgSO_4$, 0.02% w/v glucose, 1x MEM Vitamin Solution (Corning), 50 μg/mL Chloramphenicol, and 100 μg/mL Ampicillin. The cultures were incubated with shaking at 250 rpm and 18 °C until they reached an OD_{600} of 0.6, then induced with 100 mM isopropyl ß-D-1-thiogalactopyranoside (IPTG). Cells were induced for 36-48 hours with shaking at 250 rpm and 18 °C to allow for protein overexpression.

The cells were harvested by centrifugation at 11000 xg for 10 minutes at 4 °C. Cell pellets were resuspended in 10x excess lysis buffer (75 mM Tris, 300 mM NaCl, 0.2 mM EDTA, pH 7.5) with 10x w/v excess of LDR stock (100 mg/mL lysozyme,10 mg/mL DNAse, 10 mg/mL RNAse), PMSF (20 mg/mL), and Magnesium Acetate (0.1 M). The cells were rotate for 30 minutes at room temperature to fully resuspend the pellet. Cell lysis was carried out with a Fisher Scientific Sonic Dismembrator Model 505, with the pulse set to 5 s on and 5 s off at 40% amplitude and a 1/4" tip. The cells were subjected to sonication twice for 7 ½ minutes and once

for 5 minutes. After sonication, the lysed cells were rotated at 4 °C with 3% empigen BB detergent for 40 minutes to an hour. The solubilized portion was then fractionated from the insolubilized by centrifugation at 17000 xg and 4 °C for 30 minutes. The supernatant was incubated with agitation with Ni^{2+}-NTA resin overnight to allow for protein binding. The resin and supernatant mixture was centrifuged at 2700 xg to separate the resin from the supernatant and the resin was then transferred to a gravity column for protein purification. The TRPV1 VSLD protein was purified by a rinse of Buffer A (40 mM HEPES and 300 mM NaCl, pH 7.5) with 2 mM tris(2-carboxyethyl)phosphine (TCEP) and 1.5% empigen BB detergent. The column was washed with Buffer A, 2 mM TCEP, 1.5% empigen BB detergent, and 50 mM imidazole to remove any nonspecific bound protein. The column was treated with a detergent exchange buffer containing 25 mM phosphate pH 7.0, 2 mM TCEP, and 0.05% 1-palmitoyl-2-hydroxy-*sn*-glycero-3-phospho-(1′-*rac*-glycerol) (LPPG), then the purified TRPV1 VSLD protein was eluted with 25 mM phosphate pH 7.0, 2 mM TCEP, 0.1% LPPG, and 250 mM imidazole. The purified protein was concentrated using an Amicon spin filter (10000 Da molecular weight cutoff) and the protein purity was confirmed via SDS PAGE.

6.3.3 Site-Directed Spin Labeling

A 10x molar excess of dithiothreitol (DTT) was added to the purified TRPV1 VSLD protein and the mixture was purged with N_2 gas for 1 minute. The mixture was then incubated at room temperature with shaking for 24 hours to reduce any disulfide bonds. A 250 mM stock of S-(1-oxyl-2,2,5,5-tetramethyl-2,5-dihydro-1H-pyrrol-3-yl)methyl methanesulfonothioate (MTSL) (Toronto Research Chemicals) was prepared in methanol and added directly to the purified TRPV1 VSLD protein at a 20x molar excess. The solution was incubated at room temperature for 30 minutes, then at 37 °C with shaking for 3 hours, then at room temperature with shaking for the remainder of 24 hours. The labeled protein was then buffer exchanged into 25 mM phosphate pH 7.0 and 0.05% LPPG by three rounds of centrifugation at 6000 xg in Amicon spin filter tubes (10000 Da molecular weight cutoff). During each round of centrifugation 7 mL of 25 mM phosphate pH 7.0 + 0.05% LPPG was added to the filter, allowing for removal of excess spin label. After the third round of centrifugation the protein was incubated with pre-equilibrated Ni^{2+}-NTA resin overnight. The resin was transferred to a gravity column and washed with 300 mL of 25 mM phosphate pH 7.0 + 0.05% LPPG to ensure total

removal of unreacted spin label, then the protein was eluted in 25 mM phosphate pH 7.0, 0.1% LPPG, and 250 mM imidazole.

6.3.4 CW-EPR Spectroscopy

CW-EPR spectroscopy measurements were collected on a Bruker EMX X-Band spectrometer with a Premium X bridge and ER4119-HS cavity. All measurements were carried out at room temperature with a center field of G, a 150 G sweep width, 100 kHz modulation frequency, 1 G modulation amplitude, and a 10.02 mW microwave power.

6.3.5 DEER Spectroscopy

Four pulse DEER measurements were collected with a Bruker ELEXSYS E580 spectrometer equipped with a SuperQFT pulse Q-band system with a EN5107D2 resonator and 150 W amplifier. All DEER samples contained approximately 50 μM spin label, with 10% v/v glycerol as a cryoprotectant. The samples were loaded into a 1.1 mm inner diameter quartz capillary (Wilmad LabGlass, Buena, NJ). DEER data was collected using a standard four pulse sequence $[(\pi/2)\nu1 - \tau1 - (\pi)\nu1 - t - (\pi)\nu2 - (\tau1 + \tau2 - t) - (\pi)\nu1 - \tau2 - \text{echo}]$ with probe pulse widths of 8 and 16 ns, a pump pulse width of 70 ns, 120 MHz frequency difference between the pump and probe pulses, shot repetition time determined by the spin-lattice relaxation time (T_1), 100 shots per point, and 16 step phase cycling at 80 K collected out to 2 μs determined by the spin-spin relaxation time (T_2).[13] Each sample was allowed to signal average for 24 hours. DEER data were analyzed using Matlab based DEER Analysis program 2015.[20] Tikhonov regularization was used to obtain DEER distance distributions $P(r)$ in the distance domain with the constraint $P(r) > 0$.[21] The background correction was obtained by using a homogeneous three-dimensional model. The regularization parameter in the L curve was optimized for the best fit DEER time domain data.

6.3.6 DEER Distance Predictions

Interspin distances for MTSL labeled sites were modeled using coarse-grained molecular dynamics. A model of the VSLD (residues 417 - 557) from the cryo-EM structure of TRPV1 from *Rattus norvegicus* (PDB: 3J5P) was created in CHARMM-GUI membrane builder with the Martini 22p force field in a planar lipid bilayer with 452 molecules of POPC and 150 of POPG and a number of Na+ and Cl- ions to produce 150 mM total and a system with 0 net charge [7,14,15]

All subsequent simulations were run in Gromacs v2022.3.[16] The simulation was minimized and equilibrated with default run parameters generated by CHARMM-GUI. Production phase was also run with default CHARMM-GUI parameters, except with $5x10^7$ integration steps of 20 fs each for a total of 1 us. A custom MATLAB program was used to generate the predicted distance between labels in each production frame based on extension of the vector between the backbone coordinate and the SC1 coordinate of the selected residue by a factor of 2.5 and finding the distance between these extended points for different selected residues. When the observed distances for each frame were binned, they were then plotted as a histogram to show their time averaged distribution.

6.4 Results and Discussion

Several cysteine mutations were selected for TRPV1 VSLD to provide dynamic information and interhelical distances for each of the helices. L422C and A539C were successfully mutated, yielding proteins with two cysteines that can be useful for continuous wave

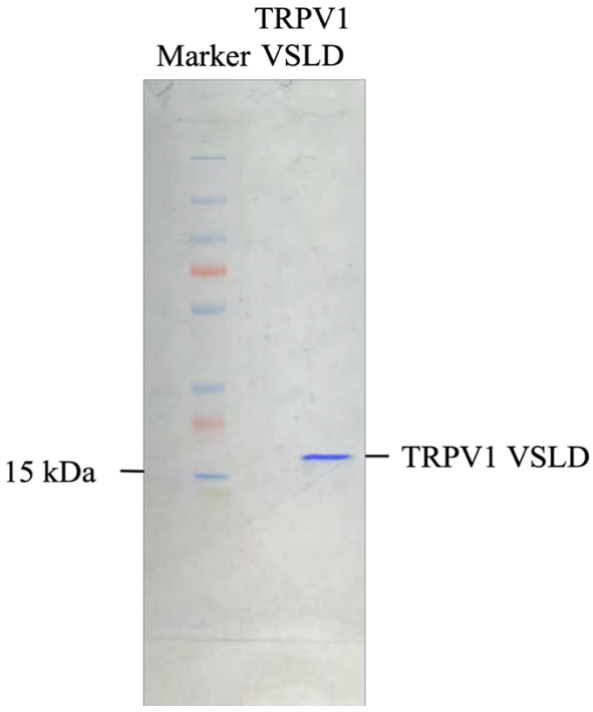

Figure 6.2. SDS-PAGE gel showing purified TRPV1 VSLD in LPPG micelles at the expected molecular weight.

(CW) EPR spectroscopy and DEER spectroscopy. L422C lies in S0, and A539C is in S4.[11,12] WT was also expressed since it has one native cysteine, so it can be used to collect CW EPR spectroscopy data. Each mutant and WT protein expressed highly with final purified protein concentrations ranging from 2.5-5 mg of protein per liter of bacterial culture. The purity was also confirmed via SDS PAGE, shown in **Figure 6.2**. The high expression levels and exceptional purity makes TRPV1 VSLD an excellent candidate for EPR spectroscopic measurements, as it requires a larger amount of protein than most other spectroscopic techniques.[17]

All mutants and WT TRPV1 VSLD successfully labeled with spin labeling efficiencies ranging from 67% to 90%. WT is the only single mutant that has been labeled so far, and it labeled at the highest overall efficiency of 90%, with L422C/C443 at 77% and A539C/C443 at 67%, according to a spin label concentration calculated by TEMPO calibration curve. At this range of spin labeling efficiency any of the available EPR techniques are accessible, including DEER spectroscopy.[13,17] A539C/C443 will need to have a higher efficiency to observe accurate distances with DEER spectroscopy, so it can either be replaced with a comparable mutant if necessary or the labeling protocol can be optimized to increase the efficiency. The CW EPR spectra for the currently available mutants are shown in **Figure 6.3.** Each sample has a spin label at position C443, which is the native cysteine, so any difference in line shape between the WT spectra and the mutants are a result of the additional cysteine. Once a cysless mutant is produced, these cysteine mutations will be labeled on their own to determine their dynamics without the native cysteine influencing the spectra and further mutations will be made to investigate the dynamics of residues spanning the entire length of VSLD. CW EPR spectroscopy can be performed at a large range of temperatures, and the spin label used can stay attached upon addition of ligands assuming the ligand used is not also a reducing agent.[18] Since TRPV1 VSLD has been found to undergo conformational changes at high temperature and after ligand binding, this labeling method can be used to determine the change in dynamics for individual side chains

under a number of different conditions, providing a better understanding of how the local environment is affected in the presence of agonists and different temperatures.[2]

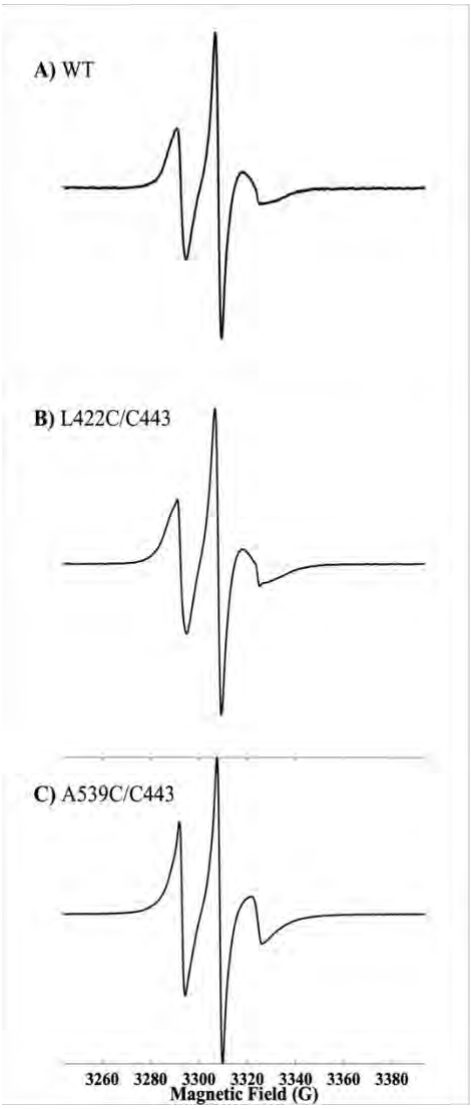

Figure 6.3. CW EPR spectra of each TRPV1 mutant currently expressed. In (A) the WT protein is labeled at the native cysteine C443. In (B) the labels are at L422C and C443, and a slight mobile component can be seen in the low and high field lines that arise from L422C. In (C), the protein is labeled at A539C and C442, and the spectra appears slightly sharper, especially in the low field line when compared to WT.

DEER measurements were conducted on the L442C/C443 mutant, with a single broad distance measured, centered at 33 Å or 3.3 nm (**Figure 6.4**). This data was collected on a sample with 77% spin labeling efficiency, and it had a modulation depth of 20%. Compared to the distance prediction based off the Cryo-EM model the distance measured with DEER spectroscopy was longer, which makes sense as the model was based off a sample in vesicles and the DEER spectrum was collected in detergent micelles. Since a vesicle is a more restrictive environment, the protein would have less freedom of movement and will sample different conformations when compared to the detergent micelle. Despite the difference between the model and experimental distance distribution, this the model can be used for now to get a quick estimate on the expected distance before the DEER data is collected. It could be improved upon by reconstituting the protein into vesicles so that the model and experimental distance distributions are taken from samples in the same membrane mimetic. The sample quality will be improved by optimizing the labeling protocol, but this is a promising preliminary result as this is the first DEER spectrum collected for this protein.[13] By increasing the spin labeling efficiency the distances collected will be more precise and the modulation depth will increase, providing better distance estimations that can be used to further refine structural details.[13] DEER measurements will also be conducted in the presence of agonists to observe distance distribution shifts that occur due to the induced conformational changes.

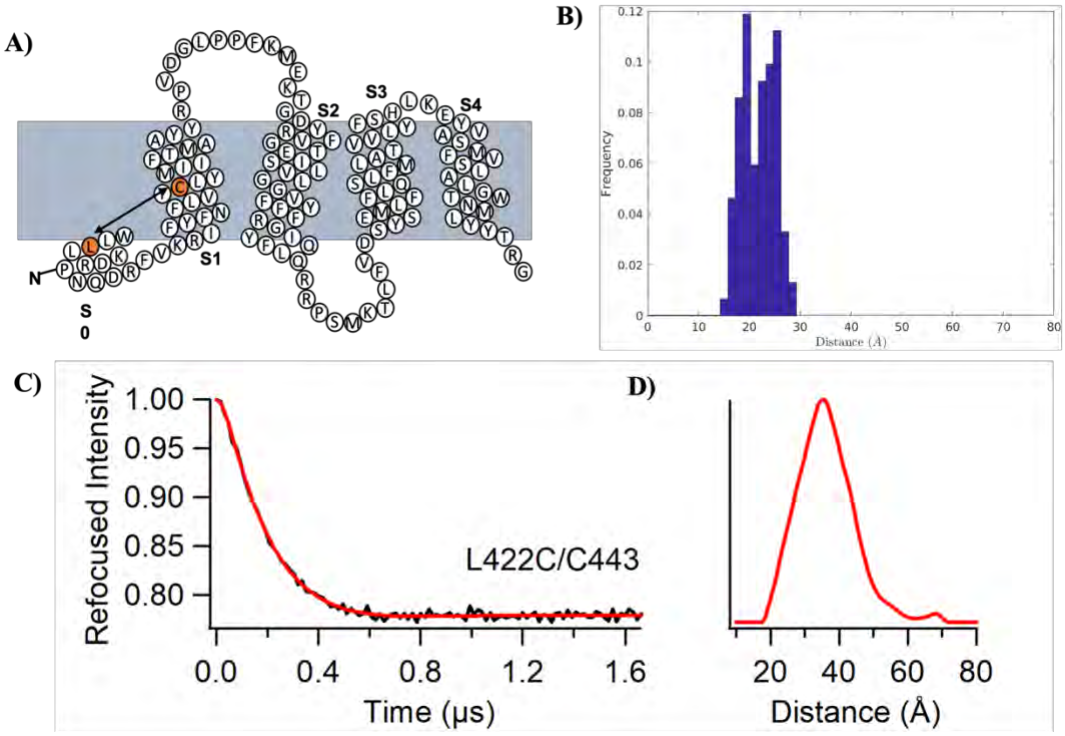

Figure 6.4. (A) Topology diagram showing the location of spin labels in orange, with an arrow to indicate the distance to be measured between them. **(B)** Distance prediction based on Cryo-EM model in POPC:POPG vesicles. Time domain **(C)** and distance distribution **(D)** data of L422C/C443.

6.5 Conclusions

This is the first time the human TRPV1 VSLD has been successfully spin labeled for the purpose of EPR spectroscopic measurements. The spin labeling efficiency is very high for a protein that hasn't been spin labeled before, which makes it a great candidate for CW and pulsed EPR experiments. By expressing more single and double cysteine mutations and subjecting these mutants to different conditions known to induce conformational changes, dynamic and structural information on this protein will be further refined.

6.6 Acknowledgements

This work was generously supported by an NIGMS/NIH Maximizing Investigator's Research Award (MIRA) R35 GM126935 grant to G.A.L.

References

(1) Benítez-Angeles, M.; Morales-Lázaro, S. L.; Juárez-González, E.; Rosenbaum, T. TRPV1: Structure, Endogenous Agonists, and Mechanisms. *Int. J. Mol. Sci.* **2020**, *21* (10), 3421. https://doi.org/10.3390/ijms21103421.

(2) Kim, M.; Sisco, N. J.; Hilton, J. K.; Montano, C. M.; Castro, M. A.; Cherry, B. R.; Levitus, M.; Van Horn, W. D. Evidence That the TRPV1 S1-S4 Membrane Domain Contributes to Thermosensing. *Nat. Commun.* **2020**, *11* (1), 4169. https://doi.org/10.1038/s41467-020-18026-2.

(3) Cao, E.; Liao, M.; Cheng, Y.; Julius, D. TRPV1 Structures in Distinct Conformations Reveal Activation Mechanisms. *Nature* **2013**, *504* (7478), 113–118. https://doi.org/10.1038/nature12823.

(4) Storozhuk, M. V.; Moroz, O. F.; Zholos, A. V. Multifunctional TRPV1 Ion Channels in Physiology and Pathology with Focus on the Brain, Vasculature, and Some Visceral Systems. *BioMed Res. Int.* **2019**, *2019*, 1–12. https://doi.org/10.1155/2019/5806321.

(5) Zhang, H.; Lin, J.-J.; Xie, Y.-K.; Song, X.-Z.; Sun, J.-Y.; Zhang, B.-L.; Qi, Y.-K.; Xu, Z.-Z.; Yang, F. Structure-Guided Peptide Engineering of a Positive Allosteric Modulator Targeting the Outer Pore of TRPV1 for Long-Lasting Analgesia. *Nat. Commun.* **2023**, *14* (1), 4. https://doi.org/10.1038/s41467-022-34817-1.

(6) Dixit, G.; Dabney-Smith, C.; Lorigan, G. A. The Membrane Protein KCNQ1 Potassium Ion Channel: Functional Diversity and Current Structural Insights. *Biochim. Biophys. Acta BBA - Biomembr.* **2020**, *1862* (5), 183148. https://doi.org/10.1016/j.bbamem.2019.183148.

(7) Liao, M.; Cao, E.; Julius, D.; Cheng, Y. Structure of the TRPV1 Ion Channel Determined by Electron Cryo-Microscopy. *Nature* **2013**, *504* (7478), 107–112. https://doi.org/10.1038/nature12822.

(8) Tominaga, M.; Tominaga, T. Structure and Function of TRPV1. *Pflüg. Arch. - Eur. J. Physiol.* **2005**, *451* (1), 143–150. https://doi.org/10.1007/s00424-005-1457-8.

(9) Kwon, D. H.; Zhang, F.; Suo, Y.; Bouvette, J.; Borgnia, M. J.; Lee, S.-Y. Heat-Dependent Opening of TRPV1 in the Presence of Capsaicin. *Nat. Struct. Mol. Biol.* **2021**, *28* (7), 554–563. https://doi.org/10.1038/s41594-021-00616-3.

(10) Yang, F.; Xiao, X.; Lee, B. H.; Vu, S.; Yang, W.; Yarov-Yarovoy, V.; Zheng, J. The Conformational Wave in Capsaicin Activation of Transient Receptor Potential Vanilloid 1 Ion Channel. *Nat. Commun.* **2018**, *9* (1), 2879. https://doi.org/10.1038/s41467-018-05339-6.

(11) Neuberger, A.; Oda, M.; Nikolaev, Y. A.; Nadezhdin, K. D.; Gracheva, E. O.; Bagriantsev, S. N.; Sobolevsky, A. I. Human TRPV1 Structure and Inhibition by the Analgesic SB-366791. *Nat. Commun.* **2023**, *14* (1), 2451. https://doi.org/10.1038/s41467-023-38162-9.

(12) Kwon, D. H.; Zhang, F.; Fedor, J. G.; Suo, Y.; Lee, S.-Y. Vanilloid-Dependent TRPV1 Opening Trajectory from CryoEM Ensemble Analysis. *Nat. Commun.* **2022**, *13* (1), 2874. https://doi.org/10.1038/s41467-022-30602-2.

(13) Jeschke, G. DEER Distance Measurements on Proteins. *Annu. Rev. Phys. Chem.* **2012**, *63* (1), 419–446. https://doi.org/10.1146/annurev-physchem-032511-143716.

(14) Marrink, S. J.; Risselada, H. J.; Yefimov, S.; Tieleman, D. P.; De Vries, A. H. The MARTINI Force Field: Coarse Grained Model for Biomolecular Simulations. *J. Phys. Chem. B* **2007**, *111* (27), 7812–7824. https://doi.org/10.1021/jp071097f.

(15) Qi, Y.; Ingólfsson, H. I.; Cheng, X.; Lee, J.; Marrink, S. J.; Im, W. CHARMM-GUI Martini Maker for Coarse-Grained Simulations with the Martini Force Field. *J. Chem. Theory Comput.* **2015**, *11* (9), 4486–4494. https://doi.org/10.1021/acs.jctc.5b00513.

(16) Pronk, S.; Páll, S.; Schulz, R.; Larsson, P.; Bjelkmar, P.; Apostolov, R.; Shirts, M. R.; Smith, J. C.; Kasson, P. M.; Van Der Spoel, D.; Hess, B.; Lindahl, E. GROMACS 4.5: A High-Throughput and Highly Parallel Open Source Molecular Simulation Toolkit. *Bioinformatics* **2013**, *29* (7), 845–854. https://doi.org/10.1093/bioinformatics/btt055.

(17) Sahu, I. D.; Lorigan, G. A. Site-Directed Spin Labeling EPR for Studying Membrane Proteins. *BioMed Res. Int.* **2018**, *2018*, 1–13. https://doi.org/10.1155/2018/3248289.

(18) Bordignon, E.; Bleicken, S. New Limits of Sensitivity of Site-Directed Spin Labeling Electron Paramagnetic Resonance for Membrane Proteins. *Biochim. Biophys. Acta BBA - Biomembr.* **2018**, *1860* (4), 841–853. https://doi.org/10.1016/j.bbamem.2017.12.009.

Chapter 7

Conclusions and Future Directions

The work in this dissertation made use of biophysical techniques to further the understanding of protein-protein interactions and aggregation, as well as the development and application of novel membrane mimetic systems.

Chapter 2 highlighted the interactions between monomers of the KCNQ1 tetramer, showing that the oligomerization of the channel does not fully rely on the interactions of the C-terminus, which has been the focus of studies in the literature. The transmembrane region alone is capable of forming a tetramer, which has never been confirmed before as previous studies have either used the full-length protein or the VSD alone.[1,2] By studying the transmembrane region in isolation, the influence of the interactions in the C-terminus was eliminated and there is now a better understanding about what is required for the channel to form the native tetramer. Knowing this, the tetramerization mechanism can be further clarified by determining which residues are involved. Known disease state mutations could be introduced into this construct to determine if these mutations hinder the tetramerization, therefore clarifying disease mechanisms, which could lead to more effective therapeutics.[2,3]

In Chapter 3, the KCNE1 protein was purified directly from the cell with a derivative of SMA polymer that is more compatible with membrane protein systems. By functionalizing the polymer and reducing the molecular weight, SMA-Neut was shown to be capable of purifying a protein that was not accessible to traditional SMA.[4] The functionalization of the polymer allows it to tolerate a wider range of pH values and the presence of divalent cations, making it suitable for use with a wider range of proteins when compared to traditional SMA. Since the previous method of KCNE1 purification involved overexpression in inclusion bodies, the SMA was introduced to the protein after the inclusion bodies were fractionated.[5] It was found that the SMA successfully purified the protein from inclusion bodies with a similar level of purity when compared to the original purification method, as shown by SDS-PAGE. By expanding the solubilization capabilities of SMA through derivatization as shown in this chapter, these polymers can be used to study the structures of other membrane proteins, potentially including proteins expressed in eukaryotic cells. This could make it possible to resolve the structures and study the dynamics of proteins that are resistant to solubilization in other membrane mimetics, since SMALPs can remove proteins directly from the native environment.

Chapter 4 focused on the protein-protein interactions between KCNQ1 and KCNE1 using CW EPR spectroscopic techniques. Previous literature has studied these interactions from a functional perspective, as well as from more dynamically restricting techniques such as crosslinking. By using EPR spectroscopy, the dynamic properties of spin labeled KCNE1 protein upon interaction with KCNQ1 was observed for the first time. The CW EPR spectra showed clear patterns for each region of KCNE1 mutants chosen. The N-terminal mutations showed a clear increase in mobility upon interaction with KCNQ1, indicating that there is a change in dynamics and conformation that is consistent with the function of that region of KCNE1, which is to interact with the voltage sensing domain (VSD) of KCNQ1 so that the channel can open and close at the appropriate timescale.[6] In the transmembrane region residues 57-59 are highly conserved and crucial for the slow activation kinetics of the I_{KS} channel. When these residues are spin labeled the spin label mobility also increases, but in this case, this indicates the interaction is disrupted as the spin label is already more restricted as it is in a helix in the middle of the bilayer. This is further supported by the other transmembrane mutants 65, 66, and 69 showing broadening upon interaction with KCNQ1. The C-terminus did not show significant changes upon the introduction of KCNQ1, which validates previous literature that the C-terminus of E1 interacts with the C-terminus of Q1, which is not present in the construct used in this chapter.[6,7] Following this study, the dynamics of the E1/Q1 complex could be further clarified by using the full length Q1 protein. This would require expression with a mammalian cell system as full length Q1 does not express in *E. Coli.* The protein could be purified from the mammalian cells or in cell EPR could be used with E1 and Q1 co-expressed in the same cells. This could further refine the dynamics of the channel and expand the study into the C-terminal region of Q1. This could also be done in the presence of cofactors and endogenous lipids such as calmodulin and PIP2, which are required *in vivo* for a fully functional channel.[8,9] This chapter has shown that the dynamics of this protein-protein interaction can be reliably measured via CW EPR spectroscopic techniques and opens the possibility for this technique to be used with other constructs of the same complex and other similar systems.

Chapter 5 explored the aggregation of full-length Tau protein using CW EPR and DEER spectroscopic techniques. Full length tau has not been studied in this way before, so it was crucial to develop a method for aggregation and spin labeling that don't disrupt the protein.[10] Detailed structural and dynamic information of Tau aggregates is crucial for the understanding of

various tauopathies. Now that the structures of several disease state aggregates are known, lab grown aggregate structures must be studied to determine their physiological relevance. By spin labeling full-length Tau instead of a truncated construct, this study provides a method by which the dynamics and structure of octadecyl sulfate (ODS) induced aggregates can be determined. Through CW and DEER measurements it was found that the spin label remains attached to the protein throughout the aggregation process and TEM images showed that the protein aggregates are of sufficient quality in the presence of spin label. The core of the aggregate has been found to be in a similar region for multiple methods of aggregation including disease state aggregates. In the case of ODS, it was found that there was not a significant change in dynamics or distances between spin labels upon aggregation, indicating that the core of the aggregate is in a different region for this inducer when compared to other methods. This could imply that the physiological significance of ODS induced aggregates is not sufficient for them to be compared to disease state aggregates. By developing this method, the core of the aggregate for other aggregation techniques could be quickly determined with a few double mutants that cover a broad range of the protein length, eliminating those that are dissimilar from disease state aggregates. This would provide researchers with a list of aggregation methods that provide the most physiologically relevant aggregates to use for further studies of aggregation inhibitors and tauopathy treatments.

Chapter 6 focused on the expression, spin labeling, CW EPR, and DEER spectroscopic studies of the human TRPV1 voltage sensing like domain (VSLD). TRPV1 is a protein that is becoming a more popular drug target after the discovery of its role in several common diseases, so a thorough understanding of the structure and dynamics is crucial for the development of new therapies.[11] The VSLD region is similar to the VSD of Q1 and is responsible for ligand binding and thermosensing, two processes that control the function of the channel.[11] This is the first time this protein has been successfully spin labeled, and the high label concentration and efficiency will allow for the use in both CW and pulsed EPR experiments. The side chain dynamics, solvent accessibility, membrane depth, and distances between residues or monomers can be determined using the labeling method used here. Cysteine mutations will be introduced in areas of interest, first taking advantage of the single native cysteine to produce doubled labeled samples ready for DEER spectroscopy. Due to the variety of agonists available the change in dynamics and structure can be studied in the presence of ligands, high temperatures, and low pH.

References

(1) Dixit, G.; Sahu, I. D.; Reynolds, W. D.; Wadsworth, T. M.; Harding, B. D.; Jaycox, C. K.; Dabney-Smith, C.; Sanders, C. R.; Lorigan, G. A. Probing the Dynamics and Structural Topology of the Reconstituted Human KCNQ1 Voltage Sensor Domain (Q1-VSD) in Lipid Bilayers Using Electron Paramagnetic Resonance Spectroscopy. *Biochemistry* **2019**, *58* (7), 965–973. https://doi.org/10.1021/acs.biochem.8b01042.

(2) Chung, D. Y.; Chan, P. J.; Bankston, J. R.; Yang, L.; Liu, G.; Marx, S. O.; Karlin, A.; Kass, R. S. Location of KCNE1 Relative to KCNQ1 in the I_{KS} Potassium Channel by Disulfide Cross-Linking of Substituted Cysteines. *Proc. Natl. Acad. Sci.* **2009**, *106* (3), 743–748. https://doi.org/10.1073/pnas.0811897106.

(3) Maljevic, S.; Wuttke, T. V.; Seebohm, G.; Lerche, H. KV7 Channelopathies. *Pflüg. Arch. - Eur. J. Physiol.* **2010**, *460* (2), 277–288. https://doi.org/10.1007/s00424-010-0831-3.

(4) Burridge, K. M.; Harding, B. D.; Sahu, I. D.; Kearns, M. M.; Stowe, R. B.; Dolan, M. T.; Edelmann, R. E.; Dabney-Smith, C.; Page, R. C.; Konkolewicz, D.; Lorigan, G. A. Simple Derivatization of RAFT-Synthesized Styrene–Maleic Anhydride Copolymers for Lipid Disk Formulations. *Biomacromolecules* **2020**, *21* (3), 1274–1284. https://doi.org/10.1021/acs.biomac.0c00041.

(5) Sahu, I. D.; Craig, A. F.; Dunagan, M. M.; Troxel, K. R.; Zhang, R.; Meiberg, A. G.; Harmon, C. N.; McCarrick, R. M.; Kroncke, B. M.; Sanders, C. R.; Lorigan, G. A. Probing Structural Dynamics and Topology of the KCNE1 Membrane Protein in Lipid Bilayers via Site-Directed Spin Labeling and Electron Paramagnetic Resonance Spectroscopy. *Biochemistry* **2015**, *54* (41), 6402–6412. https://doi.org/10.1021/acs.biochem.5b00505.

(6) Gofman, Y.; Shats, S.; Attali, B.; Haliloglu, T.; Ben-Tal, N. How Does KCNE1 Regulate the Kv7.1 Potassium Channel? Model-Structure, Mutations, and Dynamics of the Kv7.1-KCNE1 Complex. *Structure* **2012**, *20* (8), 1343–1352. https://doi.org/10.1016/j.str.2012.05.016.

(7) Kang, C.; Tian, C.; Sönnichsen, F. D.; Smith, J. A.; Meiler, J.; George, A. L.; Vanoye, C. G.; Kim, H. J.; Sanders, C. R. Structure of KCNE1 and Implications for How It Modulates the

KCNQ1 Potassium Channel † ‡. *Biochemistry* **2008**, *47* (31), 7999–8006. https://doi.org/10.1021/bi800875q.

(8) Royal, A. A.; Tinker, A.; Harmer, S. C. Phosphatidylinositol-4,5-Bisphosphate Is Required for KCNQ1/KCNE1 Channel Function but Not Anterograde Trafficking. *PLOS ONE* **2017**, *12* (10), e0186293. https://doi.org/10.1371/journal.pone.0186293.

(9) Abbott, G. W. Biology of the KCNQ1 Potassium Channel. *New J. Sci.* **2014**, *2014*, 1–26. https://doi.org/10.1155/2014/237431.

(10) Fichou, Y.; Vigers, M.; Goring, A. K.; Eschmann, N. A.; Han, S. Heparin-Induced Tau Filaments Are Structurally Heterogeneous and Differ from Alzheimer's Disease Filaments. *Chem. Commun.* **2018**, *54* (36), 4573–4576. https://doi.org/10.1039/C8CC01355A.

(11) Kim, M.; Sisco, N. J.; Hilton, J. K.; Montano, C. M.; Castro, M. A.; Cherry, B. R.; Levitus, M.; Van Horn, W. D. Evidence That the TRPV1 S1-S4 Membrane Domain Contributes to Thermosensing. *Nat. Commun.* **2020**, *11* (1), 4169. https://doi.org/10.1038/s41467-020-18026-2.